**TECHNISCHE UNIVERSITÄT MÜNCHEN**

Department Chemie

Lehrstuhl für Biotechnologie

# Functional conformations of the molecular chaperone BiP

Moritz Daniel Marcinowski

Vollständiger Abdruck der von der Fakultät für Chemie der Technischen Universität München zur Erlangung des akademischen Grades eines Doktors der Naturwissenschaften genehmigten Dissertation

| | | |
|---|---|---|
| Vorsitzender: | | Univ.-Prof. Dr. Michael Groll |
| Prüfer der Dissertation: | 1. | Univ.-Prof. Dr. Johannes Buchner |
| | 2. | Univ.-Prof. Dr. Sevil Weinkauf |
| | 3. | Univ.-Prof. Dr. Iris Antes |

Die Dissertation wurde am 01.06.2011 bei der Technischen Universität München eingereicht und durch die Fakultät für Chemie am 06.07.2011 angenommen.

*Für meine Eltern*

# 1 Index

# 2 Summary

Antibodies of the subtype IgG are composed of two heavy chains (HCs) and two light chains (LCs). The HC contains one variable ($V_H$) and three constant domains ($C_H$1-3) while LCs consist of one variable ($V_L$) and one constant domain ($C_L$). The four chains of the heterotetramer are linked via disulphide bridges. The assembly of IgGs has to be carefully monitored in the endoplasmic reticulum (ER) as the secretion of incorrectly assembled IgGs is potentially harmful for the organism. Hence, control mechanisms exist in the ER with the molecular chaperone BiP, a member of the Hsp70 family, playing an important role. Furthermore, BiP is involved in other regulatory tasks such as the unfolded protein response or the ER associated degradation pathway (ERAD).

BiP was first discovered as heavy chain binding protein and the $C_H$1 domain is the major binding site for BiP in HCs. Hence, the interaction of BiP with the $C_H$1 domain as an endogenous substrate was analyzed in detail with a focus on (i) the binding sites for BiP in the $C_H$1 domain (ii) the conformational changes of BiP in its chaperone cycle and upon binding of substrates and (iii) the alteration of BiP's cycle by the co-chaperone ERdJ3.

The introduction of point mutations in predicted BiP binding sites in $C_H$1 in this work has shown that only a subset of binding sites are recognized by BiP in a mutually exclusive manner. By a fluorescence anisotropy assay it was possible to directly follow binding of peptides corresponding to those sites in equilibrium and to analyze effects of modified peptides. So far, hydrophobicity was believed to be the only driving force for efficient binding. In this work, the influence of peptide conformations was analyzed, revealing a preference of BiP for extended conformations over kinked ones in substrates. This was shown by introducing non-proteinogenic amino acids in a central position of the peptides without changing the hydrophobicity of the peptide. By making use of different side chain substituents, aromatic systems even as large as Fmoc were shown to be bound, while linear hydrophobic side chains are not well bound by BiP.

Substrate recognition by BiP is regulated by the binding of ATP and its subsequent hydrolysis with the ADP-bound state showing high affinity. However, a detailed analysis of the underlying conformational changes within BiP was missing. Intramolecular FRET pairs were introduced in BiP and analyzed on the single molecule level in collaboration with Prof. Don Lamb (Ludwig-Maximilians-Universität, München) by single pair FRET (spFRET). The experiments revealed concerted domain movements in BiP with the nucleotide binding domain (NBD), the substrate binding domain (SBD) and the lid acting as a tripartite

molecular machine. Importantly, conformational transitions of the lid domain allow BiP to discriminate between peptide and protein substrates which are bound by BiP in different conformations. Additionally, a hitherto unknown direct interaction of substrates with the lid of BiP could be shown.

The co-chaperone ERdJ3 was previously shown to accelerate BiP's ATPase and to transfer substrates to BiP. In this work, it was shown that the ADP-bound state of BiP strongly interacts with ERdJ3 while ATP leads to only transient interactions. In the presence of ERdJ3 and ADP, a lid conformation highly similar to the $C_H1$-bound one was observed, indicating that ERdJ3 primes BiP for substrate binding. This is supported by ensemble FRET experiments where ERdJ3 accelerated $C_H1$ binding in the presence of ADP and exclusively allowed BiP binding to $C_H1$ in the presence of ATP.

Taken together, the conformational selectivity of BiP for substrates was analyzed revealing that extended stretches are bound while kinked ones are not. This expands the current view that only hydrophobicity is the driving force for substrate recognition by BiP. Additionally, the analysis of the conformational cycle of BiP revealed different conformations upon peptide or protein substrate binding, which were considered so far as equivalent, with the lid playing an important role in the discrimination of both substrate types. Importantly, ERdJ3 primes BiP for $C_H1$ binding by populating a conformation in BiP similar to the $C_H1$-bound one.

# 3 Zusammenfassung

Immunglobuline (Igs) sind komplex aufgebaute Biomoleküle des adaptiven Immunsystems höherer Eukaryoten. Sie sind im Subtyp IgG aus zwei leichten Ketten und zwei schweren Ketten aufgebaut, die kovalent mittels Disulphidbrücken verknüpft sind. Die leichte Kette besteht aus einer konstanten ($C_L$) und einer variablen ($V_L$) Domäne. Eine variable ($V_H$) und drei konstante ($C_H$1-3) Domäne bilden die schwere Kette. Durch das Heterodimer der N-terminalen variablen Domänen der leichten und schweren Kette werden Epitope mit hoher Spezifität erkannt. Die homodimeren $C_H$2 und $C_H$3 Domänen beinhalten die Effektorfunktionen für die Aktivierung des Immunsystems. Die korrekte Assemblierung und Faltung von Igs muss streng kontrolliert werden, da sonst potentiell für den gesamten Organismus schädliche Formen sekretiert werden.

Igs werden co-translational in das Endoplasmatische Retikulum (ER) sekretiert und dort assembliert. Die zwei, bzw. vier Domänen der beiden Ketten müssen korrekt falten, ihre internen Disulphidbrücken oxidieren, sowie das Heterotetramer bilden. Ig Domänen können einzeln falten, die $C_H$1 Domäne erlangt ihren gefalteten Zustand jedoch erst nach der Assoziation mit der Partnerdomäne $C_L$. Dieser effiziente Mechanismus führt zur Retention nicht-assemblierter schwerer Ketten im ER. Verantwortlich hierfür ist das molekulare Chaperon heavy chain binding protein (BiP), das stabile Komplexe mit der $C_H$1 Domäne bildet. Als Vertreter der Hsp70 Familie ist der Zyklus von BiP durch die Hydrolyse von ATP reguliert. ATP Bindung resultiert im nieder-affinen Zustand für Substrate, wohingegen die Hydrolyse des ATPs zu ADP zum hoch-affinen Zustand führt. Zusätzlich wird der Chaperon-Zyklus durch Co-Faktoren wie dem lumenalen ERdJ3 reguliert.

In dieser Arbeit wurde die Sequenzspezifität von BiP mit der $C_H$1 Domäne als natürliches Substrat, sowie der Konformationszyklus von BiP und dessen Modulation durch das Co-Chaperon ErdJ3 untersucht. Hierzu wurden die Proteine kloniert, rekombinant in *E. coli* expremiert und gereinigt.

Durch Punktmutationen in zwei vorhergesagten Bindestellen für BiP in der $C_H$1 Domäne konnte gezeigt werden, dass BiP beide Stellen im Kontext der $C_H$1 Domäne erkennt und beide alternierend gebunden werden können. Die Bindung von Peptiden, die diesen beiden Bindestellen entsprechen, konnte mittels Fluoreszenz-Anisotropie im Gleichgewicht verfolgt werden. Bislang wurde die Hydrophobizität der Bindestellen als einziges wichtiges Element für die Bindung nachgewiesen. In dieser Arbeit wurde die Konformation der Bindestellen analysiert, da durch nicht-natürliche Aminosäuren lineare oder geknickte Konformationen

der Peptide induziert werden konnten. Die Analyse zeigte, dass BiP nur lineare Sequenzen erkennt und geknickte Konformationen, trotz identischer Hydrophobizität, nicht gebunden werden. Mittels verschiedener Seitenketten-Substituenten konnte gezeigt werden, dass aromatische Systeme in zentraler Position des Peptides von BiP gebunden werden, wohingegen lineare hydrophobe Reste schlecht erkannt werden.

Der Konformationszyklus von BiP der zu den verschiedenen Substrat Affinitäten führt, ist nicht im Detail verstanden. Daher wurden in dieser Arbeit mittels Einzel-Molekül FRET Experimenten in Zusammenarbeit mit der Gruppe von Prof. Don Lamb (Ludwig-Maximilians Universität, München) die Konformationsänderungen von BiP bei Nukleotid, Peptid oder Protein Substrat Bindung untersucht. Die Ergebnisse zeigen aufeinander abgestimmte Konformationsänderungen der Domänen von BiP. Peptide wurden bisher als Minimalmodell für Proteinsubstrate verwendet, da sie mit ähnlicher Affinität an BiP binden. Interessanterweise, werden Peptide und die $C_H1$ Domäne als Proteinsubstrat jedoch von BiP in verschiedenen Konformationen gebunden. Hierbei spielt der *Lid* von BiP eine entscheidende Rolle, da er direkt mit der $C_H1$ Domäne interagiert.

ERdJ3, ein lumenales Co-Chaperon von BiP, bindet Substrate und überträgt diese auf BiP. In dieser Arbeit wurde der Einfluss von ERdJ3 auf den Konformations Zyklus von BiP sowie die Substratübertragung näher untersucht. Es konnte gezeigt werden, dass die Bindung von ERdJ3 in BiP in Anwesenheit von ADP eine Konformation ähnlich der des $C_H1$ gebundenen Zustands bewirkt und somit BiP für die Bindung des Protein-Substrats vorbereitet. Dies wird durch eine effizientere Bindung der $C_H1$ Domäne durch BiP in Anwesenheit des ERdJ3s unterstrichen.

Zusammenfassend wurde in dieser Arbeit die Selektivität von BiP für Bindestellen in Substraten untersucht und es konnte gezeigt werden, dass BiP lineare Sequenzen bindet, wohingegen geknickte Konformationen nicht erkannt werden. Dies erweitert das Verständnis der Substratspezifität von BiP, da bisher nur die Hydrophobizität der Bindestelle als wichtig erkannt wurde. Darüber hinaus konnten abgestimmte Konformationsänderungen in den Domänen von BiP bei Nukleotid und Substratbindung gezeigt werden, wobei Peptide und $C_H1$ in unterschiedlichen Konformationen gebunden werden. Der *Lid* spielt hierbei eine wichtige Rolle und dessen Konformation wird durch ERdJ3 moduliert.

# 4 Introduction

## 4.1 Protein folding

Proteins are synthesized at the ribosome as linear, unfolded polypeptide chains. During or after their biogenesis they have to adopt an intricate three-dimensional structure to fulfil their biological tasks. Exceptions are natively disordered proteins which only obtain their structure upon association with ligands or other proteins in hetero-oligomers (Fink, 2005). Protein folding is a spontaneous process governed by the information of the amino acid sequence (Anfinsen, 1973; Seckler and Jaenicke, 1992; Fersht and Daggett, 2002). It is driven by the balance of entropy and enthalpy from the unfolded state (U) to the folded native state (N) (Dill, 1990; Dill and Chan, 1997). This is represented by the concept of the folding funnel where the folded state is a minimum on the multidimensional energy landscape ((Leopold et al., 1992; Wolynes et al., 1995; Dobson and Karplus, 1999); see Figure 1).

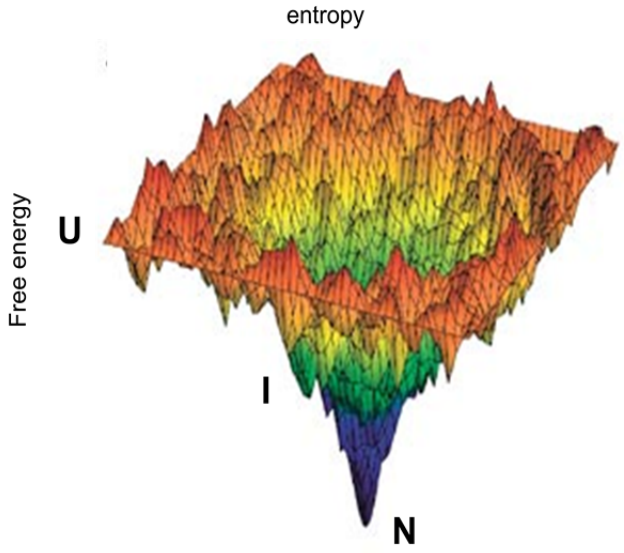


**Figure 1**
*The concept of the folding funnel*. Proteins can explore, in the balance of entropy and enthalpy, the broad accessible space in their unfolded state (U). Folding intermediates (I) are characterized by local minima and the folded native state (N) by a global minimum.
Adopted and modified from (Chaplin, 2006).

During folding, the loss of entropy is compensated by a gain in free energy due to non-covalent interactions and the folded state is usually only stabilized by an energy difference in the range of a few hydrogen bonds (Pace, 1990). Native proteins are characterized by a defined secondary, tertiary and quaternary structure. The secondary structure elements, e.g. α-helices and β-strands, are characterized by defined hydrogen bonds of the amide and carbonyl atoms of the protein backbone. The tertiary structure is defined by the three-

dimensional orientation of secondary structure elements within a polypeptide chain and the quaternary structure is the three-dimensional orientation of more than one polypeptide chain towards each other in oligomeric proteins. The main driving forces protein folding and association are hydrophobic contacts between amino acid side chains and additional non-covalent contacts such as hydrogen bonds or salt bridge formations (Dill, 1990). Proteins fold, in the simplest case, in a two-state reaction to their native state. Nevertheless, folding pathways are often characterized by intermediates which are often transient (Yon, 2001; Ptitsyn et al., 1995; Ptitsyn, 1995). These intermediates represent local minima on the folding landscape of the funnel and can be either on- or off-pathway to the native state and are characterized by a substantial fraction of native-like secondary structure content.

Proteins can be further modified after their synthesis. The most common modifications are glycosylations in the endoplasmic reticulum (ER) and the Golgi apparatus and disulphide bridge formation between two cysteine residues in the more oxidizing environment of the ER (Helenius and Aebi, 2004; Sevier and Kaiser, 2002; Feige and Hendershot, 2011). Additionally, phosphorylation, N-nitrosylation and further covalent side chain modifications are found which have a regulatory effect on protein functions (Olsen et al., 2006; Mannick and Schonhoff, 2002). Proteins can not only fold to their native state but they also form biological inactive and potential harmful side products such as aggregates and fibrils. A generalized folding pathway of a disulphide bridged protein is shown in Figure 2.

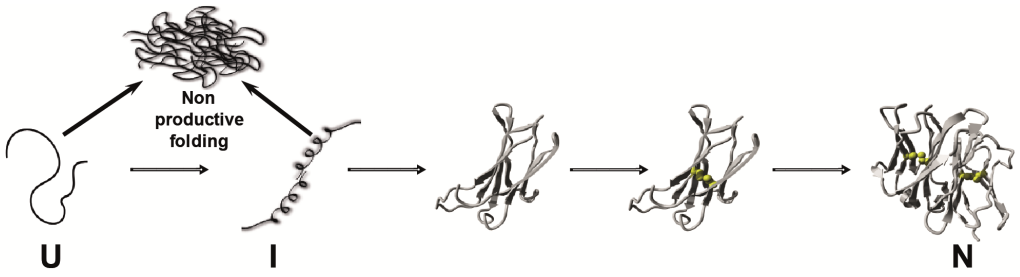


**Figure 2**
*Schematic representation of a protein folding pathway*. The unfolded state (U) folds *via* an intermediate (I) to the native state (N) including potential formation of non-productive folding side products. On the way to the native state a disulphide bridge (shown in yellow) and a dimer are formed.

## 4.2 Protein folding in the endoplasmic reticulum

The endoplasmic reticulum (ER) of eukaryotes is a unique environment for protein folding. Around one third of all newly synthesized proteins of a cell is imported into the ER (Chen et

al., 2005) and has to fold before traversing further the secretory pathway. The ER is the place for oxidative folding in the cell as a more oxidizing environment than in the cytosol is provided by a redox system consisting of the small peptidic molecules GSH and GSSG. The presence of this system allows the formation of covalent intra- or intermolecular disulphide bridges between cysteine residues. Disulphide bridges are commonly found in secreted proteins as they stabilize their folded state once they are formed by restricting the conformational space available (entropic effect) and an enthalpic component due to a restricted solvent accessible space in the unfolded state (Feige M.J. and Buchner J., 2010). Additionally, they represent an ideal tool for covalent linkage of sequence elements which may be located far away in the amino acid sequence of a protein. Glycosylation of proteins at asparagine residues of the sequence N-X-T/S, X not being proline,is also commonly found in the ER leading to a further increase in the stability and allowing the exploration of a new chemical space for the interaction and assembly of proteins *via* their covalently attached sugar residues (Helenius and Aebi, 2004). Protein folding in the ER has to be carefully monitored as un- or misfolded proteins secreted out of the cell through the secretory pathway may have harmful effects on the organism as manifested in severe diseases as for example amyloid formation in the case of an excess in antibody secretion (Buxbaum and Gallo, 1999). Therefore, a network of chaperones and further factors exists in the ER fulfilling the demanding task of ER quality control (Gregersen and Bross, 2010; Hebert and Molinari, 2007; Braakman and Bulleid, 2010).

## 4.3 Molecular chaperones

Although proteins can fold autonomously in isolation, protein folding in a crowded environment as a cell is more complex. All synthesized proteins have to fold under similar conditions concerning pH, buffer/salt concentration and temperature. Additionally, a cell is a highly crowded environment with protein concentrations in the range of 300 mg/ml and above (Ellis, 2001). The formation of aggregates and other non-productive folding products is a second order reaction thus facilitated at high protein concentration. Therefore, a cell is a very challenging place for proteins to fold. Hence, the class of molecular chaperones, i.e. folding helpers, assists proteins in cells to obtain and maintain their folded state (Walter and Buchner, 2002; Richter et al., 2010; Bukau et al., 2006). Additionally, they are also involved in the protein homeostasis due to their interplay with the protein degradation machinery of the cell (Goeckeler and Brodsky, 2010). Molecular chaperones are ubiquitous and conserved (Karlin and Brocchieri, 1998). Many of them were first discovered in the response

of cells to thermal stress and therefore named heat shock proteins (Hsps). Although many members are up-regulated upon different stresses such as temperature, ethanol, oxidizing agents and accumulation of unfolded proteins, many are constitutively expressed (Richter et al., 2010). Molecular chaperones are categorized due to their molecular weight (Figure 3).

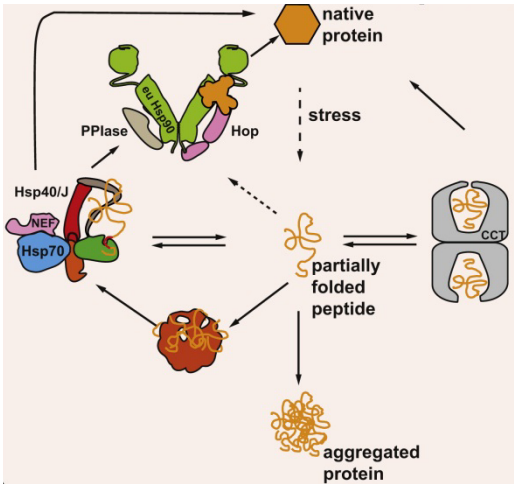


**Figure 3**
*The cytosolic chaperone network of higher eukaryotes*. The chaperone system consists of small Hsps (sHsps) shown in red, the Hsp70 system and its co-chaperones (shown in blue), a member of the Hsp60 family CCT (gray) and the Hsp90 system and its co-factors (green). The interconnection of the system in folding proteins to their native state is shown by arrows. Adopted from (Richter et al., 2010).

The class of small heat shock proteins (sHsp) is the only non-ATP dependent one. They form large oligomeric structures which bind to unfolded substrates (Haslbeck et al., 2005). Refolding to the native state can be achieved by the family of Hsp70 chaperones. Hsp70s interact with unfolded or partially folded intermediates and transfers its substrates to the Hsp90 system or releases them to fold (for details see section 4.4). Both, the Hsp70 and Hsp90 system depend on the hydrolysis of ATP and are supplemented by a variety of co-chaperones which can harbor additional functions such as regulation of their ATPase activity, PPIase (peptidyl-prolyl isomerization) or oxidoreductase activity (Wandinger et al., 2008). In contrast to Hsp70s, Hsp90s bind to later folding intermediates or highly unstable proteins (Richter and Buchner, 2006; Wegele et al., 2004). The Hsp60/CCT system is not only binding to unfolded proteins but additionally provides a cavity formed by two ring-like structures which allows encapsulated proteins to fold in a physiochemical environment different from the cytosol (Horwich and Fenton, 2009). Although different in their mode of action, chaperones are found in a cell organized in a dynamic network with substrates being transferred from one member to the other (Young et al., 2004).

## 4.4 The Hsp70 chaperone system and the ER-resident Hsp70 BiP

The Hsp70 network is found in the cytosol but also in mitochondria and the endoplasmic reticulum of cells. Hsp70s are highly conserved in sequence and their mode of action, but differences in their client specificity and their involvement in cellular processes exist (Gragerov and Gottesman, 1994; Hageman et al., 2011; Daugaard et al., 2007). The cytosolic members show broad substrate specificity and interact with early folding intermediates after their synthesis and often handover substrates to the Hsp90 system for further stabilization and folding. In organelles, however, the picture is different as substrates are imported as unfolded polypeptide chains. The Hsp70 of mitochondria, mtHsp70, is an essential factor for the import as its ATP-hydrolysis constitutes the motor for protein import. The mechanism is not clearly understood yet and both a ratching and pulling mechanism are discussed (Goloubinoff and De los, 2007).

The only member of the Hsp70 family in the ER is the heavy chain binding protein (BiP) (Munro and Pelham, 1986; Karlin and Brocchieri, 1998). It is essential, as deletion is lethal (Normington et al., 1989; Rose and Fink, 1987) and participates in important folding and quality control mechanisms of the ER (for details see 4.5). In general, Hsp70s consist of an N-terminal nucleotide binding domain (NBD) and a C-terminal substrate binding domain (SBD). The SBD can be further sub-divided into a β-sheet sandwich consisting of eight strands harboring a cleft for substrate binding and a regulatory α-helical lid consisting of five helices (A-E) (Bukau et al., 2006; Zhu et al., 1996). The domain movements in Hsp70s are coupled to the hydrolysis of ATP in the NBD although a detailed understanding is missing so far. NMR and spFRET experiments of *E. coli* DnaK and mtHsp70 have shown that binding of ATP leads to a compaction of the NBD/SBD and the hydrolysis to ADP results in looser domain contact (Woo et al., 2009; Bertelsen et al., 2009; Mapa et al., 2010). A hydrophobic linker between the NBD and SBD plays an important role in transferring the information of the bound nucleotide to the SBD (Swain et al., 2007; Vogel et al., 2006). The domain organization of Hsp70s is depicted in Figure 4.

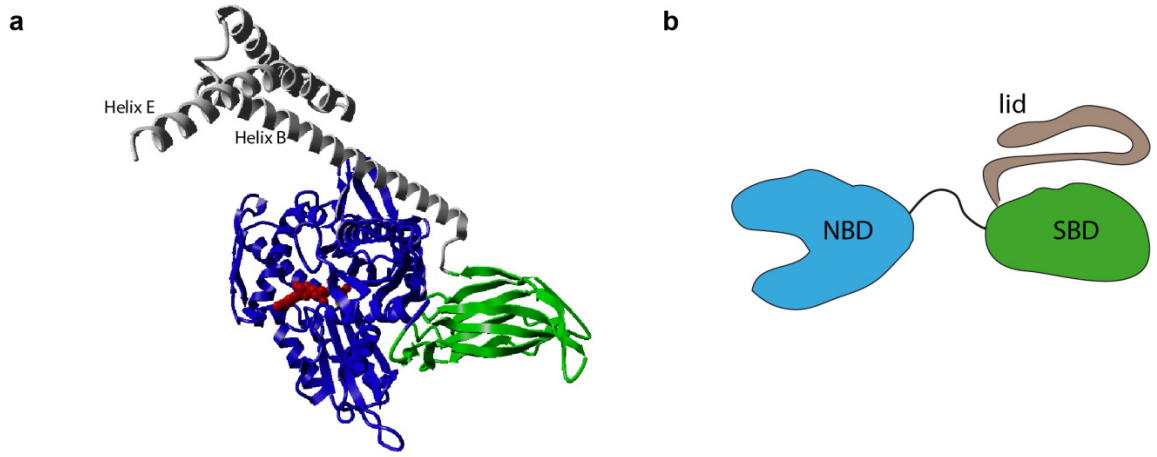


**Figure 4**
*The domain organization of Hsp70*. Hsp70s consist of an N-terminal nucleotide binding domain (blue; nucleotide in red) and a C-terminal substrate binding domain which can be sub-divided into a β-sandwich domain (green) with a cleft for substrate binding and an α-helical domain, the so-called lid (gray). The NBD is connected to the SBD via a hydrophobic linker which transfers the information of the bound nucleotide in the NBD to the SBD and is important for the domain movements in the chaperone cycle of Hsp70s. The domains are depicted (a) on the crystal structure of the Hsp70 homologue Sse1 (PDB code 3d2f) and (b) in a schematic drawing. Figure adopted and modified from (Marcinowski et al., 2011).

Hsp70s bind to substrates in a nucleotide-dependent manner. The ATP-bound state shows low substrate affinity whereas the hydrolysis to ADP results in stable and high affinity substrate complexes (Swain et al., 2007; Vogel et al., 2006). The role of the C-terminal lid is not completely understood yet and differences between Hsp70s seem to exit (Mapa et al., 2010; Gragerov and Gottesman, 1994). While the lid is required for efficient Hsp70-dependent pre-protein translocation into mitochondria and is a critical factor for cell growth if deleted in Kar2p (Tokunaga et al., 1998), the yeast orthologue of BiP, the deletion in *E.coli* DnaK leads to minor effects, although substrate binding kinetics are affected (Buczynski et al., 2001). Additionally, the lid is assigned a regulatory function for ATP binding and the release of substrates (Slepenkov et al., 2003) and for the interdomain communication in *E. coli* DnaK (Moro et al., 2004). The complete chaperone cycle of Hsp70s is regulated by co-chaperones which do not only control the hydrolysis of ATP and the exchange of ADP against ATP but some also deliver substrates.

## 4.5 The functions of BiP in the endoplasmic reticulum

BiP is a major integrator of several important functions of the ER. In general, proteins have to be transported co-translationally into the ER and have to fold and assemble (van and Braakman, 2005; Zimmermann et al., 2011). Additionally, the secretion of non-correctly

folded or assembled proteins has to be avoided due to their potential harmful effects on the complete organism (Hebert and Molinari, 2007).

As the ER is the compartment specialized in extracellular protein production, proteostasis has to be carefully monitored. Therefore, the ER has evolved several quality control as well as degradation mechanisms with BiP playing a central role in all of them (see Figure 5).

BiP is part of the ER-import pore, the SEC translocon, and gates co-translational import of proteins into the ER (Brodsky et al., 1995). BiP is sealing the import pore and interacts directly with the nascent polypeptide chain (Alder et al., 2005). The J-domain containing transmembrane protein ERdJ1 is part of the SEC translocon (for details see section 4.7) and acts as a regulatory element. While its lumenal J-domain is associated with BiP, the cytosolic domain binds to the ribosome allowing translation and guarantees binding of BiP to the nascent chain (Vembar et al., 2010). After initial binding of substrates to BiP during translation and import, most proteins fold autonomously or with the help of other ER chaperones after dissociation from BiP. However, rebinding of unfolded proteins occurs frequently also in the lumen of the ER, a process assisted by the soluble J-domain protein ERdJ3 (Shen and Hendershot, 2005; Shen et al., 2002). Additionally, stable complexes with substrates incapable to fold autonomously are observed (Vanhove et al., 2001; Nawa et al., 2007) as in the case of the heavy chain (HC) of antibodies (see section 4.9 and 4.10). Hence, BiP is an important quality check point for proteins in the ER due to stable binding of unfolded substrates. This leads to the retention of these substrates in the ER as they are hindered to follow up the secretory pathway through the Golgi due to the interaction of BiP with the KDEL receptor (Munro and Pelham, 1987).

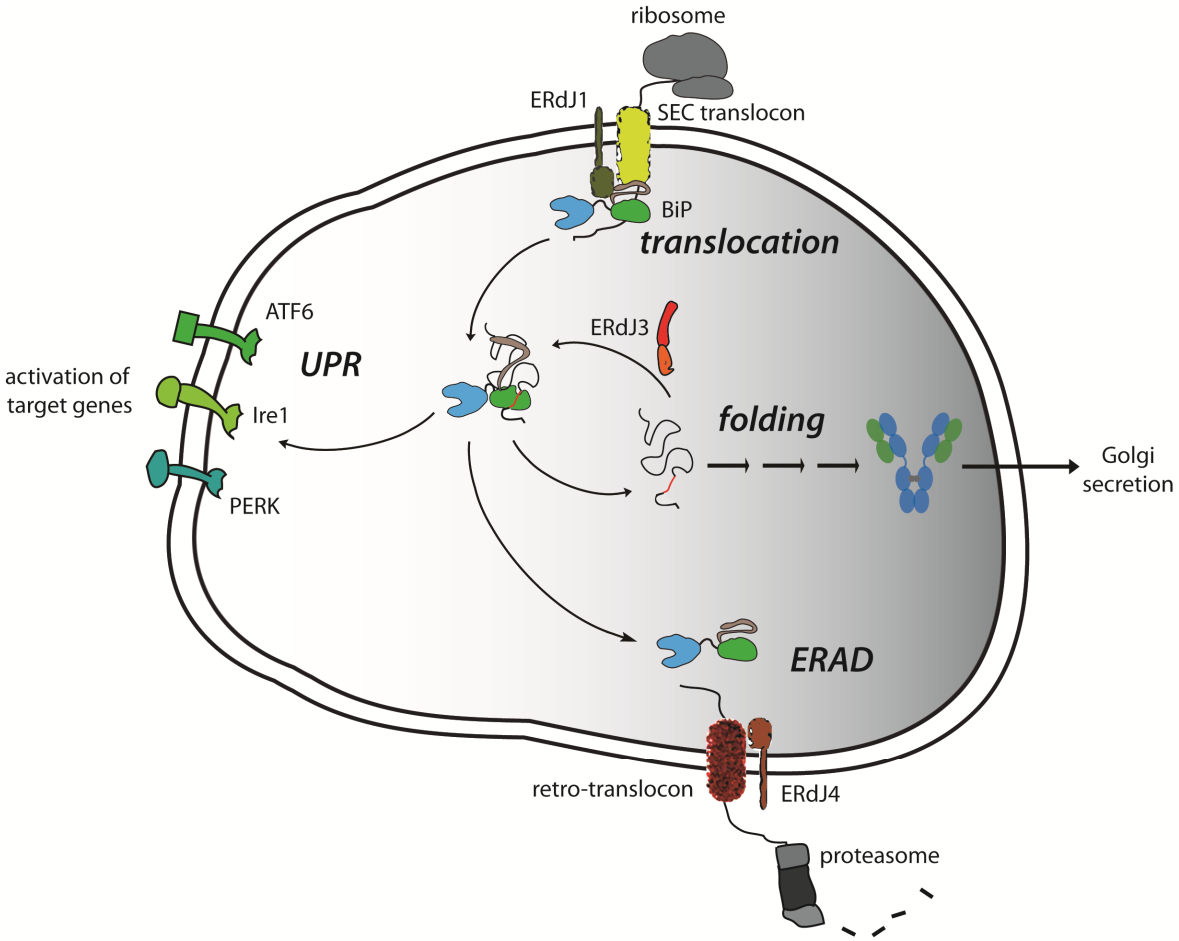


**Figure 5**
*BiP functions in the ER*. BiP is involved in the co-translational translocation of proteins into the ER as it seals the SEC translocon on its lumenal side. BiP is actively recruited to the SEC complex via the J-domain of ERdJ1. BiP binds and releases unfolded proteins in the lumen and ERdJ3 is the major co-chaperone for the folding and assembly of substrates for BiP. Upon an increase of unfolded proteins in the ER, the unfolded protein response (UPR) is activated due to lacking interaction of BiP with the transmembrane proteins ATF6, Ire1 and PERK leading to the activation of target genes (e.g. ER chaperones and factors involved in membrane biosynthesis) or a pro-apoptotic pathway. If non-glycosylated proteins fail to fold in the ER probably a switch from ERdJ-3 to ERdJ4/5 leads to retro-translocation and proteasomal degradation in the cytosol via the ER associated degradation pathway (ERAD).

BiP is involved in further quality control steps of the ER. As a part of the unfolded protein response (UPR) pathway it acts as a sensor for the load of unfolded and misfolded proteins in the ER (Ron and Walter, 2007). Upon exceeding a certain level of unfolded proteins, UPR signaling leads to the activation of transcription factors which up-regulate ER chaperones reducing the load in the ER (Otero et al., 2010; Travers et al., 2001). Three transmembrane factors build up the UPR in higher eukaryotes: ATF6, Ire1 and PERK (Yoshida et al., 1998; Tirasophon et al., 1998; Harding et al., 1999). The lumenal domains of all three proteins interact with BiP and serve as sensor domains. If the load of unfolded proteins is normal, BiP can interact with these domains, while the dissociation of BiP due to an increased

amount of unfolded proteins initiates the signaling cascade (Okamura et al., 2000). ATF6 contains a cytosolic transcription domain which is cleaved from the membrane and up-regulates ER chaperone genes and *Xbp1* transcription (Haze et al., 1999). The C-terminal part of Ire1 comprises an endoribonuclease activity which allows excision of 26 bases from the *XBP-1* mRNA transcript allowing its translation after religation. Xbp1 is a potent transcription factor for the up-regulation of ER chaperones (Calfon et al., 2002). Activated Ire1 can additionally influence the Jun kinase pathway which regulates apoptosis. PERK is an eIF-2α kinase and is involved in the regulation of apoptosis and the cell cycle via the TRAF2 pathway (Brewer and Hendershot, 2005). Hence, the UPR consists of an anti- and pro-apoptotic branch which have to be tightly regulated and in both cases, BiP release is a major lumenal signal for their activation.

The ER does not has an own protein degradation machinery and unfolded proteins have to be retro-translocated to the cytosol for proteasomal degradation, a pathway known as ER-associated degradation (ERAD) (Meusser et al., 2005). For glycosylated proteins the substrates are transferred from the Calnexin/Calreticulin system to EDEM, a trans-membrane lectin (Kanehara et al., 2007). For non-glycosylated proteins, BiP is the major sensor. The exact mechanism is still unclear but a change in the associated J-protein containing co-factors from ERdJ3 to ERdJ4/5 seems to play an important role (Dong et al., 2008). The components of the retro-translocon are still not all known, but Derlin 1-3 make up the transmembrane part and the cytosolic AAA ATPase p97 serves as a motor for the translocation. Additional components such as the J-domain containing transmembrane protein ERdJ4, the E3 ligase Hrd1 and the ubiquitin-like domain containing factor Herp are associated with the pore (Brewer and Hendershot, 2005).

The central function of BiP to fulfill all these different tasks is the binding and subsequent release of substrates in its chaperone cycle.

## 4.6 The BiP/Hsp70 chaperone cycle and its regulation

The chaperone cycle of BiP and other Hsp70 chaperones is depicted in Figure 6. The class of J-domain containing co-chaperones can bind to the interface of the NBD/SBD of Hsp70s and accelerate the hydrolysis rate of ATP to ADP (Qiu et al., 2006; Kelley, 1998; Kelley, 1999).

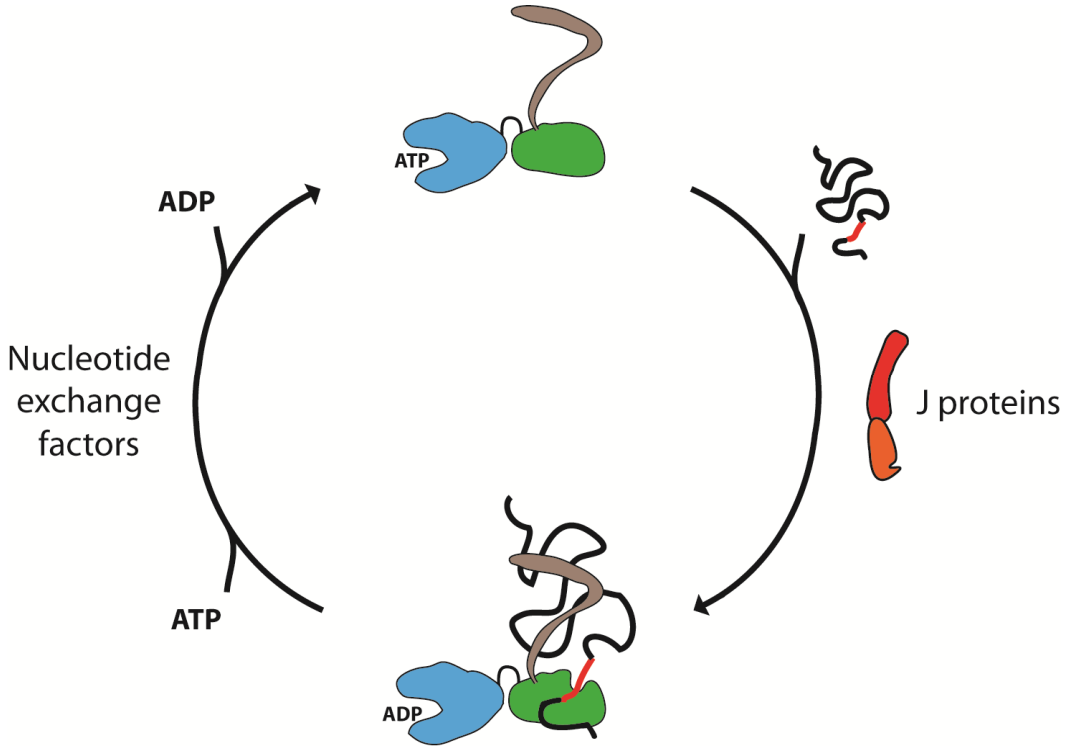


**Figure 6**
*The chaperone cycle of Hsp70*. In the ATP-bound state, Hsp70s show only low substrate affinity. J-domain containing proteins accelerate the hydrolysis of ATP and some have the additional ability to transfer bound substrates to Hsp70. The hydrolysis of ATP results in the high affinity state of Hsp70 for substrates and they are bound in a cleft in the SBD. The exchange of ADP against ATP leads to the dissociation of the substrate complex. This step is catalyzed by nucleotide exchange factors.

The J-domain comprises a highly conserved His-Pro-Asp sequence motif which is essential for binding (Tsai and Douglas, 1996). Besides the conserved J-domain, most J-proteins have additional domains comprising additional functions. Some of them carry a substrate binding domain which binds to unfolded proteins and allows the transfer of their substrates to Hsp70s. After hydrolysis of ATP and the population of the high affinity substrate complex, the bound substrate is released upon the exchange of ADP against ATP. This second important step in the chaperone cycle of Hsp70s is catalyzed by the second group of co-chaperones, the nucleotide exchange factors (NEFs) (Bukau et al., 2006).

## 4.7 BiP co-chaperones

J-domain containing co-chaperones (also named Hsp40s) interact with Hsp70s (see section 4.6). Besides accelerating the ATPase activity of their partner Hsp70, most of them fulfill additional tasks in fine-tuning the function of the Hsp70. In the ER, seven J-domain containing co-chaperones for BiP were identified so far. They are named ERdJ1-7 and can

be grouped into membrane-bound ones (ERdJ1/2/4/7) and lumenal ones (ERdJ3/5/6) (reviewed in Otero et al. (Otero et al., 2010)). Additionally, they show a high variety of additional elements like substrate binding or thioredoxin domains. While little is known about the function of ERdJ2, ERdJ6 and ERdJ7, specifically ERdJ1 was shown to be important for co-translational secretion and retro-translocation of proteins (Dudek et al., 2005) while ERdJ4 and ERdJ5 were reported to be major elements in the ERAD pathway as they are important for priming substrates for degradation (Dong et al., 2008).

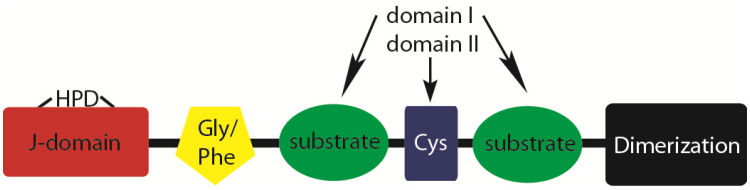


**Figure 7**
*Domain organization of ERdJ3*. The N-terminal J-domain with the conserved HPD motif (Tsai and Douglas, 1996) (red) is followed by a Gly/Phe-rich domain (yellow) and a substrate binding domain I (green), divided by a Cys-rich domain II (blue). The C-terminus is formed by the dimerization domain (black). Adopted from (Marcinowski et al., 2011).

In contrast, the soluble ERdJ3 plays an important role in the folding branch of the ER as it directly interacts with substrates and transfers them to BiP. It was first discovered in the BiP-mediated folding of antibodies and is the major co-chaperone of BiP in the maturation of these important substrates (Shen and Hendershot, 2005). Derived from sequence alignments, ERdJ3 was identified as a type I J-protein as it possesses a J-domain, a glycine/phenylalanine-rich domain, a cysteine-rich domain and a substrate binding domain (Jin et al., 2009). Additionally, ERdJ3 is up-regulated upon ER stress (Shen and Hendershot, 2005). Its domain organization is shown in Figure 7. It dimerizes via its C-terminal domain and hydrophobic residues in its substrate binding domain are important for the interaction with unfolded substrates (Jin et al., 2009; Shen and Hendershot, 2005). Unlike cytosolic type I J-domain proteins, the Cys-rich domain is not stabilized by a bound $Zn^{2+}$ ion but by two disulphide bridges.

The second class of co-chaperones in the ER, the NEFs, can be divided into two classes. The family of Hsp110 proteins shares a similar topology with Hsp70s but carry a large insertion in the β-sandwich of the SBD. Hsp110s have to bind ATP in their NBD to form hetero-dimers with Hsp70s and catalyze the release of ADP from Hsp70 (Dragovic et al., 2006; Polier et al., 2008; Weitzmann et al., 2006; Andreasson et al., 2008). Additionally, a substrate handover of Hsp70 to Hsp110 during or after the release of ADP is discussed

(Easton et al., 2000). The NBD of the ER Hsp110 Grp170 forms a face-to-face complex with the NBD of BiP and the C-terminal lid of Grp170 also interacts with the NBD of BiP (Andreasson et al., 2008). This leads to a highly similar mechanism of nucleotide exchange in BiP as for cytosolic Hsp70s (Andreasson et al., 2010). The structure of the cytosolic Hsp110 and Hsc70 is shown in Figure 8.

The second class is structurally distinct from Hsp70s although they also interact with the NBD of Hsp70s and the ER member is the BiP interacting protein BAP/SIL1 (Chung et al., 2002). It shows a different mode of action as Grp170 by destabilizing or eventually even unfolding the NBD of Hsp70s to allow ADP release. In the ER, BAP/Sil1 has a pivotal role as its deletion leads to the rare Marinesco-Sjögren syndrome resulting in ataxia, juvenile cataracts, generally some degree of cognitive delay, and very small stature (Anttonen et al., 2005; Senderek et al., 2005). This indicates that the NEFs in the ER can only partially complement their function although they catalyze the identical reaction.

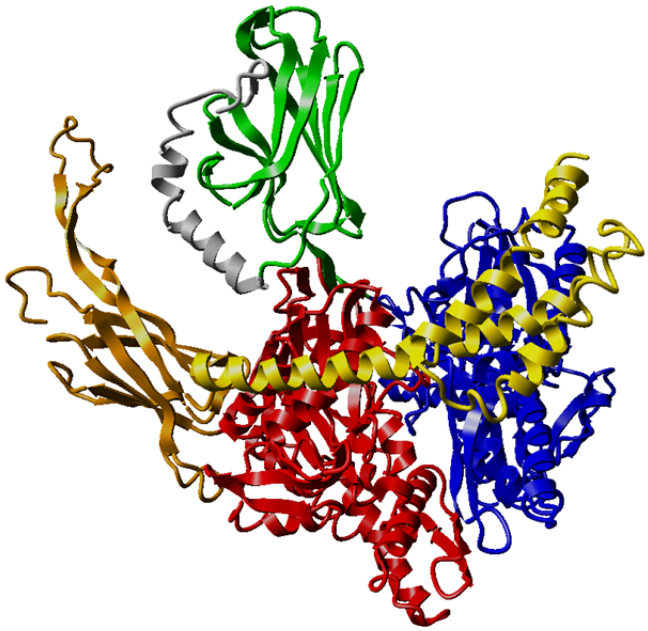

**Figure 8**
*Structure of the complex of cytosolic Hsp110/Hsc70*. Domains of Hsc 70 are colored as NBD (blue), SBD (green) and lid (gray). For Hsp110 the NBD is shown in red, the SBD as orange and the lid as yellow. Figure drawn from PDB: 3C7N.

## 4.8 Substrate recognition by BiP/Hsp70

Hsp70s recognize solvent-exposed, linear stretches of seven amino acids in peptides and unfolded proteins (Rudiger et al., 1997; Gething et al., 1995; Knarr et al., 1995; Knarr et al., 1999; Pandya et al., 2009). Previous studies on the specificity revealed alternating hydrophobic residues in binding sequences as an important feature and charged residues reduce the affinity drastically. Based on screening peptide-libraries, phage display or

determining the effect of individual peptides on BiP ATPase stimulation, an algorithm to predict binding sequences was developed (Gething et al., 1995; Knarr et al., 1995; Knarr et al., 1999; Blond-Elguindi et al., 1993). The peptidic substrate is bound in a cleft of the β-sandwich and the lid is closing tightly on top of the domain and the substrate. Besides hydrophobic interactions, hydrogen bonding of residues in the SBD of Hsp70 and the substrate peptide backbone is important (Swain et al., 2006). The X-ray structure of the SBD of the bacterial DnaK with a bound peptide substrate is shown in Figure 9.

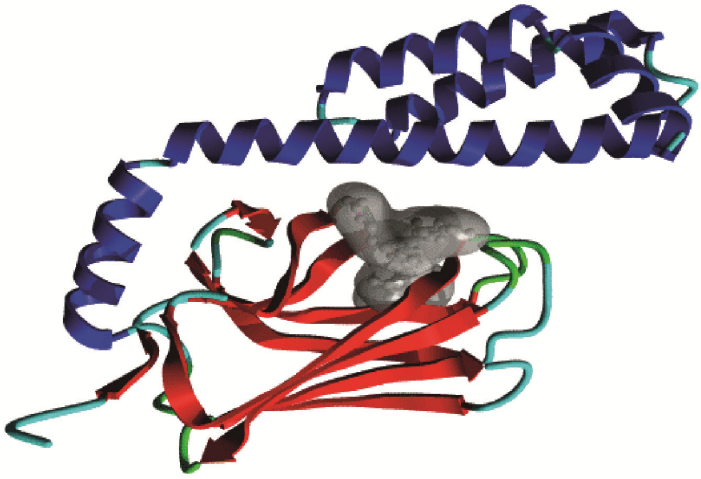

**Figure 9**
*Structure of the peptide bound SBD of DnaK*. The peptide (gray) is bound in a cleft of the β-sandwich domain (red) and the lid (blue) closes tightly over the bound peptide and the SBD. (PDB code: 1DKX).

In contrast to peptidic substrates, nothing is known about the domain movements and orientations of BiP upon binding of a protein. Peptides were taken so far as surrogates for protein substrates as similar $K_d$ values were observed for both classes of substrates.

Interaction studies of Hsp70s with endogenous protein substrates are rare. They revealed differences in the recognition of binding sites in peptides and in the context of a protein. Peptide filter assays predicted multiple binding sequences for DnaK in one of its endogenous substrates, the $\sigma^{32}$ transcription factor, but only one of them was recognized in the context of the whole protein (Rodriguez et al., 2008; McCarty et al., 1996). Therefore, an improved prediction method besides the scoring algorithm and peptide assays is needed. The hydrophobicity of the peptide seems not to be the exclusive determinant for Hsp70 binding and further information such as the conformation of the peptide may play a role and should increase the accuracy of high affinity binding site predictions.

For BiP, two studies were performed to determine binding sites in endogenous substrates. Peptides derived from the HIV-envelope protein gp160 and from antibodies predicted to bind BiP were tested for binding using the stimulation of BiP ATPase activity (Knarr et al., 1995; Knarr et al., 1999). For both substrates, a set of binding sites was determined on the peptide level. The analysis on the specificity revealed a pattern of hydrophobic residues as for other Hsp70s, with Phe or Tyr accumulating in the central position. However, an analysis on the protein level, as for $\sigma^{32}$ transcription factor, is missing. Furthermore, multiple sites in all antibody domains were predicted, although most of them only interact transiently with BiP *in vivo* and, on a domain level, only 1:1 stochiometric complexes are observed (Feige et al., 2009).

The substrate specificity of Hsp70s from different organisms and compartments varies as shown by differences in the ability of human cytosolic Hsc70, bacterial DnaK and BiP to form complexes with the high affinity binding site of the $\sigma^{32}$ transcription factor (Gragerov and Gottesman, 1994). This point is of special interest, as the sequence identity especially of the β-sandwich of the SBD, is very high. Therefore, either a regulatory element in another domain, as for example the lid, or single changes in amino acids must contribute to this finding.

## 4.9 Antibodies

Antibodies are part of the adaptive immune system and represent a highly adaptable and potent defence line against pathogens. Additionally, antibodies are recently used as therapeutics due to their high target selectivity. Antibodies are produced at very high copy numbers by secretory B-cells (1000s per second) (Sitia and Braakman, 2003). They are co-translationally imported in the ER where they fold, assemble and are covalently modified prior to their secretion via the secretory pathway (Feige et al., 2010).

The most common antibodies, immunoglobulin G (IgG), are comprised of two light chains (LCs, consisting of the $V_L$ and $C_L$ domains) and two heavy chains (HCs, with the $V_H$ and $C_H1$-3 domains). The complete IgG can be subdivided in an Fc fragment composed of the homodimer of the $C_H2$ and $C_H3$ domains and two Fab fragments composed of the heterodimer of the LC and the $V_H$ and $C_H1$ domain of the HC (Figure 10) (Huber et al., 1976).

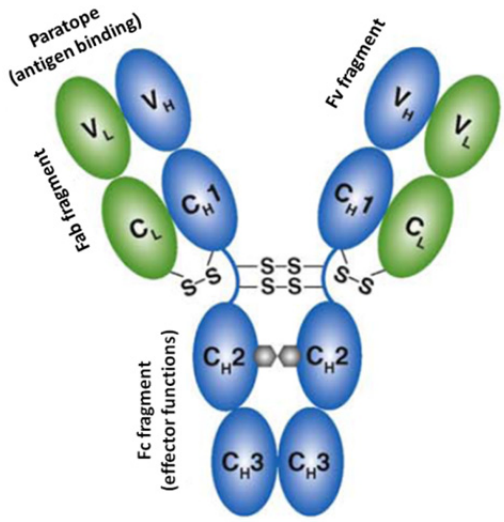


**Figure 10**
*Domain arrangement of an IgG1 antibody.* Light chains are shown in green, heavy chains in blue. S-S indicates a disulfide bridge and grey hexagons represent oligosaccharides. Functional elements of the antibody are indicated.

The variable domains, $V_H$ and $V_L$, together constitute the antigen binding site which is crucial for antibody specificity. Within each variable domain, three hypervariable regions (complementarity determining regions or CDRs) constitute the residues interacting with antigens. The constant domains form the framework of the antibody and are not subjected to variations upon clonal selection. Despite diverse amino acid sequences, the antibody domain structure is highly conserved. This so-called immunoglobulin (Ig) fold is a β-barrel structure of approximately 110 amino acids in which the two halves of the barrel are linked by a conserved disulphide bond (see Figure 11) (Huber et al., 1976). Dissecting antibodies into individual domains or fragments allowed the detection of differences in the folding of these structurally highly similar domains. The first isolated domains examined have been the $C_L$ and $C_H3$ domains. Their analysis revealed that the domains can fold autonomously and that prolyl-peptide bond cis/trans isomerization plays an important, rate-determining role (Feige et al., 2010). In the folding pathway of the $C_L$ domain, a small helix connecting two strands is the first element that adopts its native structure upon refolding and seems to guide the orientation of the rest of the protein (Feige et al., 2008). Despite their structural similarity, recent results showed that the folding pathways of the individual domains can be quite different, as the partner of $C_L$, the $C_H1$ domain cannot fold autonomously but only in the context of the $C_L$ domain (see 4.10) (Feige et al., 2010; Feige et al., 2009).

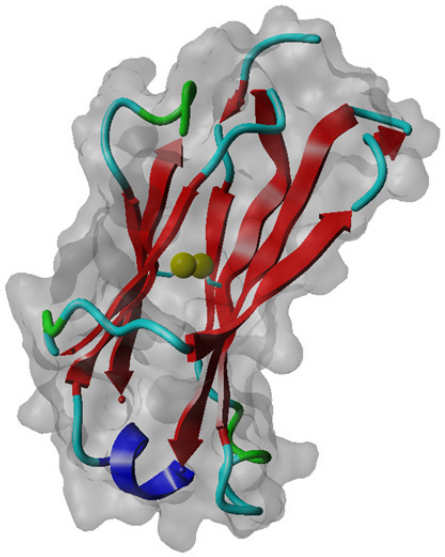

**Figure 11**
*Structure of the IgG1 $C_L$ domain.* The X-ray structure of the CL domain shows the typical features of the Ig fold. An internal disulphide bridge (shown in yellow) stabilizes a β-sandwich consisting of seven strands (red). Two helical strand-connecting elements stabilize the topology. Drawn from PDB code 1HZH**.**

## 4.10 The IgG $C_H1$ domain

The $C_H1$ domain of IgG has singular features compared to all other Ig domains. It is, in isolation, an unfolded protein but becomes structured upon association with its cognate partner, the $C_L$ domain (Feige et al., 2009; Lee et al., 1999). The final adopted structure is a typical Ig-fold with seven β-strands. The folding pathway of the $C_H1$ domain is characterized by the formation of an encounter complex with $C_L$ where certain residues in the interface are already found in a native-like environment (Feige et al., 2009). From the partially structured encounter complex, the $C_H1$ domain folds in a prolyl-isomerization controlled reaction to its native state. The second folding phase can be accelerated by peptidyl-prolyl-isomerases such as the ER-resident cyclophilin B (Feige et al., 2009). Murine IgG1 $C_H1$ possesses three *cis*-Pro bonds in its native structure but a mutational analysis showed that only isomerization of Pro 34 is crucial for folding *in vitro* and *in vivo* (Feige et al., 2009). Importantly, the internal disulphide bridge of $C_H1$ has to be formed to allow complex formation with $C_L$ and once $C_H1$ is folded, disulphide bridge formation between cysteines in the C-terminus of $C_H1$ and $C_L$ renders the reaction irreversible (Feige et al., 2009).

This association-dependent folding pathway has direct implications on the quality control and assembly of IgG. The molecular chaperone BiP was first identified in forming stable complexes with the HC of IgG in the ER preventing their secretion out of the ER in the absence of LCs (Haas and Wabl, 1983; Bole et al., 1986). In subsequent studies, the $C_H1$ domain was identified as the major interaction site as its deletion allowed the secretion of these $\Delta C_H1$-HCs and a domain swap with the LC $C_L$ domain led to the retention of these chimeric LCs in the ER (Lee et al., 1999). Hence, the $C_H1$ domain is necessary and sufficient

for the retention of unassembled heavy chains in the ER. The *in vivo* analysis of complex formation of BiP with the HC of IgG revealed that BiP does not cycle from the HC indicating the presence of very stable complexes (Vanhove et al., 2001). However, the $C_H1$ domain is not bound by BiP alone, but rather a multi-chaperone complex was found (Meunier et al., 2002). The complex is already pre-formed in the absence of the HC as substrate and assembles on the HC (Meunier et al., 2002). The predominant members in the complex, besides BiP, are ERdJ3, cyclophilin B, the Hsp90 family member Grp94, the NEF Grp170 and protein disulphide isomerase (PDI), all acting together in the folding of IgGs in the ER. The efficient retention of unpaired HCs is of special importance for the organism, as HCs carry, besides a $V_H$ domain capable of interacting with epitopes, also the complete effector domains of IgG, the Fc part. Hence, in contrast to unpaired LCs, the secretion of unpaired HCs could lead to unspecific binding of targets in the organism followed by an unwanted immune reaction mediated by the Fc part. Additionally, HCs are prone to the formation of fibrils and amyloids as the mutational loss of the $C_H1$ domain leads to the secretion of HCs in the rare HC disease resulting in toxic amyloid formation, especially in the kidney (Goossens et al., 1998).

Taken together, the $C_H1$ domain is an especially interesting substrate for studying its interaction with BiP and co-factors as it forms stable complexes *in vitro* and *in vivo* and its association and folding with the $C_L$ domain is as a major, BiP-mediated, quality control step in the maturation of antibodies.

# 5 Objective

The objective of the thesis is the analysis of the interaction of the molecular chaperone BiP with a natural client, the $C_H1$ domain of IgG *in vitro*, using recombinantly produced purified proteins. After reconstitution of complex formation, high affinity binding sites in $C_H1$, the conformational changes in BiP necessary to bind and release the substrate as well as its alteration by the co-chaperone ERdJ3 should be analyzed.

BiP was previously shown to bind to peptides derived from the $C_H1$ domain (Knarr et al., 1995). However, their recognition in the context of the complete $C_H1$ domain is not known. Studies on the bacterial DnaK substrate $\sigma^{32}$ have shown that only one out of several potential binding sites on the peptide level is recognized (Rodriguez et al., 2008; McCarty et al., 1996). As the $C_H1$ domain is the major binding site for BiP in the heavy chain of IgG (Lee et al., 1999; Feige et al., 2009), identification of the binding sites for BiP will be important for a better understanding of the assembly process of antibodies. A mutational approach for the predicted binding sites abolishing BiP binding to $C_H1$ should allow the dissection of these binding sites. So far, hydrophobic residues were identified as important elements for BiP binding but further sequential or structural features of the binding stretches necessary for stable complex formation with BiP are unknown. An approach using peptides containing non-proteinogenic amino acids substituents in a central position populating either kinked or extended forms should clarify the influence of the conformation of the substrate on BiP binding. Additionally, the plasticity of the binding groove of BiP should be targeted by amino acids with varying side chain lengths. These experiments could give rise to a better understanding of the substrate specificity of BiP and the long-term question why some substrates form stable complexes with BiP while most of them interact only transiently with BiP.

The conformational cycle of BiP and Hsp70s in general are not yet understood in detail. In this thesis, a FRET-based approach should be established to dissect these conformational changes upon nucleotide and protein or peptide substrate binding. To this end, cysteine residues should be introduced in the different domains of BiP and labeled with FRET pairs allowing the analysis by single pair FRET (spFRET) in collaboration with Prof. Don Lamb (Ludwig-Maximilians Universität, München). The experiments were aimed to answer the question of whether protein and peptide substrates are recognized differently by BiP and how the information of the bound nucleotide is transferred to the substrate binding domain and the lid.

BiP is part of a chaperone network in the endoplasmic reticulum and its function is regulated and fine-tuned by a set of co-chaperones. One of the most prominent members in IgG folding is the J-domain co-chaperone ERdJ3. Although it is known that ERdJ3 can bind and transfer substrates to BiP and stimulate its ATPase activity nothing is known about the underlying mechanism. To this end, a FRET assay to monitor substrate transfer as well as the spFRET assay to dissect conformational changes in BiP should be developed to gain insight into the function of ERdJ3.

# 6 Results

## 6.1 Protein purification

### 6.1.1 IgG domains

IgG domains were cloned and expressed as described in the material and methods section. For the IgG domains, purification protocols were established following the flow chart shown in Figure 12. Shortly, IgG domains were expressed as insoluble inclusion bodies and purified under denaturing conditions by ion exchange chromatography. To allow structure formation as well as the formation of the internal disulphide bridge of IgG domains, proteins were refolded in the presence of a redox system consisting of GSH/GSSG. The final purification step was a size exclusion chromatography (SEC) resulting in homogenous protein preparation.

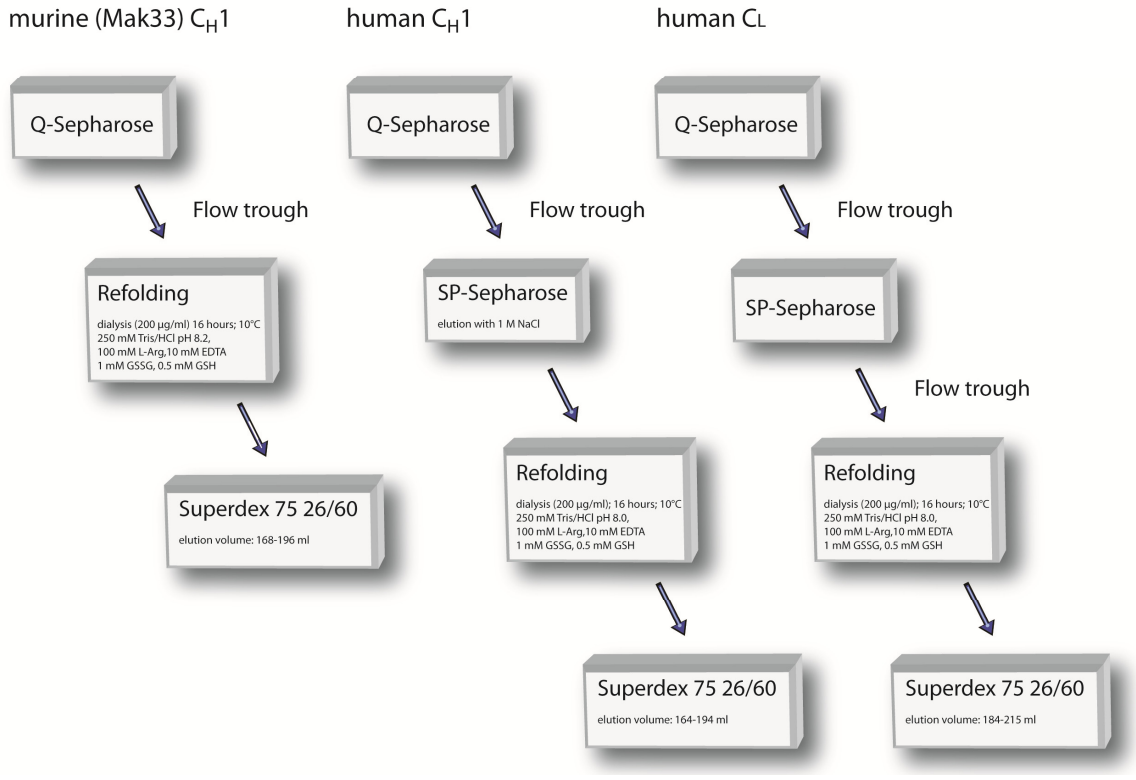


**Figure 12**
*Schematic purification protocol*. The murine $C_H1$ domain (Mak33), the human $C_H1$ and $C_L$ domain were purified by the given steps. All purifications were performed on an Äkta Prime or FPLC system.

All mutants were purified according to the flow scheme and the purity of all proteins was analyzed by SDS-PAGE and MALDI-TOF/TOF-MS to confirm homogeneity. Additionally, the correct oxidation of the internal disulphide bridge was confirmed by performing Ellman's assay (see material and methods).

### 6.1.2 BiP

The murine BiP was cloned and expressed as described in the material and methods section. The construct includes an N-terminal 6x His-tag followed by a TEV protease cleavage site. For BiP, the purification protocol was developed as depicted in Figure 13. All mutants generated in this thesis were purified identically and the purity was analyzed by SDS-PAGE and MALDI-TOF/TOF-MS to confirm homogeneity.

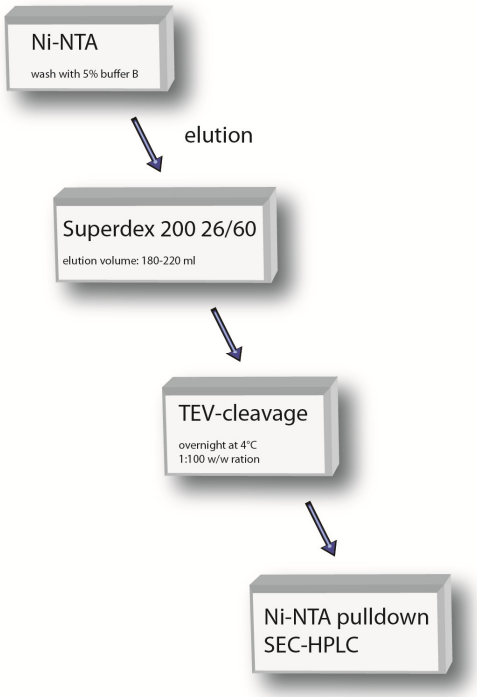


**Figure 13**
*Schematic purification protocol*. Murine BiP wild type and mutants were purified according to the given steps. All purifications were performed on an Äkta Prime or FPLC system and SEC-HPLC on a Shimadzu HPLC system with a Superdex 200 10/300 column.

### 6.1.3 ERdJ3

ERdJ3 is a glycosylated protein but recombinant production in *E. coli* only allows non-glycosylated protein expression. Hence, the protein used in this work is not glycosylated. As ERdJ3 possesses two internal disulphide bridges, it was expressed as inclusion bodies and refolded after purification. ERdJ3 was cloned with an N-terminal 6x His-tag and a TEV protease cleavage site (see material and methods). To determine optimal refolding

conditions, a screen using a genetic algorithm was performed in cooperation with Danae Baerend (TU München). The established purification protocol is shown in Figure 14 with a denaturating Ni-NTA followed by refolding and SEC. The oxidation of the internal disulphide bridges was analyzed by Ellman's assay and purity was confirmed by SDS-PAGE and MALDI-TOF/TOF-MS.

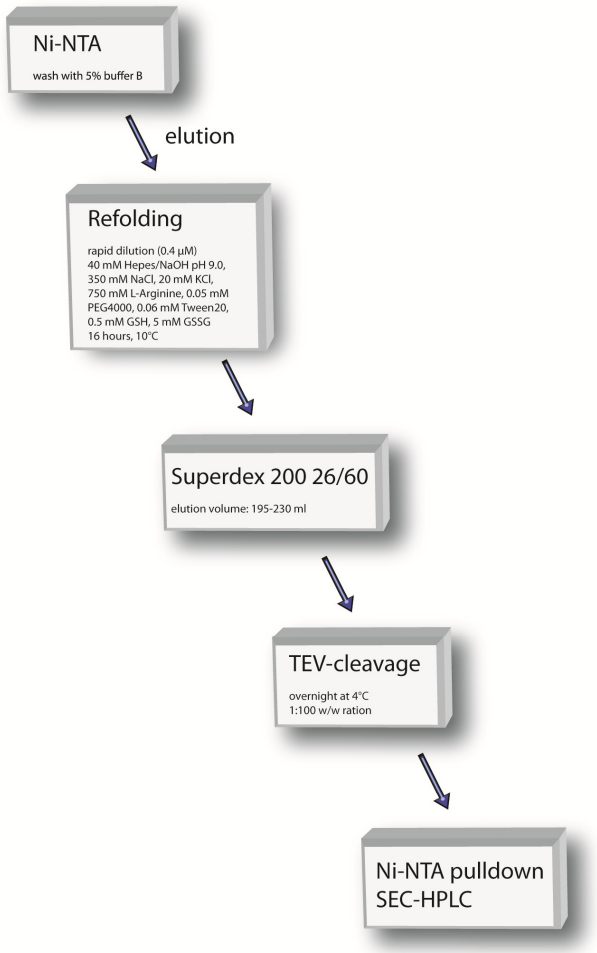


**Figure 14**
*Schematic purification protocol*. Murine ERdJ3 wildtype and mutants were purified according to the given steps. All purifications were performed on an Äkta Prime or FPLC system and SEC-HPLC on a Shimadzu HPLC system with a Superdex 200 10/300 column.

The isolated J-domain constructs of ERdJ3 were cloned as described in material and methods with an N-terminal 6x His-tag and a TEV protease cleavage site. As the isolated J-domain does not contain disulphide bridges, soluble expression in the cytosol was possible. The purification followed the protocol for BiP (see Figure 13).

## 6.2 Protein characterization

### 6.2.1 Characterization of the human IgG1 $C_H1$ domain

Proteins were characterized according to their secondary structure content by CD spectroscopy. The $C_H1$ domain of the murine IgG1 Mak33 antibody was previously shown to be unfolded in the absence of a $C_L$ domain (Feige et al., 2009). The human IgG1 $C_H1$ domain shares this feature as shown by the featureless FUV CD spectra depicted in Figure 15 and the association-coupled folding of $C_H1$ in the presence of the kappa LC $C_L$ domain.

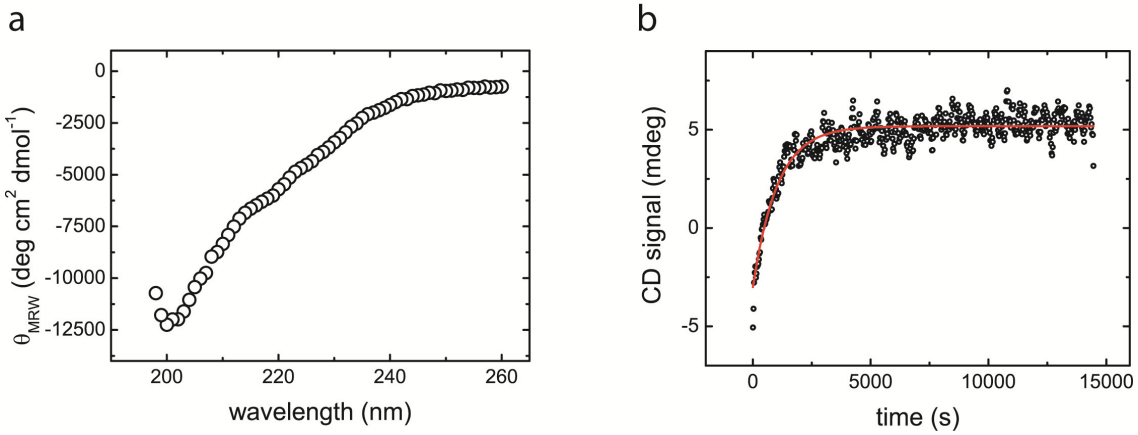


**Figure 15**
*FUV CD characterization of the human $C_H1$ domain*. (a) The human $C_H1$ domain shows a featureless FUV CD spectrum in the absence of a $C_L$ domain (protein concentration 10 µM; PBS; 25°C). (b) the addition of the folded $C_L$ domain results in an increase in secondary structure as observed at λ = 205 nm (10 µM $C_H1$; 10 µM $C_L$; PBS; 25°C).

The secondary structure formation in the association-coupled folding of the human $C_H1$ domain was determined as $k_{obs}$ = 0.058 ± 0.003 min $^{-1}$. This slow folding behavior is in good agreement with the murine $C_H1$ domain which shows a slow folding rate of $k_{obs}$ = 0.02 min$^{-1}$, as determined previously (Feige et al., 2010). Hence, the human $C_H1$ domain shares the same features as the murine $C_H1$ domain in being unstructured in isolation. In the presence of a $C_L$ domain, the human $C_H1$ folds to its native structure. The human $C_H1$ domain was used to determine the binding sequences for BiP, whereas the murine protein was used to establish BiP binding in general and for the intramolecular FRET assay to monitor BiP domain movements (see sections 6.9).

## 6.2.2 Characterization of BiP

BiP was purified in HKM buffer (50 mM Hepes/KOH pH 7.5; 150 mM KCl; 10 mM $MgCl_2$) as phosphate and Tris buffers are known to either interfere with BiP's ATPase activity or to destabilize the protein. Therefore, FUV spectra could only be measured at wavelengths above 210 nm. However, the spectrum suggests that BiP folds into its characteristic α-helix and β-sheet content according to the minimum around 220 nm as depicted in Figure 16a. An additional proof is the temperature transition of BiP showing a biphasic unfolding reaction with only the second transition being reversible (Figure 16b). The first transition shows a midpoint at T = 46°C and the second at T = 67°C.

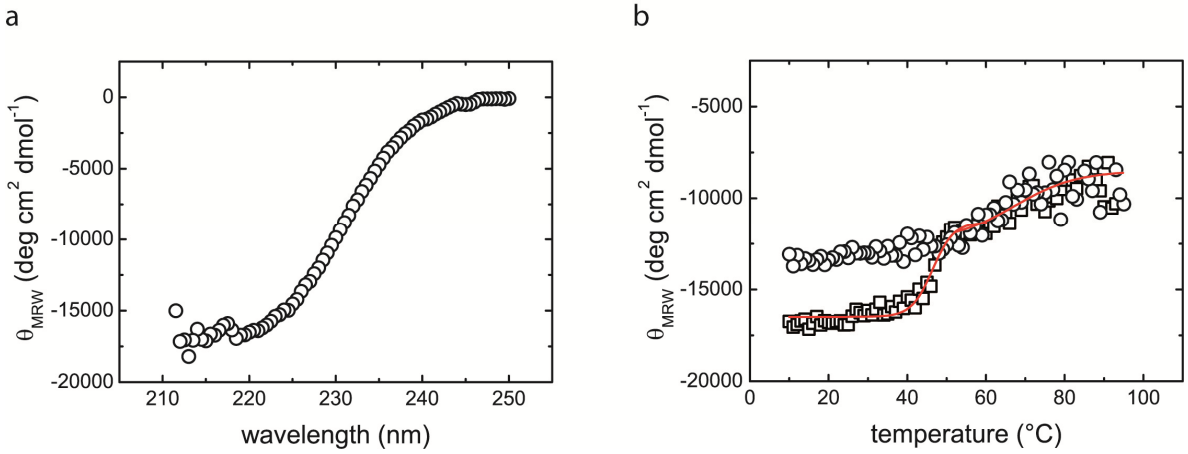


**Figure 16**
*CD characterization of BiP*. (a) CD spectrum of 5 µM BiP in HKM buffer at 25°C. (b) Temperature transition of 5 µM BiP in HKM buffer followed at the wavelength λ = 220 nm with a scanning rate of 0.2°/min. The forward transition is shown by open squares and the reverse transition by open circles. The forward transition was fit to a Bolzmann equation (red) to determine the transition midpoints.

Additionally, BiP's ATPase activity was measured in a regenerative ATPase assay and the $K_M$ could be determined as 5.1 ± 0.8 µM for low ATP concentration (see figure 17 inlay). However, BiP shows a second activity step above ~ 1 mM ATP, a feature also observed for other Hsp70s such as the cytosolic Ssa1 from *S. cerevisiae* (Dissertation Andreas Schmid, TU München). The origin of this second step is unresolved so far, but an influence of the nucleotide on the oligomerization state of BiP and therefore its activity seems most likely (Figure 17).

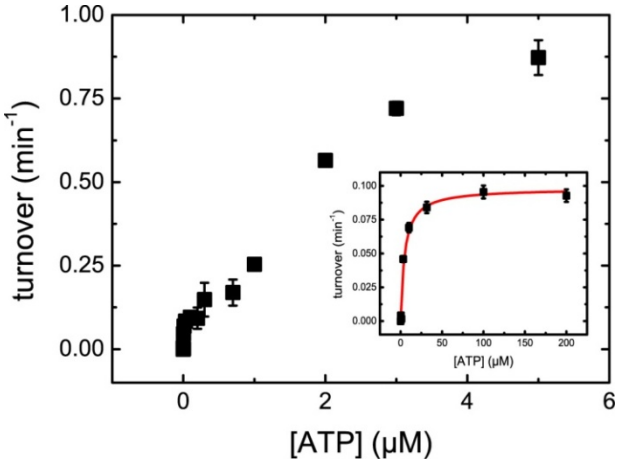


**Figure 17**
*ATPase assay of BiP followed in a regenerative assay*. 2 µM BiP was used and each concentration point was measured in triplicates. The inlay shows the determination of the $K_M$ = 5.1 ± 0.8 µM by a single-site-binding model for low ATP concentration (red). Adopted from (Marcinowski et al., 2011).

Taken together, the recombinantly expressed BiP is folded and shows temperature-induced biphasic unfolding characteristic for Hsp70s. Additionally, the ATPase activity of BiP exhibits a low $K_M$ typical for Hsp70s with turnover rates ~ 0.15 $min^{-1}$ at low ATP concentration (< 200 µM) and an activity gain above 1 mM ADP.

### 6.2.3 ERdJ3 characterization

The refolded and non-glycosylated ERdJ3 was analyzed in terms of its secondary structure by CD spectroscopy. The CD spectrum was recorded after dialysis of ERdJ3 into PBS buffer and shows typical features of a folded protein (Figure 18).

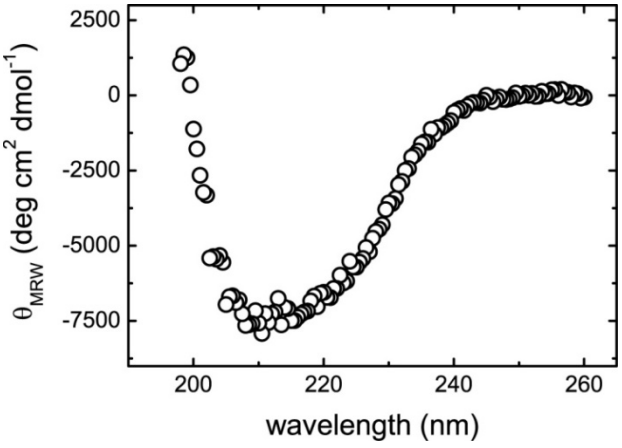


**Figure 18**
*CD analysis of ERdJ3*. 5 µM ERdJ3 was used for the measurement in PBS buffer at 25°C.

The functionality of ERdJ3 was analyzed by its ability to stimulate BiP's ATPase. Therefore, a regenerative ATPase assay was performed with varying concentrations of ERdJ3 and the activation rates were plot (Figure 19). The analysis revealed that ERdJ3 stimulates BiP maximally at a molar ration of 1:2 in agreement with the finding that ERdJ3 has to form

homodimers via its C-terminal dimerization domain to interact with BiP and a low $K_d$ can be assumed for the dimerization (see section 4.7).

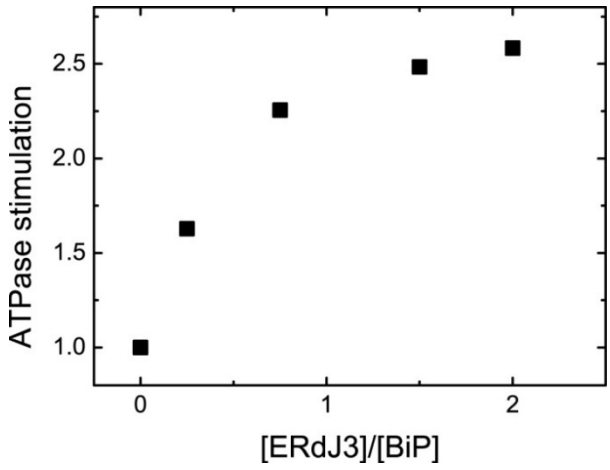


**Figure 19**
*Stimulation of BiP's ATPase by ERdJ3*. 2 µM BiP was used for the measurement in HKM buffer at 37°C in the presence of 1 mM ATP and the indicated molar amount of ERdJ3 was added and the ATPase stimulation rate calculated.

ERdJ3 harbors a J-domain which binds to the interface of BiP's NBD and SBD and stimulates the hydrolysis of ATP. A His-Pro-Asp (HPD) motif in ERdJ3 is essential for this interaction and binding can be abolished by mutating this conserved amino acid sequence to Gln-Pro-Asp (QPD) (Tsai and Douglas, 1996). For ERdJ3, three mutants were cloned and purified in this work. The full length protein with the QPD mutation in its J-domain (QPD) was analyzed as well as the isolated J-domain (J-WT) and the isolated J-domain with the QPD mutation (J-QPD). Their ability to stimulate BiP's ATPase is shown in Figure 20.

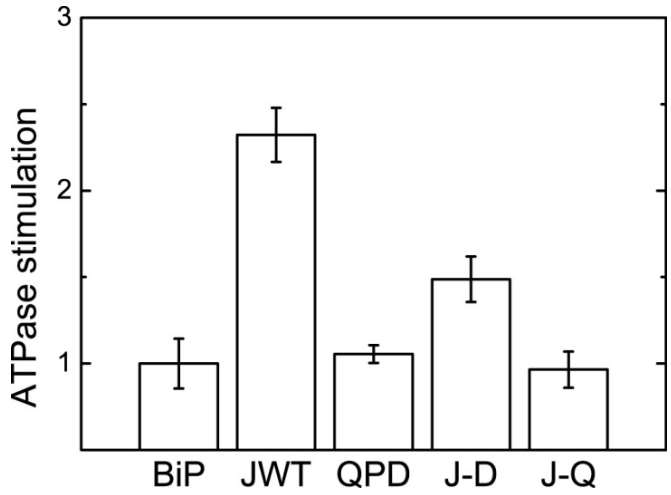


**Figure 20**
*Stimulation of BiP's ATPase by ERdJ3 mutants*. The stimulation of BiP's ATPase activity (2µM) by 4 µM ERdJ3 full length WT or the QPD mutant or 10 µM of the isolated J-domains of WT or the QPD mutant was analyzed in a regenerative ATPase assay in the presence of 1 mM ATP. (BiP: BiP only; JWT: ERdJ3 WT; QPD: ERdJ3 HPD to QPD mutation; J-D: isolated J-domain of ERdJ3; J-Q: isolated J-domain of ERdJ3 HPD to QPD mutation). Adopted from (Marcinowski et al., 2011)

The 2.5-fold ATPase stimulation rate of ERdJ3 is in very good agreement with published results for the glycosylated ERdJ3 purified from COS-1 cells as well as the loss of function concerning the ATPase stimulation of BiP upon mutation of the HPD motif to QPD (Tsai and Douglas, 1996). Interestingly, the isolated J-domain does not stimulate BiP to the same extend as the full length protein indicating that additional parts of ERdJ3 might be important for the interaction with BiP once the HPD motif is bound to the NBD/SBD interface of BiP. This point will be further clarified in detail in section 6.10.

In summary, the non-glycosylated ERdJ3 could be successfully refolded from inclusion bodies and shows its described features concerning dimerization-dependent stimulation of BiP's ATPase activity.

## 6.3 The interaction of BiP with $C_H1$

BiP was shown to bind substrates co-translationally during their synthesis into the ER. However, stable complexes with certain substrates are observed and the $C_H1$ domain is an important member of this group leading to the retention of unassembled HCs in the ER (Haas and Wabl, 1983; Bole et al., 1986; Vanhove et al., 2001). As the oxidized $C_H1$ domain is unfolded in the absence of a $C_L$ domain, yet stable and only to a certain extent aggregation prone, it represents an ideal endogenous substrate to study the interaction with BiP and its co-factors. First, the thermodynamic and kinetic parameters for this interaction were established by analytical SEC-HPLC experiments for the murine and the human $C_H1$ domain.

The $K_d$ determination revealed a rather low binding affinity of $K_d$ = 12.6 ± 0.7 µM for BiP and the oxidized murine $C_H1$ and $K_d$ = 12.9 ± 1.1 µM for the human, respectively (see Figure 21). Kinetics of the association of the murine $C_H1$ domain with BiP were performed previously and revealed a concentration dependent association reaction with very slow $k_{off}$ = 0.01 ± 0.002 $min^{-1}$ and $k_{on}$ = 0.001 ± 0.0002 $\mu M^{-1}$ $min^{-1}$ ((Feige et al., 2009), Moritz Marcinowski, Master thesis, TU München).

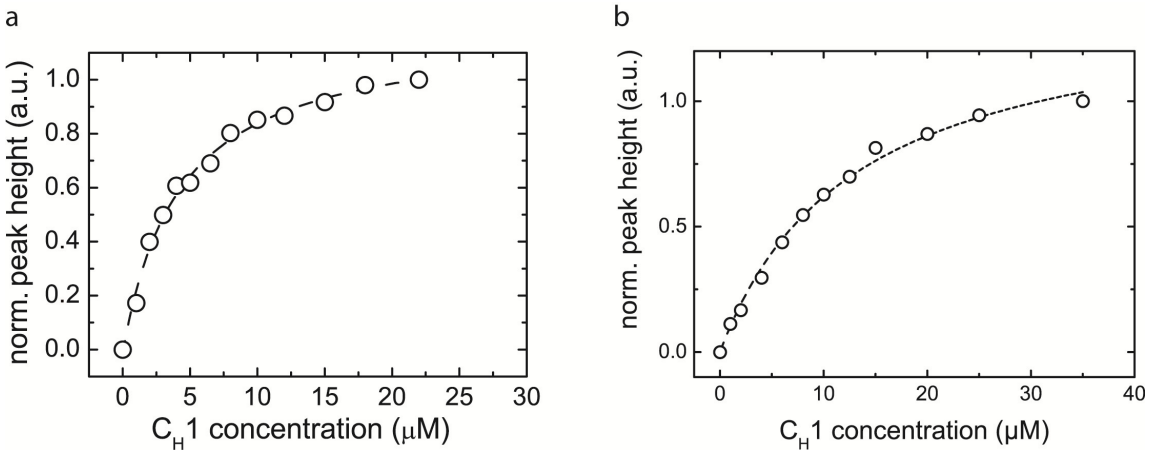


**Figure 21**
*$K_d$ determination for $C_H1$ by SEC-HPLC (Superdex 200 10/300)*. (a) the murine $C_H1$ and (b) the human $C_H1$ at 37°C in HKM in the presence of 1 mM ADP after incubation for 4 hours. Fluorescence intensities of the complex at a retention time of 26.8 min were normalized (flow rate 0.5 ml/min).

## 6.4 A mutational approach to dissect BiP binding sites in human $C_H1$

The recognition sites in the $C_H1$ domain were so far only studied by peptide libraries and seven potential binding sites were predicted within the $C_H1$ domain (Knarr et al., 1995). However, an analysis of their accessibility for BiP is missing. Therefore, a mutational approach was followed in this thesis for the human $C_H1$ domain to test for the relevance of the predicted binding sites. Within the five predicted binding sites, two sequences share a similar amino acid pattern (HTFPAVL and SVFPLAP) with a central Phe residue followed by a Pro with both flanked by small, rather hydrophobic amino acids. Both showed the highest stimulation of BiP's ATPase activity among the tested peptides (Knarr et al., 1995). First, the central Pro residue was mutated against Ala. This had different effects on the two binding sites. While the mutation of the SVFPLAP site to SVFALAP improved binding, the mutation of HTFPAVL to HTFAAVL showed a reduction of the $K_d$ for BiP to 19.2 ± 0.9 µM compared to the wt protein as shown in Figure 22a.

For the SVFPLAP sequence a reduction in affinity was only observed upon the exchange of the aromatic Phe residue against lysine (SVKPLAP) with a $K_d$ = 25.1 ± 1.6 µM as shown in Figure 22b. However, the single mutations only led to a two-fold reduction in affinity for BiP, indicating that both sites might compensate for each other. In agreement with this finding, the double mutant of the $C_H1$ domain (SVFPLAP to SVKPLAP and HTFPAVL to HTFAAVL) showed a drastically reduced binding of BiP as no complexes were observable in the tested

concentration range (Figure 22c). This indicates that only these two stretches, out of five predicted, are critical for BiP binding in the context of the complete domain.

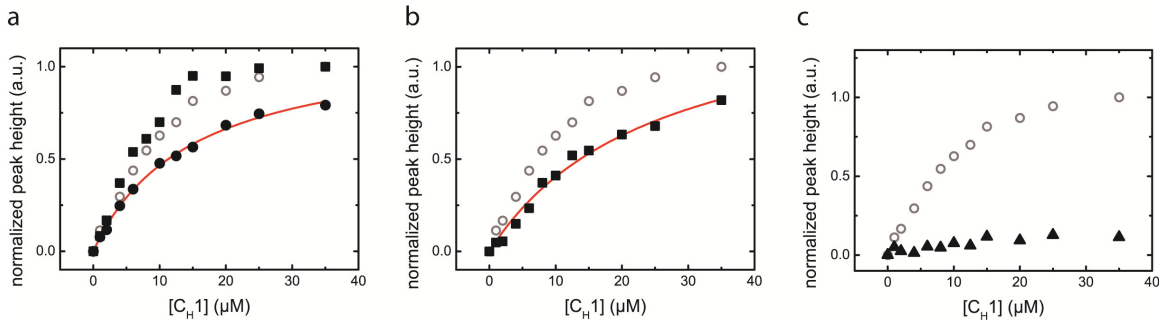


**Figure 22**
*$K_d$ determination for the mutant human $C_H1$ by SEC-HPLC (Superdex 200 10/30)*. (a) The human $C_H1$ wt is shown in gray, the SVFPLAP to SVFALAP mutant by filled squares and the HTFPAVL to HTFAAVL mutant by closed circles. (b) The human $C_H1$ wt is shown in gray and the SVFPLAP to SVKPLAP mutant in closed squares. (c) The human $C_H1$ wt is shown in gray and the double mutant (SVFPLAP to SVKPLAP and HTFPAVL to HTFAAVL) in closed triangles. All measurements were performed at 37°C in HKM in the presence of 1 mM ADP after incubation for 4 hours. Fluorescence intensities of the complex at a retention time of 26.8 min were normalized to the wt $C_H1$ domain (flow rate 0.5 ml/min). $K_d$ was determined by a fit to a single-site-binding model.

### 6.4.1 Association of the mutant $C_H1$ domains with $C_L$

The murine $C_H1$ domain was shown to fold upon association with the $C_L$ domain and folding can be monitored by changes in CD intensities (Feige et al., 2009). Here, the folding of the wild type and mutant $C_H1$ domains with a human $C_L$ domain was analyzed (see Figure 23).

The wild type as well as the HTFPAVL to HTFAAVL mutant showed association-coupled folding in the presence of the $C_L$ domain with observed rate constants $k_{obs}$ = 0.058 ± 0.003 $min^{-1}$ for wild type $C_H1$ and $k_{obs}$ = 0.041 ± 0.005 $min^{-1}$ for the mutant (Figure 23a and b, respectively). In contrast, the mutation of SVFPLAP to SVKPLAP abolished $C_L$ coupled folding of the $C_H1$ domain (Figure 23c and d, respectively).

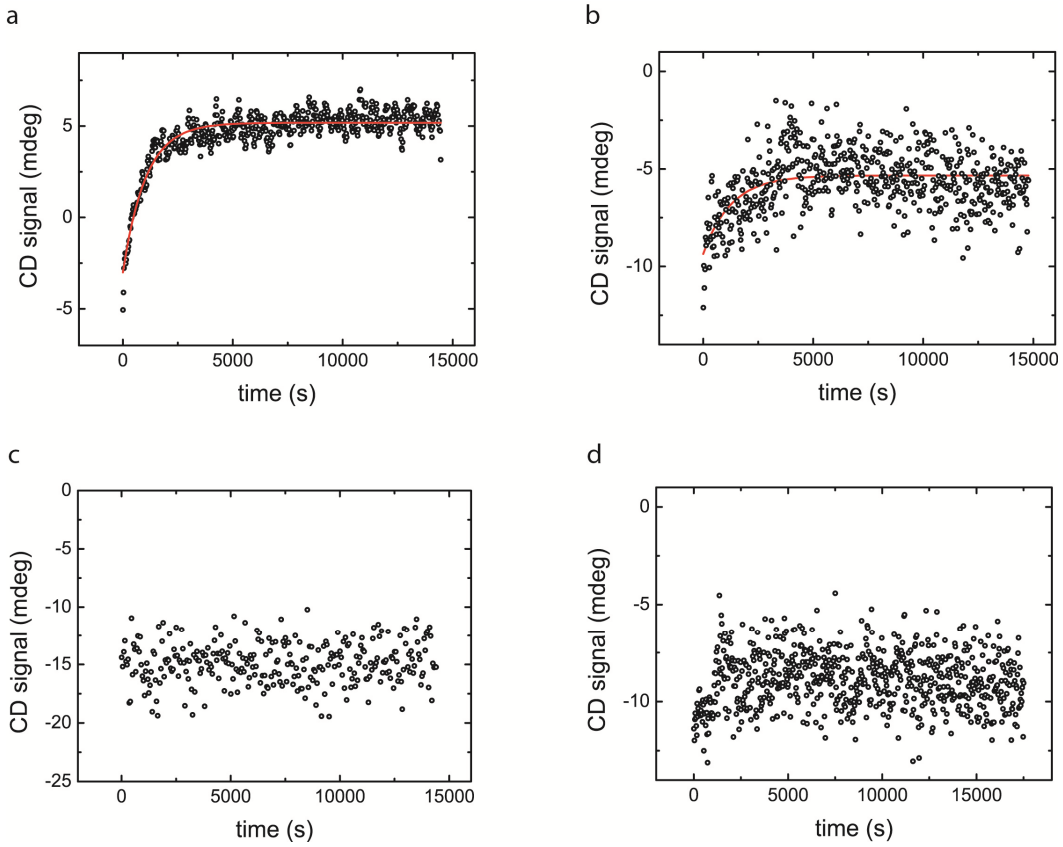


**Figure 23**
*Association of human $C_H1$ with $C_L$.* CD kinetics (wavelength λ = 205 nm) of the association of 10 µM $C_H1$ with 10 µM $C_L$ were recorded at 25°C in PBS buffer for (a) the wild type as in Figure 15, (b) the HTFPAVL to HTFAAVL mutant, (c) the SVFPLAP to SVKPLAP mutant and (d) the SVFPLAP to SVKPLAP and HTFPAVL to HTFAAVL double mutant.

## 6.5 A peptide-based assay to study association in equilibrium

As the important sites for BiP binding could be assigned by the mutational approach, the interaction of BiP with these peptide stretches was analyzed in more detail. Therefore, a peptide-based assay was chosen. Fluorescently labeled peptides were generated to study complex formation by fluorescence anisotropy in equilibrium. The peptides corresponding to wild type and mutated recognition sites were purchased with an additional C-terminal Gly-Ser-Cys linker for labeling with lucifer yellow and to avoid masking the BiP binding site in the peptide. After successful labeling (see material and methods), assays were performed in the presence of 1 mM ADP in HKM buffer at 37°C. The analysis revealed a $K_d$ = 19.3 ± 1.4 µM for the SVFPLAP binding site (Figure 24a).

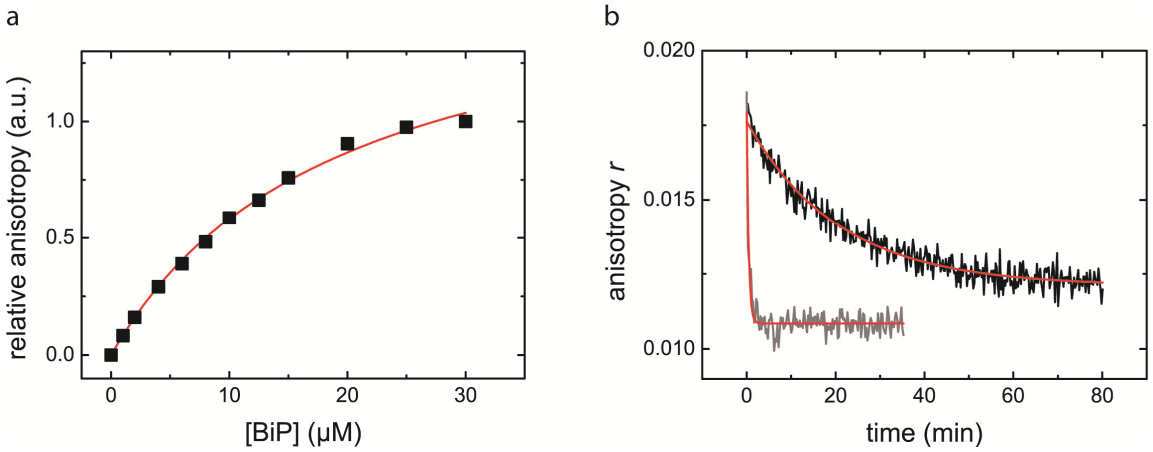


**Figure 24**
*$K_d$ determination for the SVFPLAP peptide and complex dissociation* (a) 1 µM SVFPLAPgsc-LY peptide was incubated for 4 hours with varying concentrations of BiP, 1 mM ADP, 37°C in HKM before the fluorescence anisotropy was determined and normalized. The $K_d$ was determined by a fit to a single-site-binding model. (b) Dissociation of pre-formed complexes by ATP (gray) or a 150-fold excess of unlabeled (SVFPLAP) peptide (black).

Additionally, the dissociation of the complex with either ATP or a 150-fold excess of unlabeled peptide revealed that functional complexes were formed (Figure 24b). The evaluation of the dissociation kinetics resulted in an ATP-induced dissociation rate of 2.32 ± 0.11 $min^{-1}$ and a $k_{off}$ = 0.04 ± 0.01 $min^{-1}$ for the dissociation by unlabeled peptide. This indicates that only binding of ATP but not hydrolysis is sufficient to dissociate the complex as hydrolysis under the investigated condition is an order of magnitude smaller. This finding is in good agreement with previous studies (Wei and Hendershot, 1995).

The analysis of the second, HTFPAVL, binding site revealed similar results, with a $K_d$ = 11.6 ± 0.6 µM and an experimentally determined dissociation rate $k_{off}$ = 0.04 ± 0.01 $min^{-1}$ for the dissociation by unlabelled peptide while the dissociation of a preformed complex by ATP was unchanged (Figure 25a and b). Importantly, the dissociation of the preformed complex was not altered if the unlabeled peptides with the C-terminal Gly-Ser-Cys linker were used. This shows that the linker has no influence on the binding behavior of the seven amino acid binding sequences (data not shown).

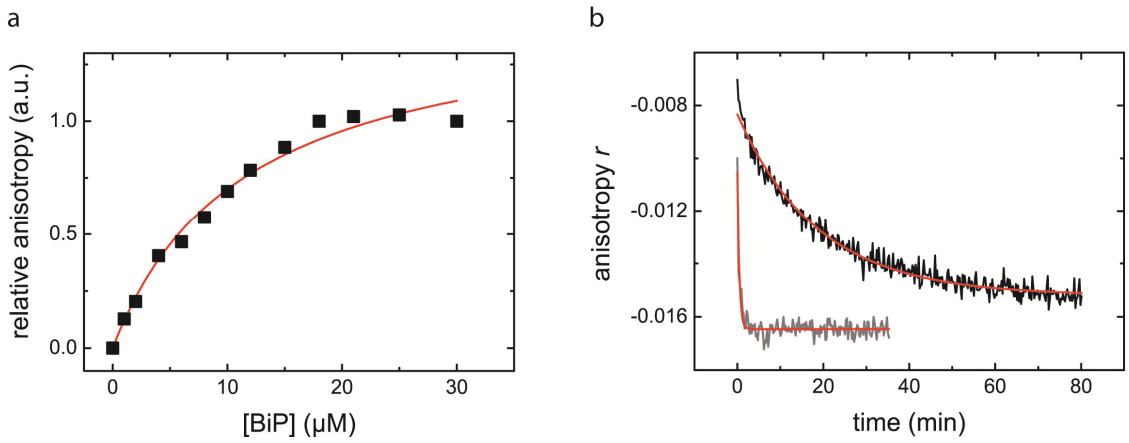


**Figure 25**
*$K_d$ determination for the HTFPAVL peptide and complex dissociation* (a) 1 µM HTFPAVLgsc-LY peptide was incubated for 4 hours with varying concentrations of BiP, 1 mM ADP, 37°C in HKM before the fluorescence anisotropy was determined and normalized. $K_d$ was determined by a fit to a single-site-binding model. (b) Dissociation of pre-formed complexes by ATP (gray) or a 150-fold excess of unlabeled (HTFPAVL) peptide (black).

Kinetics of the association of both labeled peptides with varying concentrations of BiP were followed by fluorescence anisotropy and the observed rate constants $k_{obs}$ were plot, revealing a concentration dependent association as for the complete $C_H1$ domain (Figure 26). For the SVFPLAP peptide $k_{on}$ was calculated as 0.0017 ± 0.0004 $\mu M^{-1}\,min^{-1}$ and $k_{off}$ as 0.021 ± 0.001 $min^{-1}$. The $k_{off}$ is in the range of the experimentally determined one. For the HTFPAVL binding site, the kinetic analysis revealed a $k_{on}$ = 0.001 ± 0.0002 $\mu M^{-1}min^{-1}$ and a $k_{off}$ = 0.01 ± 0.002 $min^{-1}$ which is also in good agreement with the experimentally determined one.

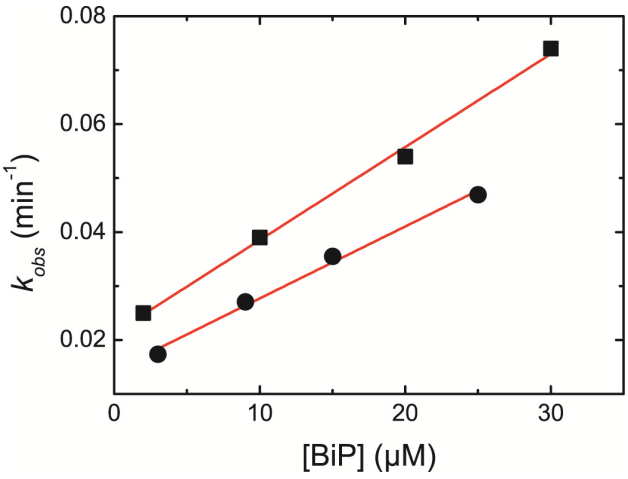


**Figure 26**
*Kinetic analysis of SVFPLAP and HTFPAVL binding to BiP*. Kinetic traces of 1 µM of the SVFPLAP peptide (filled squares) or the HTFPAVL peptide (filled circles) binding to the indicated BiP concentration at 37°C in the presence of 1 mM ADP in HKM buffer were fit to a single exponential equation to obtain the observed rate constants. By linear regression, $k_{on}$ and $k_{off}$ were determined.

In order to rule out effects of the charged termini of the synthesized peptides on binding, the HTFPAVL peptide was synthesized (Christian Becker, TU München) carrying capping groups at its N- and C-termini. Their binding behavior to BiP was addressed by performing dissociation experiments of pre-formed BiP-HTFPAVLgsc-LY complexes. As shown in Figure 27, no differences were observable and the kinetic analysis revealed an identical $k_{off}$ = 0.03 $min^{-1}$ for the capped peptide and for the peptide without terminal modifications.

Taken together, the analysis of both binding sites revealed that the two binding sites are bound with similar $K_d$ values as the complete domain in a concentration-dependent bimolecular reaction. The formed complexes are highly stable as $k_{off}$ rates are in the range of 0.03 $min^{-1}$ ± 0.01. For the concentration-dependent $k_{on}$ the high *in vivo* concentration of BiP has to be considered as well as the high local concentration of BiP at the luminal side of the SEC translocon, where newly synthesized proteins interact already co-translationally with BiP (Alder et al., 2005). Hence, the binding of the two recognition sites will be fast and efficient in the ER. The kinetic constants for the peptide interaction are given in Table 1.

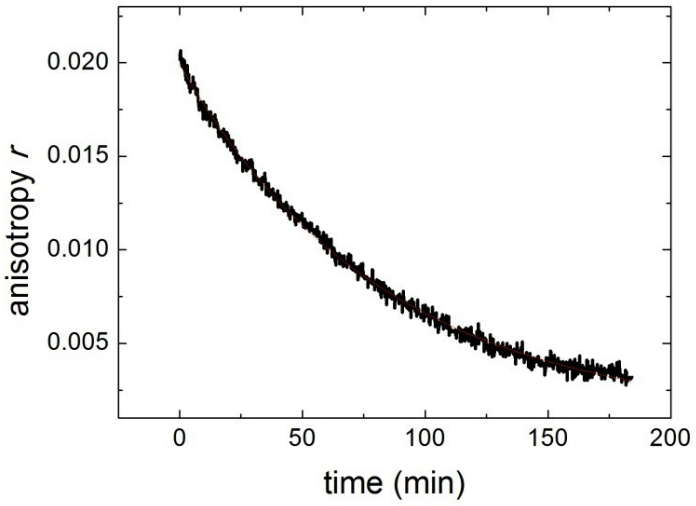


**Figure 27**
*Capping of peptide termini has no influence on complex dissociation.* Dissociation of pre-formed complexes a 150-fold excess of unlabeled (HTFPAVL) peptide (black).

| Peptide | $k_{on}$ ($\mu M^{-1}min^{-1}$) | $k_{off}$ ($min^{-1}$) | $K_d$ ($\mu M$) |
|---|---|---|---|
| **SVFPLAP** | 0.0017 ± 0.0004 | 0.021 ± 0.001 | 19.3 ± 1.4 |
| **HTFPAVL** | 0.0010 ±0.0002 | 0.010 ± 0.002 | 11.6 ± 0.6 |

**Table 1**
*$k_{on}$, $k_{off}$ and $K_d$ for peptide binding by BiP*. $k_{on}$ and $k_{off}$ were determined from linear fits of the observed rate constants $k_{obs}$ from Figure 26 with the SVFPLAP and HTFPAVL peptides. The $K_d$ values were experimentally determined (see Figure 24 and 25, respectively).

## 6.6 Analysis of the non-binding sequences

The two identified non-binding sequences were also analyzed by fluorescence anisotropy after labeling of the sequences via an added C-terminal Gly-Ser-Cys linker. The experiments were performed under identical conditions as binding of the wild type peptides. They showed the same results as for the mutations in the complete $C_H1$ domain, i.e. binding was severely impaired (Figure 28a for SVKPLAP and b for HTFAAVL, respectively). These results indicate that the loss of BiP binding of the $C_H1$ domain upon mutation of both binding sites can be attributed to the loss of binding site recognition and probably not to secondary effects distinct from the binding sites.

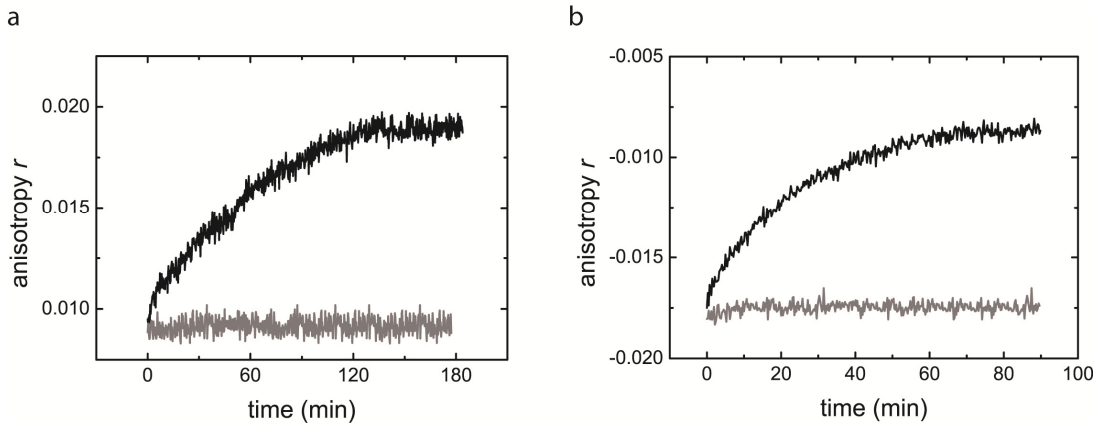


**Figure 28**
*Binding of SVKPLAP and the HTFAAVL peptide to BiP* (a) Binding of 1 µM SVKPLAPgsc-LY peptide (gray) to 15 µM BiP in the presence of 1 mM ADP, 37°C in HKM followed by fluorescence anisotropy (black wild type peptide). (b) Binding of 1 µM HTFAAVLgsc-LY peptide (gray) to 15 µM BiP in the presence of 1 mM ADP, 37°C in HKM followed by fluorescence anisotropy (black wild type peptide)

## 6.7 Non-proteinogenic amino acid substitutions in BiP binding peptides

The mutations necessary to abolish BiP binding in the two binding site differ in their character. The severe reduction of hydrophobicity and the introduction of a positive charge upon the exchange of the aromatic Phe against Lys in the SVFPLAP sequence are in agreement with the previous notion that hydrophobic residues mediate BiP binding (Gething et al., 1995; Knarr et al., 1995; Knarr et al., 1999). In contrast, the mutation of the central Pro residue in the HTFPAVL sequence to Ala leads to suppression of BiP binding, although the hydrophobicity is not affected. While the mutation of Phe to Lys in the SVFPLAP site leads to a significantly decreased score in the BiP binding site prediction algorithm, the Pro to Ala mutation in the HTFPAVL site does not. Hence, a mechanism different from the hydrophobic approach must be the reason for the non-binding HTFAAVL sequence. In crystal structures available for BiP orthologues, peptides are bound in the cleft of the SBD in a highly extended conformation (Pellecchia et al., 2000). Therefore, the influence of the peptide geometry and conformation was addressed in more detail.

In collaboration with Prof. Christian Becker at the TU München, a set of peptides with non-proteinogenic amino acid substituents for the central Pro residue in the HTFPAVL sequence was synthesized. The substituents can be grouped into classes populating (i) an extended conformation of the peptide backbone, (ii) a kinked conformation of the backbone and (iii) substituents with varying side chain lengths to explore the flexibility of the cleft in the β-sandwich of BiP´s SBD. The selected substituents are given in Figure 29 and assigned a number which will be used in subsequent experiments.

The 5-dimethyl-4-oxaproline substituent (2) exclusively allows the formation of a kinked conformation of the peptide, while the 1,4-aminobenzoic acid substituent (3) guarantees an extended conformation of the peptide as well as 1,3-aminobenzoicacid (4) which further allows the addition of side chains. As a bulky, aromatic side chain, Fmoc was chosen (6), whereas the propinyl substituent (5) allows the analysis of more linear substituents.

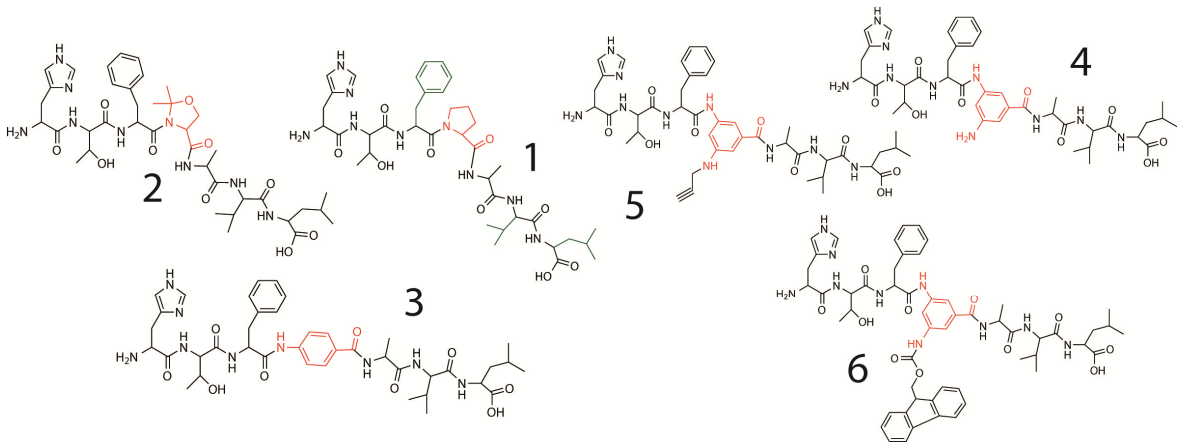


**Figure 29**
*Structure of peptides with non-proteinogenic amino acid substituents for the central Pro residue of HTFPAVL*. The central proline residue of (1) the HTFPAVL wild type peptide was exchanged against (2) 5-dimethyl-4-oxaproline, (3) 1,4-aminobenzoic acid, (4) 1,3-aminobenzoic acid, (5) propinyl substituted 1,3-aminobenzoic acid or (6) Fmoc substituted 1,3-aminobenzoic acid. The hydrophobic residues in the wt sequence are highlighted in green.

The synthesized peptides were tested for their ability to dissociate complexes of BiP with the lucifer yellow labeled wild type HTFPAVL peptide. Complexes were pre-formed in the presence of ADP and complex dissociation was initiated by the addition of a 150-fold excess of the unlabeled peptides 2-6 (Figure 30). The complex dissociation by the unlabeled wild type HTFPAVL peptide is shown in Figure 25b.

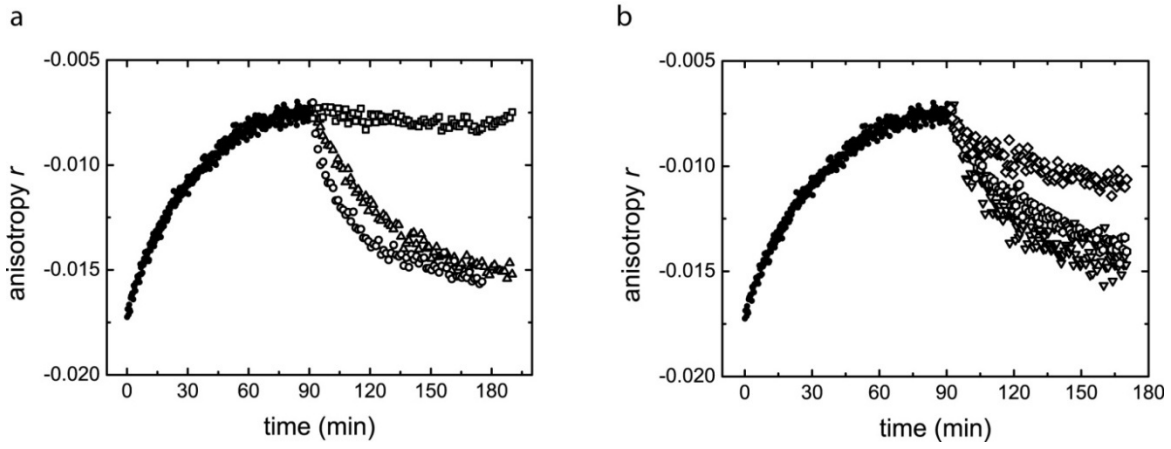


**Figure 30**
*The ability of the substituted peptides to dissociate wild type complexes with BiP*. Complex formation of 15 µM BiP with 1 µM wild type HTFPAVLgsc-LY were formed in the presence of 1 mM ADP in HKM buffer at 37°C and followed by fluorescence anisotropy (filled circles in a and b). After reaching equilibrium, a 150-fold excess of (a, open circles) unlabeled wild type peptide, (a, open squares) peptide 2 (5-dimethyl-oxoproline), (a, open triangles) peptide 3 (1,4-aminobenzoicacid), (b, reverse open triangles) peptide 4 (1,3-aminobenzoicacid), (b, open diamonds) peptide 5 (propinyl) or (b, open pentagons) peptide 6 (Fmoc) was added and complex dissociation followed.

The kinked peptide 2 showed no effect on the preformed complexes as no decay in the fluorescence anisotropy of the bound wt peptide was observable (Figure 30a). In contrast, peptide 3 dissociated the complex efficiently with a rate constant $k_{obs}$ = 0.024 ± 0.002 $min^{-1}$ comparable to the unlabeled wt peptide. These results indicate that besides hydrophobicity the conformation of the peptide has a so far unknown impact on complex formation with elongated conformations being highly favored over kinked ones. The set of peptides with the central proline residue exchanged against 1,3-aminobenzoic acid allowing the further modification of the amino-group with either a propinyl or Fmoc substituent showed a surprising binding behavior. While the rather small propinyl substituent resulted in only moderate binding, the large Fmoc substituent efficiently dissociated the BiP wt–peptide complex as well as the non-substituted 1,3-aminobenzoic acid peptide (Figure 30b).

These results indicate that BiP favors extended conformations of peptides over kinked ones even if the hydrophobicity of the peptide side chain is not altered. Additionally, the binding cleft shows a high degree of flexibility, as even a bulky Fmoc substituent in the central position can bind to BiP efficiently. However, the flexibility seems to tolerate only aromatic substituents, as the rather small propinyl substituent showed only moderate binding efficiency.

## 6.8 The role of the lid of BiP

### 6.8.1 Lid deletion mutants of BiP

The lid of Hsp70s consists of 5 helices (A-E) and its role is discussed controversially in literature. On the one side, an essential role of the lid is reported *in vivo*, especially for the mitochondrial Hsp70 (mtHsp70) and the *S. cerevisiae* homologue Kar2p of BiP. For both, defects in growth and import of proteins into the organelle are described (Tokunaga et al., 1998; Strub et al., 2003). On the other side, the lid deletion of *E. coli* DnaK revealed a faster $k_{off}$ rate of substrates if deleted, but no severe limitations were reported (Buczynski et al., 2001). Therefore, the function of the lid of BiP was studied in more detail by a deletion process with the lid truncated helix by helix from the C-terminus. The constructs are shown in Figure 31. The C-terminus of BiP carries an additional feature distinct from other Hsp70s with the KDEL ER-retention-sequence and an additional ten amino acid long part which is predicted to be unfolded.

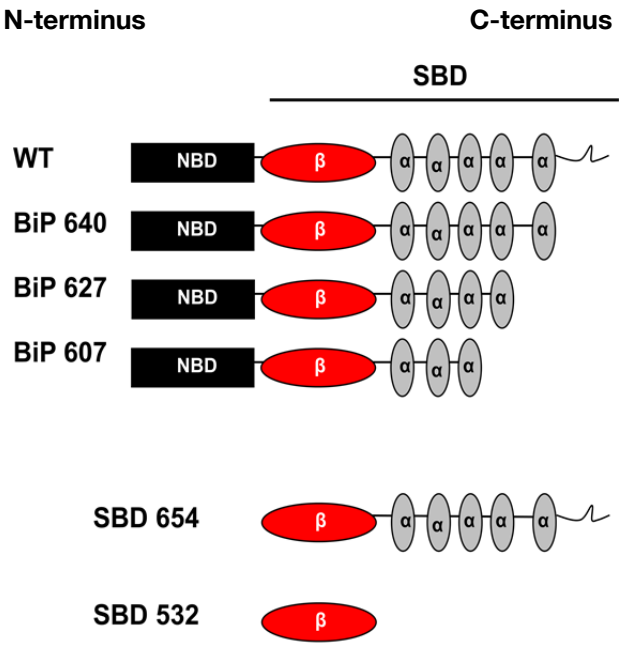


**Figure 31**
*Schematic representation of the lid deletion mutants*. Two types of mutants were generated, either containing the NBD or the isolated SBD constructs. The C-terminal 14 amino acids of BiP contain the ER retention KDEL sequence and a region predicted to be unfolded.

In this thesis, two different types of constructs were analyzed. Proteins containing the complete NBD and SBD were a kind gift of Roland Heym (Master thesis, TU München) and those containing only the SBD were cloned, expressed and purified in this thesis. The truncated versions containing the NBD were subjected to the analysis of peptide binding by the fluorescence anisotropy assay with the HTFPAVL wild type peptide. In contrast, the SBD constructs were analyzed by SEC-HPLC as the change in anisotropy was not sufficient for reliable evaluation of the data.

The results show, that the lid is critical for binding of the peptide substrate, as the deletion of helix E already leads to an abolished substrate interaction (Figure 32). Importantly, the NBD/SBD communication is not altered by the deletion of the C-terminal 14 amino acids as the release of the bound peptide by converting ADP to ATP still works. The completely truncated version of BiP with the NBD could not be purified in contrast to the isolated SBD. Hence, the analysis for substrate binding for the complete lid truncation could only be measured for the SBD without the NBD.

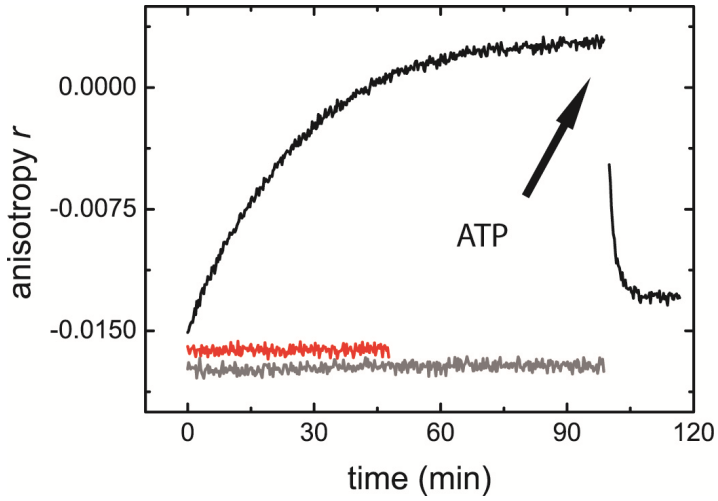


**Figure 32**
*HTFPAVL binding by lid deletion mutations of BiP (including the NBD) followed by fluorescence anisotropy*. Measurements were performed with 15 µM of the 640 construct (black), 627 construct (red) or the 607 construct (gray) and 1 µM of the HTFPAVLgsc-LY peptide in the presence of 1 mM ADP at 37°C in HKM. The conversion of ADP to ATP was performed by addition of phosphoenolpyruvate and pyruvate kinase.

In case of a complete lid truncation, very efficient substrate binding was observable for the peptide and also the $C_H1$ domain. Analysis was performed by SEC-HPLC, as the change in anisotropy was too small even for the isolated SBD containing the complete lid. The SBD 640 construct showed no difference from the full length BiP (data not shown) and the analysis for the SBD 532 construct is given in Figure 33. The analysis for HTFPAVL peptide binding revealed a $K_d$ = 6.7 ± 1.1 µM what is 2-fold below the $K_d$ of full length BiP. A similar effect is observed for binding of the murine $C_H1$ domain where the $K_d$ could be determined as $K_d$ = 3.6 ± 0.3 µM which is three-times below the $K_d$ of full-length BiP for the murine $C_H1$ domain (Marcinowski et al., 2011). Hence, the isolated SBD of BiP with the lid completely deleted, is able to bind a peptide or a protein as substrate with even higher affinity than the full length protein including the lid.

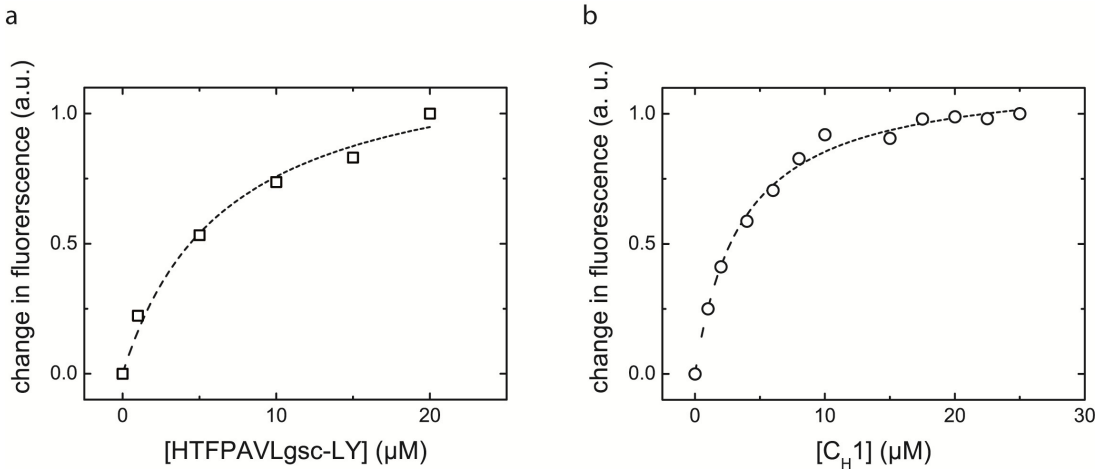


**Figure 33**
*Binding of HTFPAVL peptide and the murine $C_H1$ domain to BiP SBD 532 by SEC-HPLC (Superdex 200 10/30)*. (a) Binding of 1 µM BiP to varying concentration of the HTFPAVLgsc-LY peptide in the presence of 1 mM ADP, 37°C in HKM was analyzed by SEC-HPLC. (b) Binding of 1 µM BiP to varying concentration of the murine $C_H1$ domain in the presence of 1 mM ADP, 37°C in HKM was analyzed by SEC-HPLC. Both experiments were measured after incubation for 4 hours. Fluorescence intensities of the complex at a retention time of 33 min for the peptide and 30.1 min for the $C_H1$ domain were normalized (flow rate 0.5 ml/min).

These, on the first view controversial results, indicate that the lid undergoes a conformational transition upon deletion which may result in self-binding of a part of the lid in the SBD cleft or other sterical hindrances. This hypothesis is supported by an X-ray structure of the cytosolic bovine Hsc70 with a truncated lid. The structure shows an unfolded region within helix A which is tightly bound in the cleft of the SBD (PDB: 1YUW). This explanation is in agreement with the fact that the complete deletion of the lid leads to highly efficient substrate binding whereas partial truncations abolish the interaction with substrates. However, the lid of the BiP orthologue Kar2p from *S. cerevisiae* is described as an important element for cell viability, especially under stress conditions (Tokunaga et al., 1998) and the open question whether the lid interacts with the substrate or has only a regulatory function on the NBD and SBD was addressed by cross-linking experiments.

### 6.8.2 The interaction of the lid with the murine $C_H1$ domain

To analyze the interaction of the lid with the $C_H1$ domain, site-specific cross-linking experiments with the bi-functional cross-linker benzophenone-4-maleimide (BPM) were performed. BPM carries a maleimide entity for covalent linkage to cysteine residues and the benzophenone entitiy can be photo-activated. For crosslinking, a set of BiP mutants was generated. First, the two authentic cysteine residues which are dispensable for its

function in vitro were exchanged against serine. Second, single cysteine residues were incorporated at the positions 518 or 636, respectively. The residue 518 is located adjacent to the cleft in the β-sandwich of the SBD and serves as a negative control. In contrast, the residue 636 is located at the end of helix E of the lid. Crosslinks were performed by pre-incubating BiP single cysteine mutants with BPM prior to complex formation with an excess of the CH1 domain in HKM buffer in the presence of ADP and photo-activation of BPM. Analysis was performed by SDS-PAGE and MALDI-TOF/TOF-MS (Figure 34).

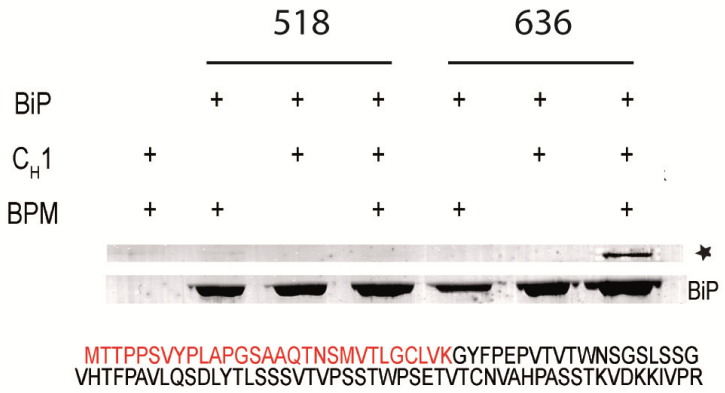


**Figure 34**
*Cross-links of the single cysteine mutants BiP 518 and BiP 636 with murine $C_H1$ by BPM*. The cysteine mutants were incubated for 2 hours with BPM prior to complex formation with $C_H1$ in the presence of 1 mM ADP. After activation of the bi-functional cross-linker BPM with UV-light at $\lambda = 350$ nm for 10 minutes, samples were analyzed by SDS-PAGE. BiP, murine $C_H1$ and BPM were added as indicated. The lower lane corresponds to non-cross-linked BiP. The cross-linking product (asterisk) was analyzed by MALDI-TOF/TOF MS after tryptic digestion. The identified peptide of the $C_H1$ domain is marked in red in the complete sequence of the $C_H1$ domain. Adopted from (Marcinowski et al., 2011).

The cross-link experiment revealed a physical interaction of the lid with the bound substrate, the $C_H1$ domain, as a cross-link was only observable for the BiP 636 construct. Additionally, the analysis of cross-link products by tryptic digestion and MALDI-TOF/TOF-MS revealed that at least the C-terminal part of the $C_H1$ is cross-linked to BiP. To further study the function of the lid and the domain movements of BiP upon binding of nucleotides, peptide and protein substrates, an intramolecular FRET system was established.

## 6.9 An intramolecular FRET assay to study BiP's domain movements

In order to study domain movements and conformations of BiP, an intramolecular FRET assay was established. The BiP mutant without the two endogenous cysteines of BiP was used as a template to generate double cysteine mutants at defined positions for fluorescent labeling. In total, four labeling positions were chosen. The SBD was labeled at position 166, the SBD β-sandwich at position 518 and the lid at positions 583 and 636, respectively. The combination of two mutations in one BiP molecule allows monitoring the conformation of the respective domains towards each other. The substituted amino acids were all solvent-exposed glycines or serines. The labeling positions are depicted in Figure 35.

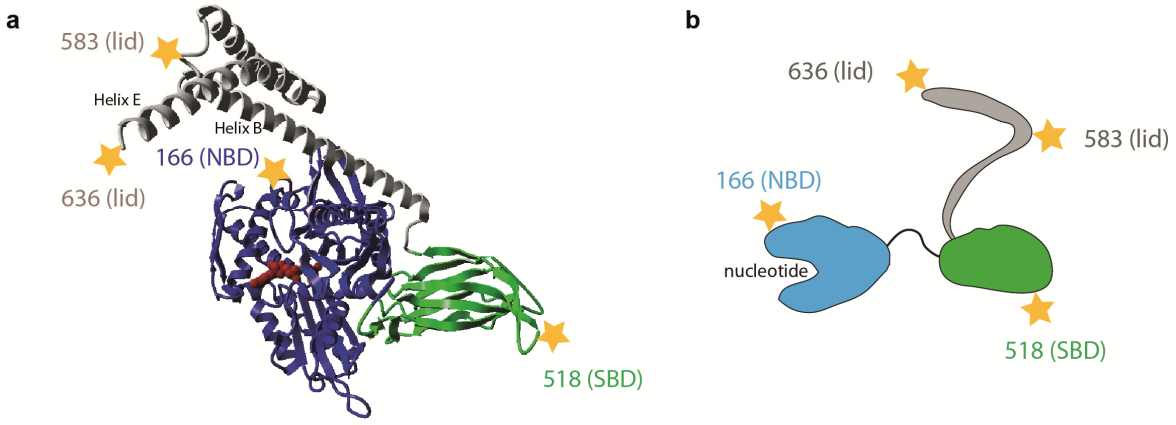


**Figure 35**
*Labeling positions within BiP for FRET measurements*. (a) The labeling positions for spFRET measurements are highlighted in the crystal structure of the Hsp70 homologue Sse1 (PDB code 2QXL). The domains are color-coded (blue: NBD; green: SBD β-sandwich; grey: lid; nucleotide: red). (b) A schematic diagram of BiP with the domains and label positions marked as in panel a. Adopted from (Marcinowski et al., 2011).

The generated cysteine mutants were first assayed concerning their ATPase activity and their ability to bind the substrates (Table 2). The analysis revealed that the engineered mutants show identical behavior as the wild type protein concerning the hydrolysis of ATP and substrate binding and therefore do not interfere with the function of BiP.

| | ATPase turnover ($min^{-1}$) | $C_H1$ binding $K_d$ (µM) | Peptide binding $K_d$ (µM) |
|---|---|---|---|
| **Wild type** | 0.25 ± 0.01 | 7.4 ± 0.2 | 11.6 ± 0.6 |
| **166/518** | 0.22 ± 0.03 | 8.2 ± 0.3 | 10.8 ± 0.4 |
| **166/636** | 0.28 ± 0.02 | 7.1 ± 0.2 | 12.1 ± 0.5 |
| **518/583** | 0.24 ± 0.01 | 8.5 ± 0.4 | 10.1 ± 0.4 |
| **518/636** | 0.22 ± 0.02 | 7.5 ± 0.1 | 11.1 ± 0.7 |

**Table 2**
*ATP turnover and substrate binding by the engineered cysteine mutants of BiP*. The turnover of ATP by BiP wild type and the cysteine mutants was analyzed in a regenerative ATPase assay in the presence of 1 mM ATP. The association of the murine $C_H1$ domain with BiP wild type and the cysteine mutants was analyzed by SEC-HPLC experiments at 37°C in the presence of 1 mM ADP. The $K_d$ value for the binding of the Lucifer Yellow labeled HTFPAVL peptide was determined by fluorescence anisotropy titrations in the presence of 1 mM ADP at 37°C. Adopted from (Marcinowski et al., 2011).

Next, labeling of the cysteines with Atto532 and Atto647 was performed. A statistical labeling procedure was applied, as both dyes were added in identical excess over the double cysteine mutant of BiP. Hence, the statistical distribution for double-labeled BiP molecules is ~ 50%. Therefore, ensemble FRET measurements are expected to show only low FRET efficiency changes and single pair FRET (spFRET) was used to dissect the conformational changes in BiP. The measurements were carried out in collaboration with Prof. Don Lamb and data were recorded and evaluated by Matthias Höller (LMU München). Details concerning measurement parameters and technical setup can be found in (Marcinowski et al., 2011) and the thesis of Matthias Höller.

All measurements shown in this thesis are adopted from (Marcinowski et al., 2011).The slow $k_{off}$ rates of the substrates predispose the system for spFRET analysis, as complexes are kinetically stable after the dilution to the pM concentration, necessary for spFRET measurements. Additionally, the method allows the discrimination of multiple conformation and species which are not accessible by ensemble FRET measurements.

### 6.9.1 spFRET analysis of the NBD/SBD conformation

The domain orientations of the NBD and the SBD towards each other were analyzed for the FRET pair 166/518.

The measurements revealed that in the absence of nucleotides and upon binding of ADP the NBD and SBD are in loose contact with each other, whereas binding of ATP or the non-hydrolyzable analogue AMP-PNP led to a smaller distance of the two domains. This finding is in good agreement with previous studies on other Hsp70s (Mapa et al., 2010; Bertelsen et al., 2009) (Figure 36). For binding of the substrates, i.e. the HTFPAVL peptide and the $C_H1$ domain, a different picture emerges. While peptide binding resulted in no major changes in comparison to the ADP-bound state of BiP, the binding of the $C_H1$ domain gave a smaller distance between the two domains. This finding is surprising, as peptides were taken so far as equivalent minimal models for substrate binding to Hsp70s in general. However, the results obtained suggest a so far unknown influence of the nature of the interacting substrate on the relative conformation of the NBD and SBD domains.

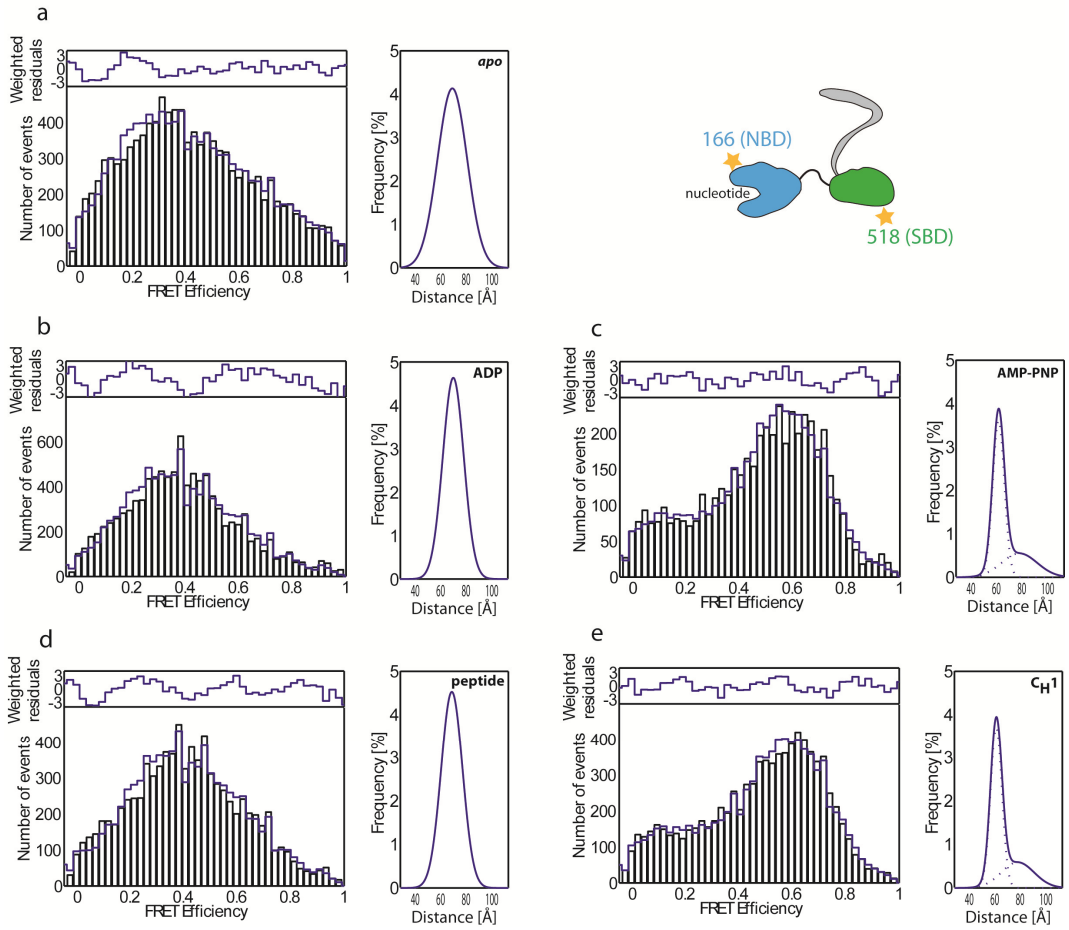


**Figure 36**
*Single pair FRET analysis of BiP 166/518 in the presence of nucleotides and substrates.* For the analysis of NBD/SBD conformations, FRET efficiencies for the double-labeled BiP 166/518 construct (the labeling sites are shown in the schematic cartoon) were measured using single pair FRET experiments (a) in the absence of nucleotides, (b) in the presence of 1 mM ADP or (c) 1 mM AMP-PNP or for the complex of BiP 166/518 with (d) the HTFPAVL peptide and (e) the murine $C_H1$ domain formed in the presence of 1 mM ADP prior to the measurements. Sample preparation with substrates was performed under high substrate excess during the incubation as well as in the dilution steps necessary for the single pair FRET experiments immediately prior to the measurement. The bars indicate the number of events for the FRET efficiency and the line represents the result from the PDA. The reduced residuals are shown in the upper panel. The plot on the right shows the distance distribution determined using PDA. Adopted from (Marcinowski et al., 2011).

## 6.9.2 spFRET analysis of the SBD/lid conformation

As a direct interaction of the lid with the $C_H1$ domain was shown, a more detailed analysis of the lid orientation towards the substrate binding domain was performed. To this end, the 518/636 double-labeled construct was used. For all investigated conditions, three distinct orientations of the lid towards the SBD were observed indicating that the lid is a flexible

entity. However, the conformations are not dynamic below the ms timescale (Marcinowski et al., 2011).

The three conformations were populated to very different degrees in the presence of nucleotides and substrates. The addition of ADP led to only minor changes compared to the *apo*-state of BiP with the lid closed over the SBD. In contrast, AMP-PNP binding resulted in a complete opening of the lid, as the FRET efficiency decreased and the low FRET population was the most predominant one. Upon addition of the HTFPAVL peptide and ADP, the lid closed over the SBD and the bound substrate, as the high FRET population is the main species. This finding is in good agreement with crystal structures of BiP homologues where the lid closes tightly over the SBD and the peptide bound in the cleft of the β-sandwich (Pellecchia et al., 2000). The binding of the $C_H1$ domain occurs in a complete different orientation of the lid as compared to the peptide. The lid was open in the $C_H1$-bound state as the low FRET population was the predominant one. This reveals a so far unknown function of the lid upon protein substrate binding. The lid interacts directly with the bound substrate and does not close on the SBD but remains in the open conformation (Figure 37, a-e).

The next question addressed was if the lid behaves as a single entity or whether the 5 helices of the lid adopt different conformation upon binding of nucleotides or substrates. Therefore, the 518/583 construct with the labeling position at the end of helix A was used and subjected to identical measurements as the 518/636 construct (Figure 38, f-j).

The obtained results show an identical behavior of the labeling position at the end of helix A (583) and the position at the end of helix E (636). For the 518/583 construct also three conformational states were observable with each populated to a different extent upon addition of nucleotides or substrates. As for 518/636, the *apo*- and ADP-bound state had a closed conformation of the lid over the SBD, whereas AMP-PNP addition leads to lid opening. For the peptide and the $C_H1$ domain, a controversial behavior was again observable, as the peptide is bound with a closed lid, whereas the $C_H1$ domain leads to an opening of the lid. As the pattern of lid conformations towards the SBD is identical for the labeling position at the end of helix A and helix E one can assume that the lid moves as a single entity and no detectable rearrangements in the packing of the helices of the lid occur upon nucleotide or substrate binding.

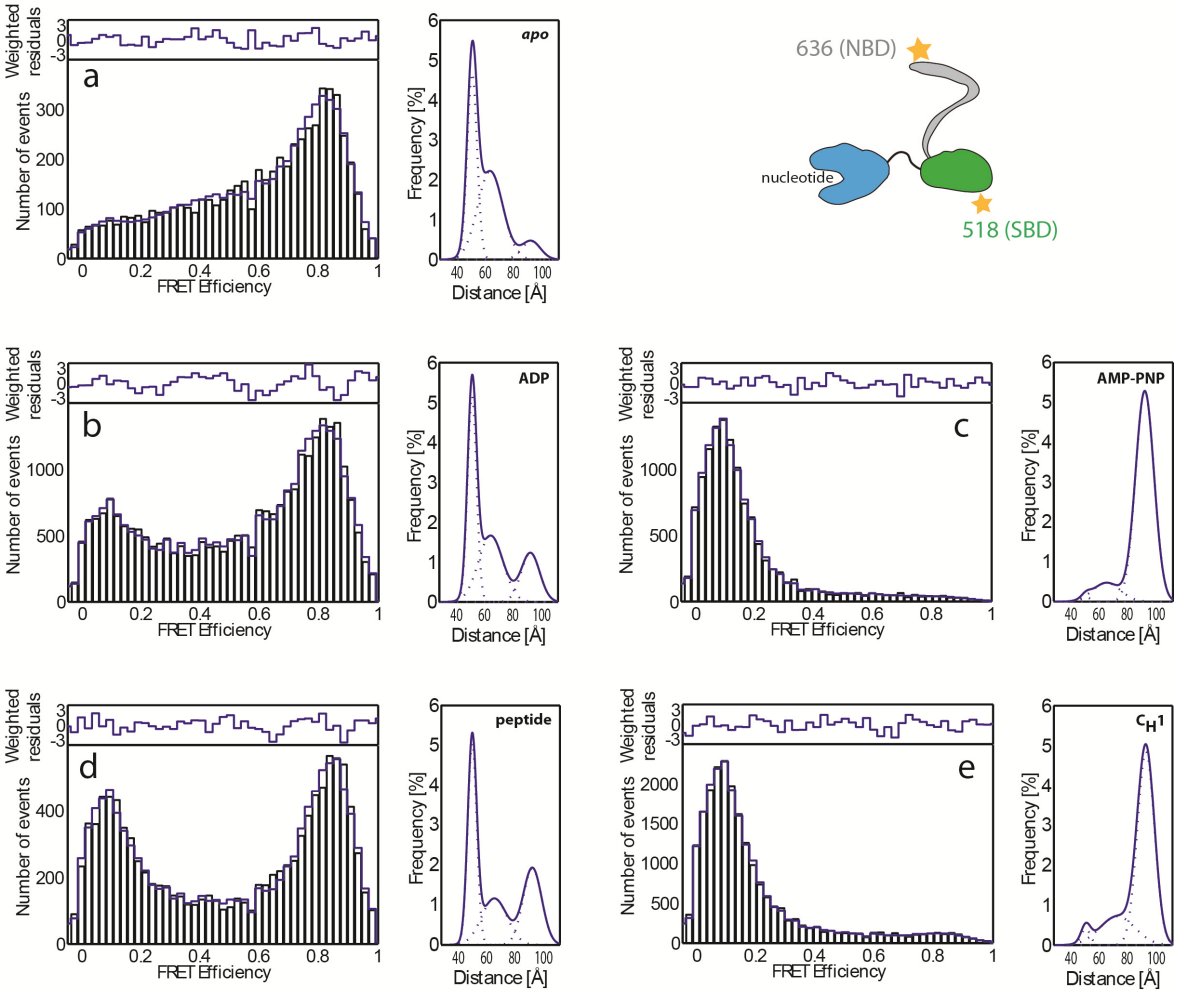


**Figure 37**
*Single pair FRET analysis of BiP 518/636 in the presence of nucleotides and substrates*. For the analysis of SBD/lid conformations, FRET efficiencies for the double-labeled BiP 518/636 construct (the labeling sites are shown in the schematic cartoon) were measured using single pair FRET experiments (a) in the absence of nucleotides, (b) in the presence of 1 mM ADP or (c) 1 mM AMP-PNP or for the complex of BiP 518/636 with (d) the HTFPAVL peptide and (e) the murine $C_H1$ domain formed in the presence of 1 mM ADP prior to the measurements. Sample preparation with substrates was performed under high substrate excess during the incubation as well as in the dilution steps necessary for the single pair FRET experiments immediately prior to the measurement. The bars indicate the number of events for the FRET efficiency and the line represents the result from the PDA. The reduced residuals are shown in the upper panel. The plot on the right shows the distance distribution determined using PDA. Adopted from (Marcinowski et al., 2011).

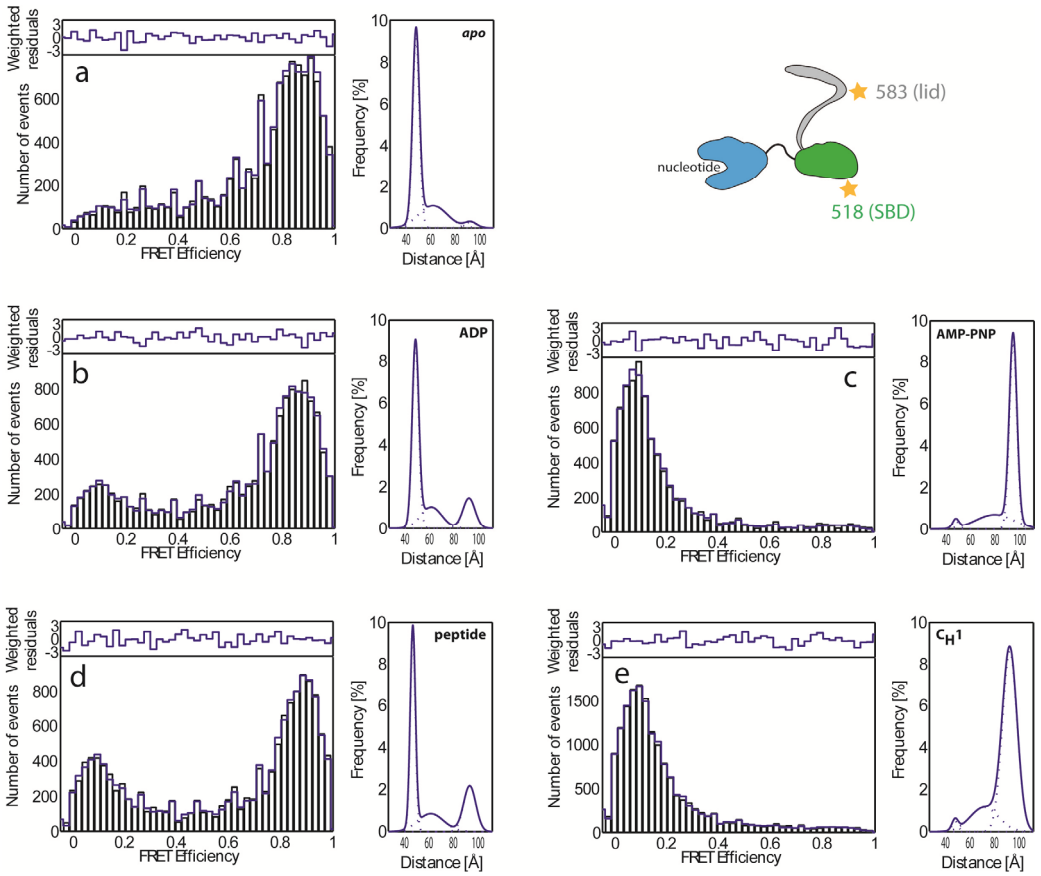


**Figure 38**
*Single pair FRET analysis of BiP 518/583 in the presence of nucleotides and substrates*. For the analysis of SBD/lid conformations, FRET efficiencies for the double-labeled BiP 518/583 construct (the labeling sites are shown in the schematic cartoon) were measured using single pair FRET experiments (a) in the absence of nucleotides, (b) in the presence of 1 mM ADP or (c) 1 mM AMP-PNP or for the complex of BiP 518/583 with (d) the HTFPAVL peptide and (e) the murine $C_H1$ domain formed in the presence of 1 mM ADP prior to the measurements. Sample preparation with substrates was performed under high substrate excess during the incubation as well as in the dilution steps necessary for the single pair FRET experiments immediately prior to the measurement. The bars indicate the number of events for the FRET efficiency and the line represents the result from the PDA. The reduced residuals are shown in the upper panel. The plot on the right shows the distance distribution determined using PDA. Adopted from (Marcinowski et al., 2011).

Distances for the spFRET experiments were calculated by Matthias Höller (LMU) using the Photon Distribution Analysis (PDA) with one to three Gaussian distributions of donor-acceptor distances and, when necessary, a small fraction of a zero-FRET (donor-only) species (see Table 3).

| | | Subpopulation 1 | | | Subpopulation 2 | | | Subpopulation 3 | | | Donor only | |
|---|---|---|---|---|---|---|---|---|---|---|---|---|
| | | % | d (Å) | σ (Å) | % | d (Å) | σ (Å) | % | d (Å) | σ (Å) | % | $\chi^2$ |
| **166/518** | apo | 97.0 | 66 | 12 | - | - | - | - | - | - | 3.0 | 2.00 |
| **166/518** | ADP | 96.4 | 67 | 8 | - | - | - | - | - | - | 3.6 | 4.80 |
| **166/518** | AMP-PNP | 30.9 | 75 | 14 | 66.5 | 58 | 5 | - | - | - | 2.6 | 2.29 |
| **166/518** | ADP/Peptide | 95.3 | 66 | 8 | - | - | - | - | - | - | 4.7 | 2.59 |
| **166/518** | ADP/$C_H1$ | 30.5 | 75 | 13 | 66.7 | 58 | 5 | - | - | - | 2.7 | 1.59 |
| **166/518** | ERdJ3/apo | 95.5 | 69 | 11 | - | - | - | - | - | - | 4.5 | 1.87 |
| **166/518** | ERdJ3/ADP | 46.9 | 70 | 13 | 48.9 | 57 | 5 | - | - | - | 4.2 | 1.06 |
| **166/518** | ERdJ3/AMP-PNP | 42.4 | 73 | 11 | 55.7 | 58 | 5 | - | - | - | 1.9 | 0.92 |
| **166/518** | ERdJ3/ATP | 26.2 | 73 | 14 | 72.4 | 57 | 5 | - | - | - | 1.4 | 1.52 |
| **166/518** | ERdJ3 domain/ADP | 96.1 | 68 | 8 | - | - | - | - | - | - | 3.9 | 6.35 |
| **166/518** | ERdJ3 QPD / ADP | 37.3 | 72 | 11 | 60.8 | 58 | 4 | - | - | - | 1.9 | 1.50 |
| **166/518** | ERdJ3/$C_H1$/ATP | 58.8 | 70 | 11 | 36.9 | 56 | 3 | - | - | - | 4.3 | 0.72 |
| **518/636** | apo | 7.7 | 90* | 7* | 41.0 | 48 | 4 | 50.0 | 61 | 9 | 1.3 | 1.36 |
| **518/636** | ADP | 20.4 | 90* | 7* | 41.4 | 49 | 3 | 36.7 | 62 | 9 | 1.5 | 2.77 |
| **518/636** | AMP-PNP | 87.3 | 90 | 7 | 0.9 | 48* | 3* | 11.8 | 63 | 10 | 0.0 | 1.03 |
| **518/636** | ADP/Peptide | 31.8 | 90* | 7* | 40.6 | 47 | 3 | 26.4 | 63 | 9 | 1.1 | 1.85 |
| **518/636** | ADP/$C_H1$ | 74.1 | 91 | 6 | 3.4 | 48* | 3* | 22.5 | 71 | 13 | 0.0 | 1.78 |
| **518/636** | ERdJ3/apo | 9.0 | 94* | 8* | 47.6 | 49 | 4 | 42.7 | 63 | 9 | 0.8 | 2.26 |
| **518/636** | ERdJ3/ADP | 78.5 | 93 | 8 | 4.5 | 49* | 4* | 17.0 | 64 | 9 | 0.0 | 1.77 |
| **518/636** | ERdJ3/AMP-PNP | 74.9 | 95 | 9 | 3.7 | 49* | 4* | 21.4 | 68 | 11 | 0.0 | 1.82 |
| **518/636** | ERdJ3/ATP | 78.8 | 94 | 8 | 2.3 | 49* | 4* | 18.9 | 67 | 12 | 0.0 | 1.26 |
| **518/636** | ERdJ3 domain/ADP | 12.6 | 90* | 8 | 50.5 | 49 | 3 | 36.2 | 64 | 10 | 0.7 | 3.00 |
| **518/636** | ERdJ3 QPD / ADP | 75.6 | 93 | 6 | 3.4 | 48* | 3 | 21.0 | 68 | 11 | 0.0 | 8.85 |
| **518/636** | ERdJ3/$C_H1$/ADP | 67.6 | 87 | 6 | 5.5 | 48* | 5 | 26.9 | 66 | 10 | 0.0 | 4.07 |
| **518/583** | apo | 3.6 | 91* | 5* | 64.1 | 47 | 3 | 31.5 | 60 | 12 | 0.7 | 1.03 |
| **518/583** | ADP | 18.4 | 90 | 5* | 59.2 | 47 | 3 | 22.3 | 60 | 9 | 0.1 | 1.05 |
| **518/583** | AMP-PNP | 69.9 | 93 | 3 | 2.7 | 46* | 3* | 27.4 | 78 | 16 | 0 | 1.77 |
| **518/583** | ADP/Peptide | 27.4 | 92 | 5* | 50.3 | 45 | 2 | 22.4 | 60 | 11 | 0 | 1.85 |
| **518/583** | ADP/$C_H1$ | 77.9 | 91 | 6 | 1.9 | 46* | 3* | 20.3 | 70 | 12 | 0 | 1.49 |

**Table 3**
*Photon distribution analysis*. The photons from an individual burst were divided into 1 ms time bins and the respective FRET efficiencies summed up in a histogram. The results were each fit using the Photon Distribution Analysis (PDA) with one to three Gaussian distributions of donor-acceptor distances and, when necessary, a small fraction of a zero-FRET (donor-only) species (due to blinking and photobleaching of the acceptor within a time bin, which it is not possible to remove completely even with pulsed-interleaved excitation). For each distribution, the respective population number (%), peak distance (d), and distribution width (σ) are given. An asterisk (*) indicates that the respective value had been fixed. Fit parameters were fixed when it was apparent that the data could be fit consistently with the same distributions determined in the presence of other factors but the width and/or relative population of the distribution was not sufficient for determining these values unambiguously. In some cases, a third subpopulation was necessary to describe the data. However, due to the broad FRET distributions, it was difficult to determine the third subpopulation with high precision and hence, the results are shown in grey. Adopted from (Marcinowski et al., 2011).

## 6.10 The role of ERdJ3 in the chaperone cycle of BiP

The BiP co-chaperone ERdJ3 is a member of the J-domain protein family and is a major co-chaperone of BiP in the folding of IgG. It was shown to stimulate BiPs ATPase activity moderately and to bind and transfer substrates to BiP (Jin et al., 2009; Shen and Hendershot, 2005). However, little is known about the mechanistic aspects of ERdJ3 in this complex. Hence, substrate binding, nucleotide dependent binding to BiP and the influence of ERdJ3 on BiP's conformation were analyzed. The purification and basic characterization of the non-glycosylated and refolded ERdJ3 is shown in section 6.1.3 and 6.2.3.

### 6.10.1 The interaction of ERdJ3 with murine $C_H1$ and BiP

The co-chaperone ERdJ3 of BiP was shown to bind substrates in its domains I and II and to deliver them to BiP. The IgG HC was shown to be an important substrate *in vivo* (Haas and Wabl, 1983). The unfolded $C_H1$ domain was used as a model for ERdJ3 binding and compared to the binding behavior of BiP. Additionally, the nucleotide dependency of ERdJ3 binding to BiP was assessed. Surface plasmon resonance (SPR) measurements were performed and evaluated kinetically. ERdJ3 forms complexes with the $C_H1$ domain characterized by fast $k_{on}$ = 1.2 ± 0.03 $\mu M^{-1}$ $min^{-1}$ and $k_{off}$ = 0.27 ± 0.07 $min^{-1}$ values in comparison to BiP as shown in Figure 39. The $K_d$ value was calculated as 0.2 µM revealing higher affinity of ERdJ3 for the $C_H1$ domain compared to BiP.

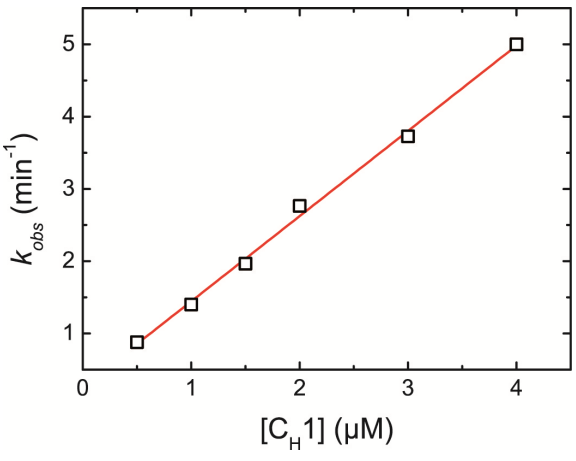


**Figure 39**
*Murine $C_H1$ binding to ERdJ3 as determined by SPR*. ERdJ3 was coupled to a CM5 SPR chip and varying concentrations of $C_H1$ were injected. The traces were fit single-exponentially to determine the time constants for binding and the resulting rate constants were plot against the $C_H1$ concentration. By linear regression, $k_{on}$ and $k_{off}$ were determined (30°C in HKM buffer at a flow rate of 20 µl/min and 35 µl samples were injected). Adopted from (Marcinowski et al., 2011).

### 6.10.2 ERdJ3 does not bind the same sites in $C_H1$ as BiP

J-proteins were reported to bind different sites in unfolded proteins then their Hsp70 counterparts. To test this hypothesis in the case of ERdJ3 and BiP, fluorescence anisotropy was measured with ERdJ3 and the peptides representing the high affinity binding sequences of BiP in the $C_H1$ domain. None of the tested peptides showed binding to ERdJ3 in the tested concentration range (20 µM ERdJ3 and 1 µM peptide). A representative experiment is shown for the HTFPAVL sequence in Figure 40.

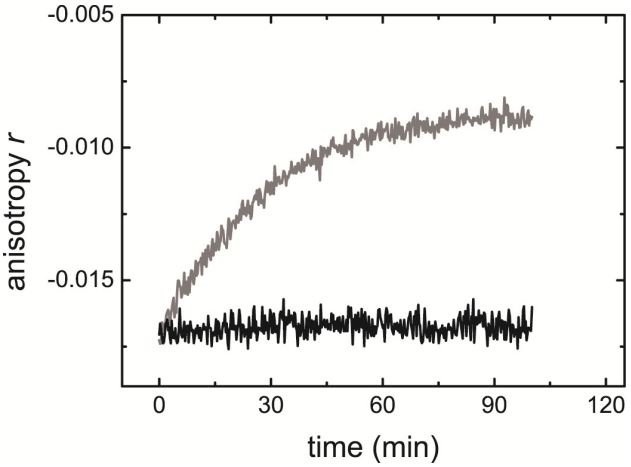


**Figure 40**
*HTFPAVL peptide binding by ERdJ3.* 1 µM HTFPAVLgsc-LY peptide was incubated with 20 µM ERdJ3 in HKM buffer at 37°C and the change in fluorescence anisotropy was followed (black). As a control, binding of 10 µM BiP was analyzed in the presence of 1 mM ADP (gray).

### 6.10.3 Nucleotide dependency of ERdJ3 binding to BiP

The binding of ERdJ3 to BiP was also analyzed by SPR experiments in the presence of either ADP or ATP to determine the high affinity state of BiP for ERdJ3 interaction. The observed rate constants were extracted from the SPR measurements with ERdJ3 coupled to the chip and BiP incubated with either 1 mM ATP or 1 mM ADP 15 minutes prior to the measurements. The evaluation showed a concentration-dependent association of ERdJ3 with BiP in the presence of ADP (Figure 41) with $k_{on}$ = 0.14 ± 0.008 $\mu M^{-1}$ $min^{-1}$ and $k_{off}$ = 0.77 ± 0.006 $min^{-1}$. In the presence of ATP, no concentration dependency was observed. The observed rate constant of ~ 1.0 $min^{-1}$ revealed a rate-limiting step for the association reaction, roughly similar to the ERdJ3-accelerated ATP hydrolysis of BiP under these conditions (Figure 41).

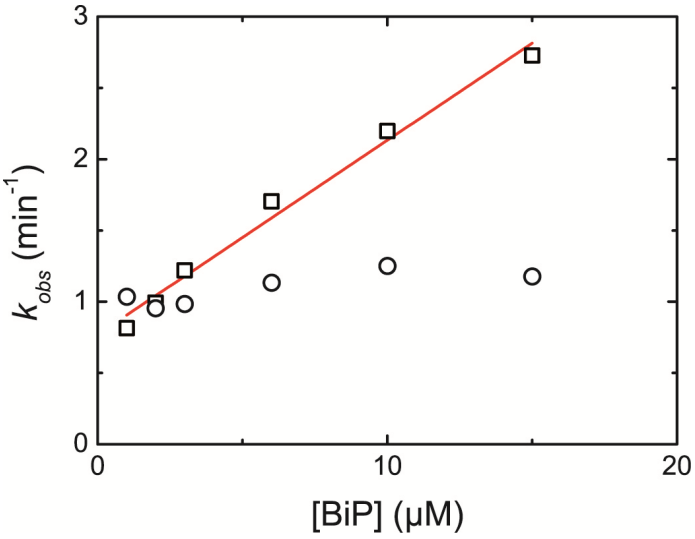


**Figure 41**
*Nucleotide-dependent BiP binding to ERdJ3 determined by SPR*. ERdJ3 was coupled to a CM5 SPR chip and varying concentrations of BiP pre-incubated with 5 mM ADP (open squares) or 5 mM ATP (open circles) were injected. The traces were fit single-exponentially to determine the time constants for binding and the resulting observed rate constants were plot against the BiP concentration. By linear regression, $k_{on}$ and $k_{off}$ were determined (30°C in HKM buffer at a flow rate of 20 µl/min and 35 µl samples were injected). Adopted from (Marcinowski et al., 2011).

These experiments indicate that ERdJ3 associates transiently with the ATP-bound state of BiP, accelerating the ATPase activity of BiP before forming stable complexes with BiP in the ADP-bound state.

### 6.10.4 spFRET analysis of the influence of ERdJ3 on BiP

To study the influence of ERdJ3 on the domain orientations of BiP, the established spFRET assay was used. For the *apo*- and ATP- or AMP-PNP-bound conformation of BiP, no influence upon the addition of ERdJ3 was observable. In contrast, as already indicated by the SPR measurements, ERdJ3 bound stably to the ADP-bound state of BiP and induced a looser contact between the NBD and SBD as well as an opening of the lid. These results were obtained for the 166/518 construct and the 518/636 construct, respectively (Figure 42 and data not shown).

The measurements revealed that ERdJ3 binds to the ADP-bound state of BiP and leads to an opening of the lid and a tighter contact of the NBD and SBD (Figure 42), a conformation similar to the $C_H1$-bound one. ERdJ3 binds to the NBD/SBD interface via a conserved HPD motif in its J-domain leading to the acceleration of BiP's ATPase (Shen and Hendershot, 2005). Although the isolated J-domain is sufficient to stimulate BiP's ATPase to a certain extent (1.5-fold, compared to 2.5-fold of the full length ERdJ3), the binding of the isolated J-

domain had no influence on BiP conformations in our spFRET setup irrespective of the nucleotide used (data not shown). This indicates that BiP conformations induced by full length ERdJ3 are not only the result of J-domain binding to the NBD/SBD interface but that an additional binding site exists.

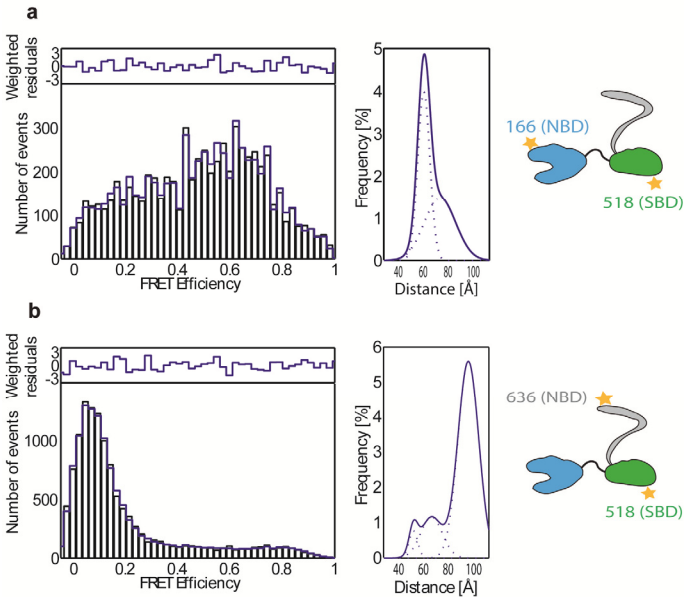


**Figure 42**
*Analysis of the influence of ERdJ3 on the conformation of BiP in the presence of ADP*. (a) double-labeled BiP 166/518 was used to investigate the NBD-SBD conformation and (b) double-labeled 518/636 to investigate SBD/lid conformations. Experiments were performed in the presence of 1 mM ADP in HKM. The bars indicate the number of events for the given spFRET efficiency and the line represents the result from the PDA. The reduced residuals are shown in the upper panel. The plots on the right show the distance distribution determined using PDA. Adopted from (Marcinowski et al., 2011).

Taken together, ERdJ3 seems to prime BiP for the protein accepting state, i.e. with an open lid, to allow more efficient binding besides the acceleration of BiP's ATPase activity to generate the ADP-bound high affinity state of BiP. However, a substrate-like binding of ERdJ3 to the cleft of the SBD cannot be ruled out and therefore a FRET assay was developed to monitor substrate binding by BiP directly.

### 6.10.5 A FRET assay to monitor $C_H1$ binding to BiP

The complex formation of $C_H1$ and BiP was monitored in an ensemble FRET assay. The murine $C_H1$ domain was labeled *via* an artificially introduced cysteine at the N-terminus with Atto647 as acceptor dye and the single cysteine mutant 636 of BiP with Atto532 as donor dye. Complex formation was monitored by changes in the fluorescence of the donor dye.

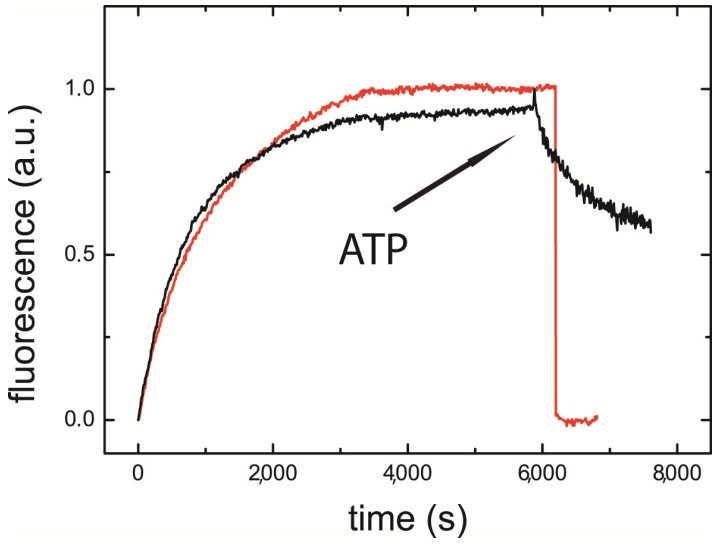


**Figure 43**
*Ensemble FRET measurements of BiP-$C_H1$ complex formation.* Experiments were performed at 37°C with 2 µM BiP 636 labeled with Atto532 and 3 µM $C_H1$ N-Cys labeled with Atto647 in the presence of 1 mM ADP. Binding was monitored In the absence (red; $k_{obs}$ = 0.05 $min^{-1}$) and presence of 5 µM ERdJ3 (black; $k_{obs}$ = 0.07 $min^{-1}$). After reaching equilibrium, ADP was converted into by addition of phosphoenolpyruvate and pyruvate kinase. (Adopted from (Marcinowski et al., 2011)).

As depicted in Figure 43, complex formation of the murine $C_H1$ domain and BiP could be monitored by the ensemble FRET assay in the presence of 1 mM ADP. Upon the enzymatic conversion of ADP to ATP, the complex dissociated very fast as already observed for the dissociation of the BiP-peptide complex (see section 6.5). Binding of $C_H1$ to BiP was slightly diminished in the presence of ERdJ3 but association kinetics were 1.5-fold accelerated. This indicates that ERdJ3 can transfer the bound $C_H1$ domain to BiP, accelerating binding to the ADP-bound state of BiP. This finding is in good agreement with the SPR measurements which showed a concentration-dependent association of ERdJ3 to ADP-bound BiP (see section 6.10.3). Interestingly, the dissociation of the complex by ATP was hampered in the presence of ERdJ3. The $C_H1$ domain dissociated slowly and not completely from BiP indicating a stabilizing effect of ERdJ3 on the $C_H1$-BiP complex (Figure 43). The influence of ERDJ3 on binding of $C_H1$ to BiP was further analyzed in the presence of ATP allowing the complete hydrolysis cycle of BiP to proceed. Under the investigated conditions, no complex formation was observable in the absence of ERdJ3. Additionally, the mutant of ERdJ3 with the HPD motif in the J-domain exchanged against QPD had no influence on binding, as the ATPase activity of BiP cannot longer be stimulated by the J-domain of ERdJ3. In contrast, addition of wild type ERdJ3 allowed efficient complex formation in the presence of ATP. Interestingly, binding of $C_H1$ to BiP is faster in the presence of ATP then with ADP and is in the range of the rate constant for ATP hydrolysis under the investigated conditions (see Figure 44).

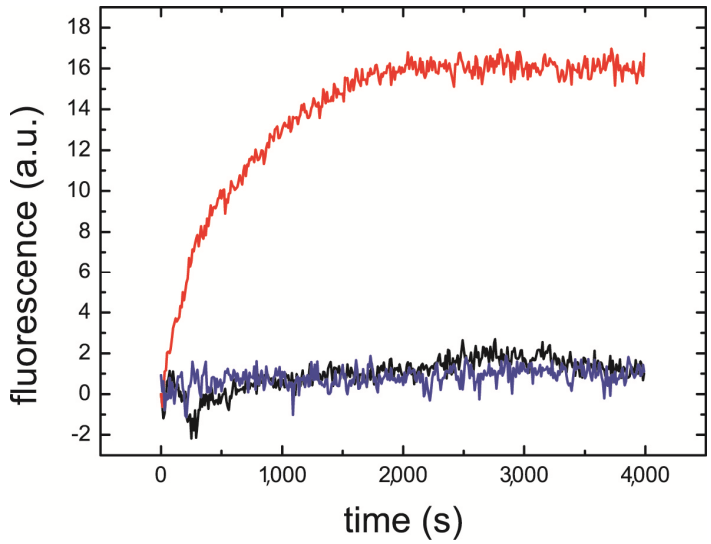


**Figure 44**
*Ensemble FRET measurements of BiP-$C_H1$ complex formation.* Experiments were performed at 37°C with 2 µM BiP 636 labeled with Atto532 and 3 µM $C_H1$ N-Cys labeled with Atto647. Complex formation was studied in the presence of 1 mM ATP without ERdJ3 (black), with 5 µM ERdJ3 (red; $k_{obs}$ = 0.1 $min^{-1}$) or with 5 µM ERdJ3-QPD (blue) added. Adopted from (Marcinowski et al., 2011)

Together with the SPR and spFRET data, a possible mechanism for the modulation of BiP by ERdJ3 is suggested. ERdJ3 interacts transiently with the ATP-bound state of BiP and accelerates hydrolysis. After hydrolysis, ERdJ3 forms stable complexes with BiP. If the $C_H1$ domain is present, ERdJ3 efficiently transfers it to BiP in the presence of ATP with only a minor acceleration of binding in the ADP-bound state of BiP. The question whether transfer occurs during or after the hydrolysis of ATP by BiP cannot be answered by the set of experiments performed. As ERdJ3 binding to the ADP-bound state of BiP leads to an opening of the lid, the question arose whether this has functional implications, as the conformation highly resembles the $C_H1$-bound one of BiP (see section 6.9.2). If this were the case, the efficient transfer of $C_H1$ from ERdJ3 to BiP is achieved by ERdJ3 priming the conformation of BiP for the protein substrate accepting state.

As the substrate peptide is bound to BiP with the lid in a closed conformation we tested on the influence of ERdJ3 on peptide binding.

### 6.10.6 Peptide binding to BiP in the presence of ERdJ3

The influence of ERdJ3 on peptide binding to BiP was analyzed by fluorescence anisotropy with the HTFPAVL sequence with a C-terminal GSC linker added for labeling with lucifer

yellow. Complex formation was analyzed in the presence, absence or after addition of ERdJ3 to pre-formed complexes. The experiments revealed an inhibitory effect of ERdJ3 on peptide-BiP association. Importantly, ERdJ3 does not bind the HTFPAVL peptide and therefore does not compete with BiP for the substrate (see section 6.10.2). Upon addition of ERdJ3, complex formation of the peptide with BiP is slower and less efficient then in the absence as shown in Figure 45.

Furthermore, ERdJ3 does not only suppress peptide binding if added together with BiP but is also able to dissociate pre-formed complexes if added after reaching equilibrium.

These findings support the model of ERdJ3's function as shown for binding of the $C_H1$ domain. As it primes the lid in its open conformation, peptide binding is reduced as the peptide is bound in the closed lid conformation of BiP and therefore binds less efficient if ERdJ3 is present. However, a substrate-like recognition of ERdJ3 cannot completely be ruled out but as $C_H1$ binding in its presence is more efficient it does not seem likely.

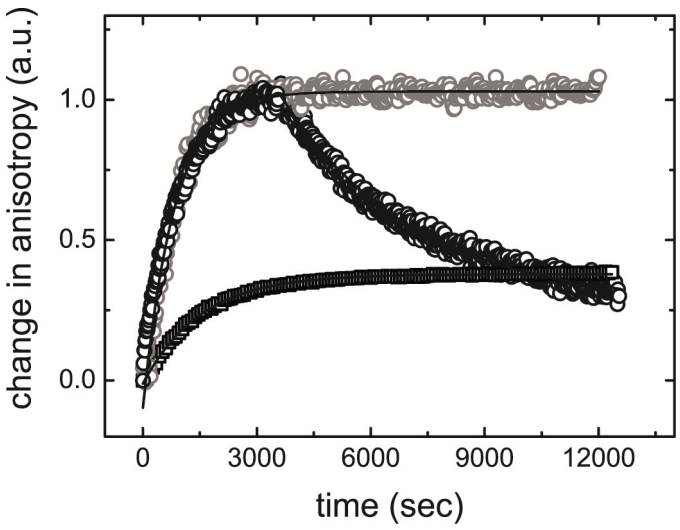


**Figure 45**
*The influence of ERdJ3 on peptide binding by BiP.* Peptide binding to 5 µM BiP was analyzed by the change in anisotropy of 1 µM lucifer yellow labeled HTFPAVL peptide with 1 mM ADP in the absence (open gray circle) of ERdJ3, in the presence of 7.5 µM ERdJ3 (open black squares) and upon addition of 7.5 µM ERdJ3 after complex formation (open black circle).

# 7 Discussion

## 7.1 $C_H1$ binding by BiP

The $C_H1$ domain was identified as the major BiP binding site in heavy chains (HCs) of IgG *in vivo* (Lee et al., 1999; Haas and Wabl, 1983; Bole et al., 1986). The *in vitro* reconstitution revealed stable complex formation of an isolated human $C_H1$ domain with a concentration-dependent $k_{on}$ and a slow $k_{off}$ rate. The kinetic parameters, as well as a $K_d$ value in the low µM range ($K_d$ = 12.6 ± 0.7 µM), are in good agreement with the previously addressed binding of a murine $C_H1$ domain to BiP ($K_d$ = 12.9 ± 1.1 µM, $k_{off}$ = 0.01 ± 0.002 $min^{-1}$ and $k_{on}$ = 0.001 ± 0.0002 $\mu M^{-1} min^{-1}$) (Feige et al., 2009). Taken together, a moderate affinity and concentration-dependent $k_{on}$ and slow $k_{off}$ rates seem to be a general feature of $C_H1$ domains from different organisms. Whether this holds also for other IgG subtypes and even other Ig isoforms is not clear yet. The determined kinetic parameters allow a description of the interaction of the $C_H1$ domain and BiP in the endoplasmic reticulum (ER). BiP is part of the SEC-translocon and already interacts co-translationally with nascent chains (Brodsky et al., 1995; Alder et al., 2005). Hence, the local concentration at the SEC-translocon is high and efficient binding of the $C_H1$ domain by BiP occurs. After binding, stable complexes of $C_H1$ and BiP are formed with low dissociation rates ($k_{off}$ ~0.01 $min^{-1}$) clearly favoring the bound state. However, no cycling of HCs from BiP is observed *in vivo* and additional factors further stabilizing the complex might be involved (Vanhove et al., 2001). A good candidate for this task is the lumenal J-domain co-factor of BiP, ERdJ3. The function and effects of ERdJ3 on BiP and $C_H1$ will be discussed in more detail in section 7.5.

## 7.2 High affinity binding sites for BiP in $C_H1$

The $C_H1$ domain is unfolded in the absence of its cognate partner domain $C_L$ and the high affinity binding sites in the context of the complete $C_H1$ domain were unknown so far. Analysis of $C_H1$ binding sites for BiP was so far only performed at the peptide level. A scoring algorithm had been developed based on phage display and the ATPase stimulation rates of BiP, identifying hydrophobic residues as important elements for BiP binding (Gething et al., 1995; Knarr et al., 1995; Knarr et al., 1999; Blond-Elguindi et al., 1993). Importantly, this does not only hold for BiP but was also for other members of the Hsp70 family (Rudiger et al., 1997; Pandya et al., 2009; Gragerov and Gottesman, 1994). However, a detailed analysis of the features of substrates, especially of those important for stable

complex formation and not only transient interaction with BiP is missing as well as the comparison of binding sites on the peptide and protein level. Hence, the $C_H1$ domain and peptides derived thereof were analyzed in this work. In previous studies, several peptides derived of all Ig domains were identified to stimulate BiP's ATPase, as an indirect proof of binding (Knarr et al., 1995). Within the $C_H1$ domain, five sites were shown to stimulate BiP's ATPase with the SVFPLAP and HTFPAVL sequences showing highest stimulation rates (Knarr et al., 1995). Hence, mutants to abolish BiP binding were generated in this work and targeted these two sequences. Interestingly, the two binding sites could compensate for each other in the case of single mutants with only minor effects on the affinity of BiP, indicating that both are recognized alternatively by BiP. In contrast, the mutation of both binding sites abolished BiP binding under the tested conditions. It should be noted that an influence of the internal disulphide bridge cannot be ruled out, as the reduced human $C_H1$ is aggregation-prone and could therefore not be analyzed.

The two identified stretches share interesting features. Both are part of the interface with the $C_L$ domain, once $C_H1$ is folded (see Figure 46). This finding explains the absence of $C_H1$:BiP:$C_L$ triple complexes *in vitro* and *in vivo* as BiP and $C_L$ compete for the same stretches in $C_H1$ causing either retention in the ER (interaction with BiP) or association-coupled folding (interaction with $C_L$) of the $C_H1$ domain. Additionally, the His residue of the HTFPAVL binding site was shown to be part of the encounter complex of the $C_H1$ domain with $C_L$ already possessing a native-like environment at this early stage of assembly-coupled folding of $C_H1$.

Importantly, the two binding sites are also highly conserved among $C_H1$ domains of different IgG subclasses and to certain extent in the other Ig isoforms as shown in the sequence alignment in Figure 47.

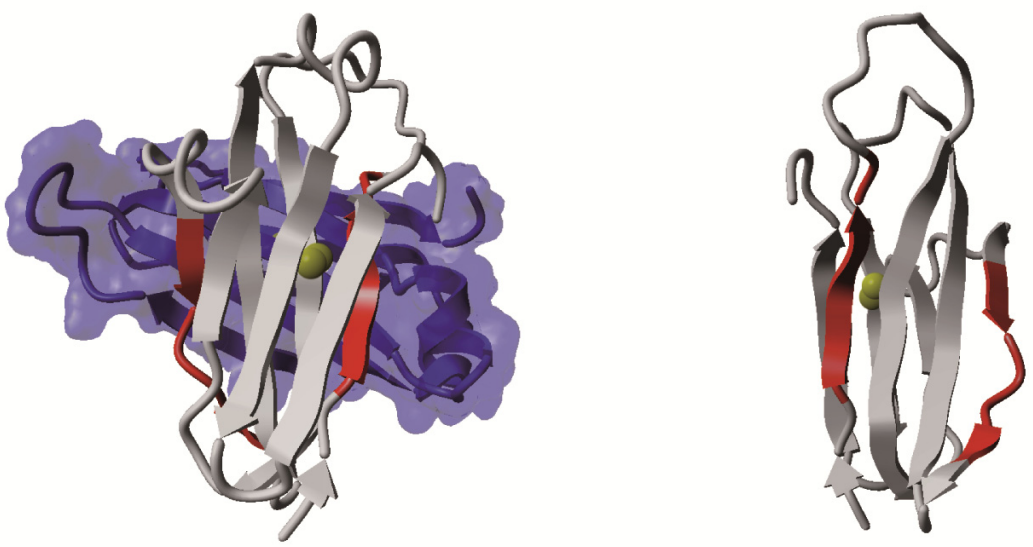

**Figure 46**
*BiP binding sites in $C_H1$*. BiP binding sites are highlighted in red in the $C_H1$ domain (gray). The left panel shows their location in the interface with the $C_L$ domain (blue) while the right panel shows the 180° view on the $C_H1$ domain. The disulphide bridges are given as yellow balls. Figure drawn from PDB code 12E8.

On the amino acid level, both identified stretches also share identical residues. An aromatic Phe residue is located at position 3 of both sequences, conferring a high degree of hydrophobicity to the stretches. The Phe is followed by a Pro residue in both cases and the central motif is flanked by further hydrophobic residues. The two point mutations identified in this work differ in their mode of action. While the SVFPLAP binding site could only be suppressed on the protein and peptide level by a mutation of the Phe residue to Lys, a Pro to Ala exchange in the HTFPAVL site was sufficient to suppress binding to BiP. This finding led to the hypothesis that further elements than hydrophobicity might be involved in the recognition of substrates by BiP. Pro is known to populate either a *cis* or *trans* conformation in the peptide backbone resulting in a more (*cis*) or less (*trans*) kinked conformation of the peptide backbone (Fischer et al., 1998). Additionally, Pro adds a higher rigidity to the surrounding backbone residues. As for the HTFPAVL binding site a Pro to Ala exchange abolished BiP binding, a synthetic chemistry approach was chosen to test whether the conformation of the peptide is important. Either kinked or extended backbones were populates by the introduction of non-proteinogenic amino acids at the Pro position. Additionally, the plasticity of BiP's binding groove was explored by the insertion of different side chain lengths.

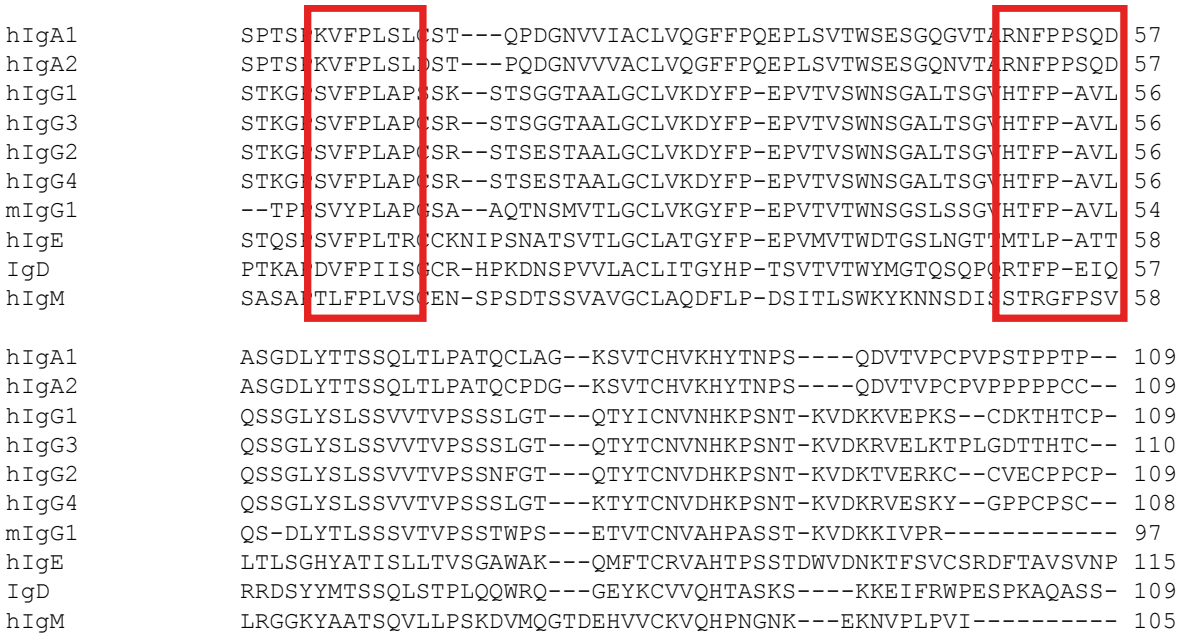


**Figure 47**
*Sequence alignment of Ig $C_H1$ domains.* Sequences of human Ig $C_h1$ and the murine Mak33 IgG1 domains were aligned using the clustalW tool. The two in IgG1 identified BiP binding sites are boxed in red.

## 7.3 Conformational selectivity of BiP

To test for the conformational selectivity of BiP for substrates, competition experiments of wild type BiP:HTFPAVL complexes with peptides containing non-proteinogenic amino acid substituents were analyzed. These experiments revealed that an exchange of the central Pro residue in the HTFPAVL motif against 1,4-aminobenzoic acid was comparable in its dissociation efficiency to the wild type sequence. In contrast, the 5-dimethyl-4-oxaproline substituent showed no displacement of the wild type peptide indicating abolished binding to BiP. As 1,4-aminobenzoic acid leads to the formation of an extended conformation within the peptide and 5-dimethyl-4-oxaproline to a stably kinked conformation, BiP seems to favor extended conformations over kinked ones. Interestingly, in X-ray structures of BiP homologues such as the bacterial DnaK the substrate peptide is also bound in a highly extended conformation in the substrate binding groove (Zhu et al., 1996; Pellecchia et al., 2000).

Upon the introduction of different side chain lengths at the additional amino group of 1,3-aminobenzoic acid, surprising results were obtained. While the rather short aliphatic propinyl substituent could not displace the wild type peptide, the large triple-ring aromat Fmoc could. This indicates a high plasticity of BiP's substrate binding groove for aromatic

residues although secondary effects as binding of the Fmoc entity on top or beside the binding groove cannot be ruled out. MD simulations and molecular docking might give a more detailed explanation of the plasticity of the binding groove of BiP.

## 7.4 The chaperone cycle of BiP and the role of the lid

The chaperone cycle of Hsp70s in general is regulated by the binding of ATP and its subsequent hydrolysis in the nucleotide binding domain (NBD). The ATP-bound state shows low substrate affinity, while ADP leads to efficient substrate binding (Goloubinoff and De los, 2007; Woo et al., 2009). The information of the bound nucleotide is transferred to the substrate binding domain (SBD) via a hydrophobic linker connecting both domains (Swain et al., 2007; Vogel et al., 2006). For bacterial DnaK, binding of ATP was reported to result in a close contact between the NBD and SBD while ADP loosens the contact (Bertelsen et al., 2009). However, a detailed analysis of the conformational changes within Hsp70s especially also including the lid domain is missing. Hence, a single particle FRET (spFRET) approach was followed in this thesis in collaboration with the group of Don Lamb (Ludwig-Maximilians-Universität, München) to dissect the conformational changes within BiP upon nucleotide and $C_H1$ vs. peptide binding. Two artificial Cys residues were introduced in the NBD, SBD or at two positions in the lid. Combination of two of these residues labeled with donor and acceptor dyes allowed the analysis of the distances between the corresponding domains. Importantly, the deletion of the two native Cys, the introduction of the new Cys and labeling with the dyes, had no influence on ATP hydrolysis and substrate binding by BiP.

For the NBD/SBD-labeled construct 166/518, the same domain orientations were observed as for DnaK upon nucleotide binding. Surprisingly, binding of $C_H1$ and the HTFPAVL peptide derived from the $C_H1$ domain had a controversial effect. While the peptide bound to BiP in the ADP-state showed no differences to the ADP-only state, binding of the $C_h1$ domain resulted in a tighter domain contact then the ADP-only state of BiP.

This effect was also observed for the domain distances between the SBD and the C-terminus of the lid (518/636). In general, the lid adopts three different conformations and the most prominent is discussed. The lid was in an open conformation upon ATP binding while ADP binding led to closing of the lid on top of the SBD. This was also found for the peptide bound to the ADP-state of BiP. This finding is in good agreement with X-ray structures of the isolated SBD of the homologue DnaK complexed with a substrate peptide. In this

structure, the lid closes on top of the SBD when the peptide is bound in the substrate binding groove (Zhu et al., 1996; Pellecchia et al., 2000). Additionally, a single molecule study on the mitochondrial Hsp70 showed the closing of the lid in the ADP and ADP/peptide-bound conformation (Mapa et al., 2010).However, binding of the $C_H1$ domain leads to an opening of the lid again adopting an antithetic conformation to the peptide bound form of BiP. The lid was in close contact with the bound $C_H1$ domain and might even interact physically with the bound $C_H1$ domain as shown by the crosslink between $C_H1$ and the C-terminus of the lid. An analysis of the dynamics of the system was not possible by the chosen approach and transient interactions cannot be ruled out if the lid is dynamic in the adopted conformations. Nevertheless, the additional interaction of the lid with parts of the bound substrate fits to the observation of 1:1 stochiometric complexes of BiP and $C_H1$ although two heptameric binding sites are found within the domain.

Different modes of actions are discussed for the lid function. On the one side, a sequential model with the different helices of Hsp70s moving independently and on the other hand a concerted mechanism has been suggested (Zhu et al., 1996; Mayer et al., 2000). The finding that the labeling position at the end of Helix A showed the same behavior in the distances to the SBD (518/583) then the C-terminal labeling position of the lid (518/636) strongly supports the notion that the lid acts as an entity. Hence, the correlated conformational changes between the NBD and SBD domains and the lid might be seen as a relay mechanism for the coupling of the ATPase activity of the NBD to substrate binding in the SBD.

The conformational cycle of BiP is depicted in Figure 48, highlighting the different conformations of BiP upon peptide or $C_H1$ binding. The apo- and ADP-bound and peptide-bound conformation of BiP are highly similar with a predominantly closed lid and a loose SBD/NBD contact. Upon binding of ATP the lid opens and the NBD/SBD come into close contact. Importantly, the $C_H1$ domain is bound in a conformation with an open lid and close NBD/SBD contact and the lid is in contact with the $C_h1$ domain. Hence, BiP acts as a tripartite machine and discriminates between protein and peptide substrates.

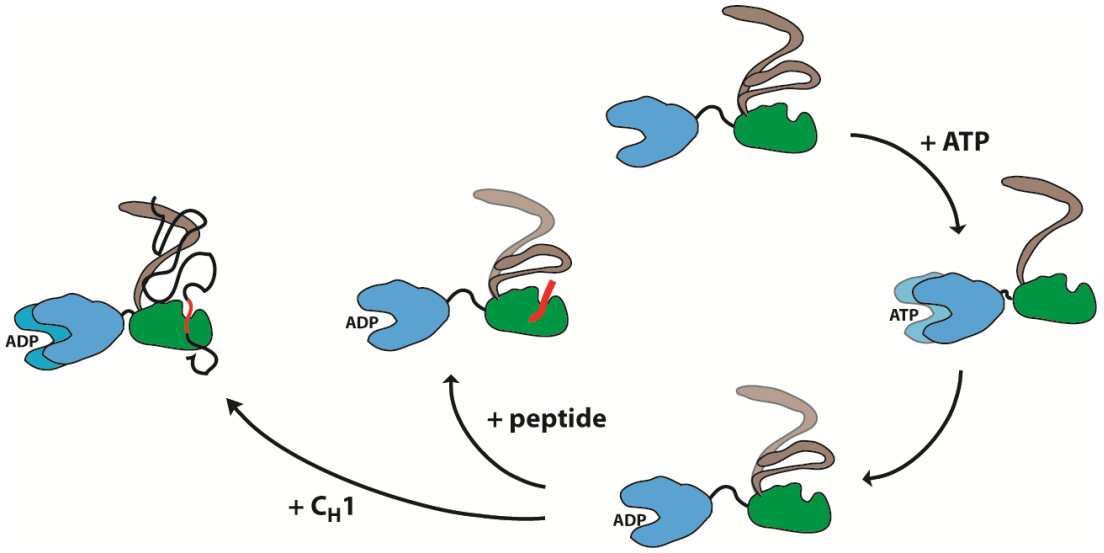


**Figure 48**
*A model for BiPs chaperone cycle and substrate discrimination*. The NBD is color-coded in blue, the SBD β-sandwich in green and the lid in grey. For multiple domain conformations, both are shown with the predominant conformation in the darker color. The interdomain distance of BiP changes upon binding of ADP or ATP. In the ATP-bound state, the NBD/SBD distance shows variations, whereas the lid is flexible in the *apo*- or ADP-bound state. The peptide is bound in the presence of ADP in a conformation similar to the ADP-only state whereas binding of the $C_H1$ domain leads to a widely opened lid and a tighter NBD/SBD coupling. Additionally, the lid interacts with the bound protein.

Having identified the lid as an important control element, deletion studies were performed and their influence on peptide and $C_H1$ binding was tested. For DnaK, higher $k_{on}$ and $k_{off}$ rates had been described for the lid deletion mutants (Buczynski et al., 2001) as well as a stabilizing effect on the SBD (Moro et al., 2004). Additionally, mutations in the lid increased the chaperone activity of DnaK (Aponte et al., 2010). In contrast, the *in vivo* analysis of the *S. cerevisiae* orthologue Kar2p of BiP and the mitochondrial mtHsp70 showed growth and import defects (Strub et al., 2003; Tokunaga et al., 1998). The partial deletion of BiP's lid resulted in a complete loss of substrate binding. However, the complete deletion, resulting in a lidless SBD, caused efficient peptide as well as $C_H1$ binding with increased affinity. This finding might argue that a partial deletion leads to unfolding of the lid and subsequent self-binding in the substrate binding groove of BiP blocking it for substrates. This notion is in agreement with an X-ray structure of bovine cytosolic Hsc70 where a truncated lid is bound in the binding groove of the SBD (Jiang et al., 2006).

Taken together, the lid was identified as an important regulatory element for the discrimination of peptide and protein substrates but it is dispensable for the binding of the isolated SBD to substrates.

## 7.5 The role of ERdJ3

ERdJ3 was reported to stimulate BiP's ATPase and to actively bind and transfer substrates to BiP (Jin et al., 2009; Shen and Hendershot, 2005). ERdJ3 is a member of the DnaJ type I family as it harbors an N-terminal J-domain, followed by a Gly/Phe-rich domain, a Cys domain, a domain I and II and a C-terminal dimerization domain. In contrast to cytosolic members of this family, ERdJ3 does not complex a $Zn^{2+}$ ion in its Cys domain but forms two internal disulphide bridges. Hence, soluble production of ERdJ3 was not possible in *E. coli* and refolding conditions were screened in collaboration with Danae Baerend, TU München. Successful refolding was confirmed by CD spectroscopy and a stimulation rate of ~2.5-fold of BiP's ATPase as reported for ERdJ3 purified from human cell culture (Jin et al., 2009; Shen and Hendershot, 2005).

ERdJ3 was shown to bind substrates in its domains I and II and to transfer them to BiP. ERdJ3 does not recognize the same binding sites as BiP as the $C_H1$-derived peptides of the high affinity binding sites for BiP showed no interaction with ERdJ3. This is also the case for the bacterial DnaK and its J-domain co-chaperone DnaJ (Rodriguez et al., 2008). Binding of the $C_H1$ domain was analyzed by surface plasmon resonance spectroscopy (SPR) and fast $k_{on}$ and $k_{off}$ rates were determined in comparison to BiP. The calculated $K_d$ value was also ~ 15-fold lower than for BiP. Hence, a kinetic model for the substrate transfer in the lumen is possible, with ERdJ3 binding with low affinity and fast $k_{on}$ rates to the $C_H1$ domain and transferring it to BiP which then forms stable complexes with $C_H1$.

To test for the interaction of ERdJ3 with BiP, nucleotide-dependent SPR experiments were performed. ERdJ3 only interacts transiently with BiP in the ATP-bound state as no concentration-dependency was observed and the observed rate constant was similar to the stimulated ATPase activity of BiP by ERdJ3. However, in the presence of ADP, or after hydrolysis, ERdJ3 formed stable complexes with BiP and showed concentration-dependent binding.

The substrate transfer efficiency of ERdJ3 to BiP was analyzed by an ensemble FRET assay. Binding of $C_H1$ to BiP was accelerated in the presence of ERdJ3 1.5-fold, while ERdJ3 exclusively allowed $C_H1$ binding to BiP if ATP was present. Interestingly, the fact that the dissociation of BiP:$C_H1$ was decreased in the presence of ERdJ3 indicates that triple complexes are forming and that ERdJ3 stabilizes the complex against dissociation. This finding is in good agreement with *in vivo* experiments were ERdJ3 is present and no cycling of heavy chains from BiP was observed (Vanhove et al., 2001).

The question how ERdJ3 achieves this modulation of BiP was answered by the spFRET assay. ERdJ3 induced no conformational changes in BiP in the absence of nucleotides or in the presence of ATP. Hence, the acceleration of BiP's ATPase is either not detectable with the chosen spectroscopic markers or too transient. In contrast, ERdJ3 caused major conformational changes of BiP in the ADP-bound state. The presence of ERdJ3 led to an opening of the lid and a tighter contact between the NBD and SBD of BiP. The observed conformations were highly similar to those of BiP in the $C_H1$-bound state. Therefore, a function for ERdJ3 is hypothesized in priming it for the protein substrate accepting state. Importantly, the conformation of BiP was not further altered upon the addition of $C_H1$. Additionally, the isolated J-domain of ERdJ3 and a mutant which is no longer able to bind to BiP via the conserved HPD motif (Tsai and Douglas, 1996; Shen and Hendershot, 2005) failed to induce these conformations. In order to test for the priming hypothesis, peptide binding to BiP was analyzed in the presence and absence of ERdJ3 as the peptide is bound in a conformation of BiP with a closed lid. Peptide binding to BiP was significantly reduced in the presence of ERdJ3 and the addition of ERdJ3 to pre-formed BiP:peptide complexes led to a partial release of the peptide from BiP, probably caused by an opening of the lid.

Taken together, ERdJ3 modulates the BiP chaperone cycle at several steps: ERdJ3 binds to substrate proteins with high affinity and a fast $k_{off}$ rate. ERdJ3 interacts transiently with BiP in the ATP state and stimulates BiP's ATPase activity. During or after the stimulated hydrolysis of ATP, the substrate protein is transferred to BiP and ERdJ3 concomitantly stabilizes the open lid conformation, which is required for efficient substrate protein binding (Figure 49). The chaperone cycle is completed by the exchange of ADP against ATP and the release of ERdJ3 and the bound substrate.

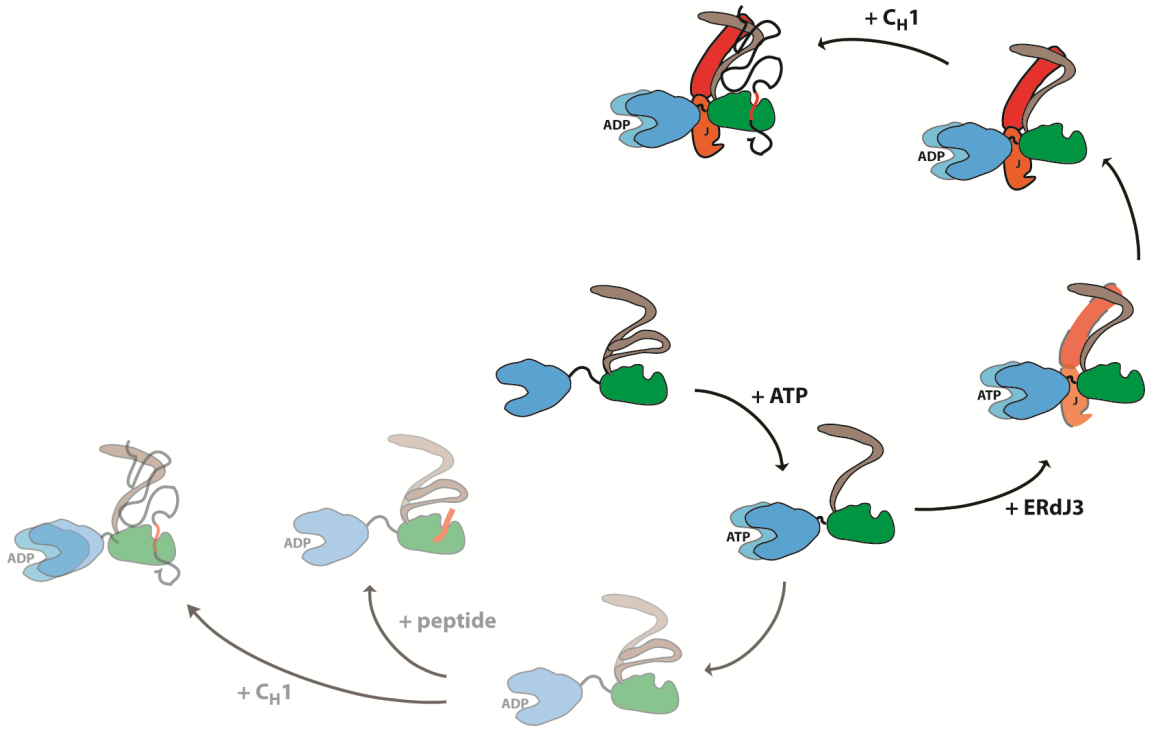


**Figure 49**
*A model for the modulation of BiP's chaperone cycle by ERdJ3*. The model for the chaperone cycle of BiP in the absence of ERdJ3 is shown in transparence (for information see Figure 48). ERdJ3 (J-domain in orange, remaining domains in red; for simplicity ERdJ3 is not shown as a dimer) regulates the chaperone cycle of BiP in transiently binding to the ATP bound state (dashed lines) and accelerating BiP's ATPase activity by binding to the NBD/SBD interface *via* its conserved J-domain. Additional contacts of ERdJ3 are needed to form stable complexes with BiP which prime the lid for protein binding after hydrolysis. After protein substrate transfer to BiP in the ADP-bound state, ERdJ3 protects the complex against dissociation by nucleotide exchange.

# 8 Materials and methods

Methods are derived from standard methods developed at the chair of biotechnology, TU München.

## 8.1 *E. coli* strains

| Strains | Geno- / Phenotype | Source / Reference |
|---|---|---|
| *E. coli* XL1 Blue | *rec*A1 *end*A1 *gyr*A96 *thi*-1 *hsd*R17 *sup*E44 *rel*A1 *lac* [F'proAB *lac*IqZDM15 Tn10 (*Tet*R)] | Stratagene, La Jolla, USA |
| *E. coli* BL21 (DE3) | F– *omp*T hsdS(rB– mB–) *dcm*+ *Tet*r *gal* l (DE3) *end*A *Hte* [*arg*U *ile*Y *leu*W *Cam*R] | Stratagene, La Jolla, USA |

## 8.2 Bacterial vectors

| Name | Vector | Origin | Cloning site |
|---|---|---|---|
| Murine $C_H1$ | pet28a | Matthias Feige, TU München | |
| Murine $C_H1$ N-Cys | pet28a | Matthias Feige, TU München | |
| Codon optimized human $C_H1$ | pSport | Matthias Feige, TU München | |
| Human $C_H1$ | pet28a | Matthias Feige, TU München | NcoI / HindIII |
| Human $C_H1$ VF-VK | pet28a | This work | NcoI / HindIII |
| Human $C_H1$ FP-FA | pet28a | This work | NcoI / HindIII |
| Human $C_H1$ VF-VK/FP-FA | pet28a | This work | NcoI / HindIII |
| Murine BiP cDNA clone | | RZPD | |
| BiP WT | pProex-HT | This work | BamHI / XhoI |
| BiP Δ Cys | pProex-HT | This work | BamHI / XhoI |
| BiP Δ Cys T518 Cys | pProex-HT | This work | BamHI / XhoI |
| BiP Δ Cys S636 Cys | pProex-HT | This work | BamHI / XhoI |
| BiP Δ Cys T166/T518 Cys | pProex-HT | This work | BamHI / XhoI |
| BiP Δ Cys T518/S583 Cys | pProex-HT | This work | BamHI / XhoI |
| BiP Δ Cys T518/S636 Cys | pProex-HT | This work | BamHI / XhoI |
| BiP SBD 654 | pProex-HT | This work | XbaI / XhoI |
| BiP SBD 532 | pProex-HT | This work | XbaI / XhoI |
| Murine ERdJ3 cDNA clone | | RZPD | |
| ERdJ3 WT | pProex-HT | This work | NcoI / XhoI |
| ERdJ3 QPD | pProex-HT | This work | NcoI / XhoI |
| ERdJ3 J-domain WT | pProex-HT | This work | NcoI / XhoI |
| ERdJ3 J-domain QPD | pProex-HT | This work | NcoI / XhoI |

## 8.3 Primer

| | Name | Sequence | Restriction site |
|---|---|---|---|
| cloning | BiP_Bam_fwd | TTTTGGATCCGAGGAGGAGGACAAG | BamHI |
| | BiP_Xho_rev | AAAACTCGAGTTACTACAACTCATCTTT | XhoI |
| | BiP418 Xba Fwd | TTTTCTAGAAATAATTTTGTTTAACTTTAAGAAGGAGATAT ACCATGGATGTTTGTCCCCTT | XbaI |
| | BiP532 Xho Rev | AAACTCGAGTTATTAGCGGTTTTGGTCATT | XhoI |
| | BiP654 Xho Rev | AAACTCGAGTTACTACAACTCATCTTT | XhoI |
| | ERj3_NcoI_fwd | TTTTCCATGG GGC GAGATTTCTAT AAGATCCTG | NcoI |
| | ERj3_XhoI_rev | TTTTCTCGAGCTACTAATAGCCCTGCAGCCCGTTGTACA | XhoI |
| Quick change | QC_hCH1_VK_fwd | CCAAAGGTCCGAGCGTGAAACCGCTGGCACCGAGC | |
| | QC_hCH1_VK_rev | GCTCGGTGCCAGCGGTTTCACGCTCGGACCTTTGG | |
| | QC_FPL_YAL_F | CCCCCATCTGTCTATGCACTGGCCCCTGGATCT | |
| | QC_YPL_YAL_R | AGATCCAGGGGCCAGTGCATAGACAGATGGGGG | |
| | QC_hCh1+_FAA_f | GGTGTTCATACCTTTGCGGCAGTTCTGCAGAGC | |
| | QC_hCh1+_FAA_r | GCTCTGCAGAACTGCCGCAAAGGTATGAACACC | |
| | QC_BiP532_taa_f | AATGACCAAAACCGCTAAACACCTGAAGAAATT | |
| | QC_BiP532_taa_r | AATTTCTTCAGGTGTTTAGCGGTTTTGGTCATT | |
| | QC_BiP_C1toS_f | GGGACCACCTATTCCTCGGTCGGTGTGTTCAAG | |
| | QC_BiP_C1toS_r | CTTGAACACACCGACCGAGGAATAGGTGGTCCC | |
| | QC_BiP_C2toS_f | GTACTGCTTGATGTTTCTCCCCTTACACTTGGT | |
| | QC_BiP_C2toS_r | ACCAAGTGTAAGGGGAGAAACATCAAGCAGTAC | |
| | QC_BiP_T166C_f | GGAAAGAAGGTTTGCCATGCAGTTGTTACT | |
| | QC_BiP_T166C_r | AGTAACAACTGCATGGCAAACCTTCTTTCC | |
| | QC_BiP_T518C_f | GCTGAAGACAAAGGTTGTGGAAACAAAAACAAAAT | |
| | QC_BiP_T518C_r | ATTTTGTTTTTGTTTCCACAACCTTTGTCTTCAGC | |
| | QC_583Cys_Fwd | AAAGAAAAGCTGTGCGGTAAACTTTCTTCT | |
| | QC_583Cys_Rev | AGAAGAAAGTTTACCGCACAGCTTTTCTTT | |
| | QC_BiP_T636C_f | AGCAAACTCTATGGATGTGGAGGCCCTCCCCCA | |
| | QC_BiP_T636C_r | TGGGGGAGGGCCTCCACATCCATAGAGTTTGCT | |
| | J_stop_f | CGGTGAAGAAGGCTAAAAAGATGGCCATC | |
| | J_stop_r | GATGGCCATCTTTTTAGCCTTCTTCACCG | |
| | QC_J3_QPD_fwd | GCCCTGCAGCTCCAGCCTGACCGGAACCC | |
| | QC_J3_QPD_rev | GGGTTCCGGTCAGGCTGGAGCTGCAGGGC | |

## 8.4 Chemicals

| Chemical | Origin |
|---|---|
| Acrylamide (38%, 2% Bisacrylamide) | Roth (Karlsruhe, Germany) |
| Agarose, ultra pure | Roth (Karlsruhe, Germany) |
| Ammoniumperoxodisulfate (APS) | Roche (Mannheim, Germany) |
| Ampicillin | Roth (Karlsruhe, Germany) |
| Adenosyl-imidodiphosphate (AMP-PNP) | Roche (Mannheim, Germany) |
| Adenosin-5'-diphosphate (ADP), disodium salt | Roche (Mannheim, Germany) |
| Adenosin-5'-triphosphate (ATP), disodium salt | Roche (Mannheim, Germany) |
| Bacto Agar | Difco (Detroit, USA) |
| Bacto Tryptone | Difco (Detroit, USA) |
| Bacto Yeast Extract | Difco (Detroit, USA) |
| Benzophenone-4-maleimide (BPM) | Invitrogen (USA) |
| Bromphenolblue S | Serva (Heidelberg, Germany) |
| Complete Protease Inhibitor Cocktail Tablets | Roche (Mannheim, Germany) |
| Coomassie Brilliant-Blue R-250 | Serva (Heidelberg, Germany) |
| 5,5' Dithio-bis-Nitrobenzoic acid (DTNB) | Sigma (St. Louis, USA) |
| 1,4-Dithiothreitol (DTT) | Roth (Karlsruhe, Germany) |
| Ethylendiamintetraacidic acid (EDTA) | Merck (Darmstadt, Germany) |
| Ethidiumbromide | Sigma (St. Louis, USA) |
| Formaldehyde, 37% p.A. | Roth (Karlsruhe, Germany) |
| Glutaraldehyd, 25% in water | Serva (Heidelberg, Germany) |
| Glycerol, 99 % | ICN, Costa Mesa, USA |
| Glycine | Roth (Karlsruhe, Germany) |
| N-(2-Hydroxyethyl)-piperazin-N'2-ethansulfonic acid (HEPES) | ICN (Costa Mesa, USA) |
| Isopropanol | Roth (Karlsruhe, Germany) |
| Isopropyl-β-D-thiogalaktopyranosid (IPTG) | Roth (Karlsruhe, Germany) |
| Kanamycin | Roth (Karlsruhe, Germany) |
| β-Mercaptoethanol, pure | Merck (Darmstadt, Germany) |
| Sodiumdodecylsulfat (SDS) | Roth (Karlsruhe, Germany) |
| N,N,N',N'-Tetramethylethylendiamin (TEMED) | Roth (Karlsruhe, Germany) |
| Polyoxyethylen-Sorbitan-monolaurat (Tween 20) | Merck (Darmstadt, Germany) |
| Restriction enzymes | New England Biolabs (Beverly, USA) |
| T4-Ligase | Promega (Madison, USA) |
| Tris-(Hydroxymethyl)-aminomethan (Tris) | ICN (Costa Mesa, US) |
| Urea, p.a. | Roth (Karlsruhe, Germany) |

All other reagents were p.a. quality and purchased from Merck (Darmstadt, Germany) except of fluorescence labels. For the preparation of buffers double distillate water was used.

## 8.5 Fluorescence label

| Label | supplier |
|---|---|
| Atto 532 maleimide | AttoTec (Germany) |
| Atto 647 maleimide | AttoTec (Germany) |
| Lucifer Yellow iodacetamide | Invitrogen (USA) |

## 8.6 Markers and kits

| | |
|---|---|
| BiaCore amine coupling kit | BiaCore Inc. (Uppsala, Sweden) |
| 1 kb DNA ladder molecular weight standard | New England Biolabs (Beverly, USA) |
| Wizard® Plus SV Mini-Preps DNA purification kit | Promega (Madison, USA) |
| High Pure PCR Product Purification Kit | Promega (Madison, USA) |
| Low-Range-molecular weight marker | BioRad (München, Germany) |

## 8.7 Chromatography material

| | |
|---|---|
| Ni-NTA (5 ml) | GE Healthcare (Freiburg Germany) |
| Q-Sepharose | GE Healthcare (Freiburg Germany) |
| SP-Sepharose | GE Healthcare (Freiburg Germany) |
| Superdex 75 Prep Grade (26/60) | GE Healthcare (Freiburg Germany) |
| Superdex 200 Prep Grade (26/60) | GE Healthcare (Freiburg Germany) |
| Superdex 75 10/300GL (HPLC) | GE Healthcare (Freiburg Germany) |
| Superdex 200 10/300GL (HPLC) | GE Healthcare (Freiburg Germany) |

Q- and SP-sepharose columns were self-packed with a volume of 75 ml each.

## 8.8 Buffers

| **Molecular Biology** | | |
|---|---|---|
| TAE (50x) | 2M | Tris/acetate pH 8.0 |
| | 50 mM | EDTA |
| BJ (10x) | 50% (v/v) | glycerol |
| | 10 mM | EDTA pH 8.0 |
| | 0.2% (w/v) | bromphenoleblue |
| | 0.2% (w/v) | xylencyanol |

| **Protein chemical buffers** | | |
|---|---|---|
| SDS running buffer (10x) | 250 mM | Tris/HCl pH 6.8 |
| | 2 M | glycine |
| | 1% (w/v) | SDS |
| Laemmli sample buffer (5x) | 312.5 mM | Tris/HCl pH 6.8 |
| | 10% (w/v) | SDS |
| | 50% (v/v) | glycerol |
| | 2.5% (v/v) | β-mercaptoethanol |
| | 0.05% (w/v) | bromphenolblue |
| separating gel buffer (4x) | 250 mM | Tris/HCl pH 8.8 |
| | 0.8% (w/v) | SDS |
| stacking gel buffer (2x) | 250 mM | Tris/HCl pH 6.8 |
| | 0.4% (w/v) | SDS |
| Fairbanks A | 2.5 g | Coomassie Brilliant Blue R 250 |
| | 250 ml | ethanol |
| | 80 ml | acetic acid |
| | adjust to 1 l with $H_2O$ | |
| Fairbanks D | 250 ml | ethanol |
| | 80 ml | acetic acid |
| | adjust to 1 l with $H_2O$ | |

| **Protein purification buffers** | | |
|---|---|---|
| Q-Sepahrose buffer A | 50 mM | Tris/HCl pH 7.5 |
| | 5 M | urea |
| | 10 mM | EDTA |
| Q-Sepahrose buffer B | 50 mM | Tris/HCl pH 7.5 |
| | 5 M | urea |
| | 10 mM | EDTA |
| | 1 M | NaCl |
| Ni-NTA buffer A (ERdJ3) | 50 mM | Hepes/KOH pH 7.5 |
| | 3 M | GdmCl |
| | 1 mM | β-mercaptoethanol |
| Ni-NTA buffer B (ERdJ3) | 50 mM | Hepes/KOH pH 7.5 |
| | 3 M | GdmCl |
| | 1 mM | β-mercaptoethanol |
| | 500 M | imidazol |
| Ni-NTA buffer A (BiP) | 50 mM | Hepes/KOH pH 7.5 |
| | 300 mM | KCl |
| Ni-NTA buffer B (BiP) | 50 mM | Hepes/KOH pH 7.5 |
| | 300 mM | KCl |
| | 500 M | imidazol |
| HKM buffer | 50 mM | Hepes/KOH pH7.5 |
| | 150 mM | KCl |
| | 10 mM | $MgCl_2$ |
| PBS buffer | 8 g | NaCl |
| | 0.2 g | KCl |
| | 1.44 g | $Na_2HPO_4 \cdot 2\ H_2O$ |
| | 0.24 g | $KH_2PO_4$ |
| IB preparation buffer | 100 mM | Tris/HCl pH 7.5 |
| | 150 mM | NaCl |
| | 10 mM | EDTA |

## 8.9 Equipment and computer programs

| device | origin |
|---|---|
| **Absorption Spectrophotometers** | |
| Varian Cary 100 Bio UV-Vis-Spectrophotometer | Varian (Palo Alto, USA) |
| **Circular dichroism spectropolarimeter** | |
| Jasco J715 including PTC 343 Peltier temperature device | Jasco (Groß-Umstadt, Germany) |
| **Fluorescence Spectrophotometer** | |
| Spex FluoroMaxIII spectrofluorimeter equipped with anisotropy polarizers | Jobin Yvon (München, Germany) |
| **Chromatography devices** | |
| ÄKTA FPLC | GE Healthcare (Freiburg Germany) |
| **HPLC devices** | |
| Shimadzu HPLC system equipped with autosampler | Scimadzu (München, Germany) |
| **Gel electrophoresis devices** | |
| Hoefer Mighty Small II | GE Healthcare (Freiburg, Germany) |
| **Power amplifier** | |
| LKB-GPS 200/400 | Amersham Bioscience (Freiburg, Germany) |
| Pharmacia EPS 3500, 301 and EPS 1001 | GE Healthcare (Freiburg, Germany) |
| **Analytical Balance** | |
| BP 121 S | Satorius (Göttingen, Germany) |
| BL 310 | Satorius (Göttingen, Germany) |
| **Centrifuges** | |
| Rotina 46 R Centrifuge | Hettich (Tuttlingen, Germany) |
| Eppendorf-Centrifuge 5415 C | Eppendorf (Hamburg, Germany) |
| Avanti J25, JA-10 and JA-25.50-Rotor | Beckmann (Vienna, Austria) |
| **Additional Equipment** | |
| Eppendorf-Thermomixer | Eppendorf (Hamburg, Germany) |
| Magnetic stirrer Heidolph MR2000 | Heidolph (Kehlheim, Germany) |
| pH-Meter - WTW | WTW (Weilheim, Germany) |
| Incubator | New Brunswick Scientific (Nürtingen, Germany) |
| Water bath Haake F6-K | Haake (Karlsruhe, Germany) |

| | |
|---|---|
| Cell Disruption Apparatus | Basic Z Constant Systems (Warwick, UK) |
| Centricon 10/30/100- microconcentrators | Millipore (Bedford, USA) |
| Dialysis tubes Spectra/Por (6-8 kDa) | Spectrum (Houston, USA) |
| Cuvettes 1.5 mL | Zefa (Munich, Germany) |
| **Computer Programs** | |
| Adobe CS | Adobe Systems (San Jose, USA) |
| Microsoft Office 2007 | Microsoft (Unterschleißheim, Germany) |
| Origin 8 | OriginLab (Nothhampton, USA) |

## 8.10 Molecular methods

### 8.10.1 Cultivation and storage of *E. coli*

*E. coli* was cultivated in a thermostated incubator at 30°C or 37°C either on LB plates or in LB liquid media. Strains were selected by addition of appropriate antibiotics to the media, hence selecting cells containing the corresponding resistance genes either on the plasmid or in the genome. Liquid cultures were inoculated from fresh overnight cultures or by transferring single colonies from plates. Bacterial division was monitored at 600 nm ($OD_{600nm}$ = 1 corresponding to approx. $8x10^8$ cells/ml). For long-term storage, 5 mL of a freshly inoculated culture were centrifuged at 5,000 x g and the sediment was resuspended in 1 mL medium. 300 µl 50 % glycerol were added to 700 µl of bacterial suspension resulting in a 15% glycerol culture stock. The culture was frozen using liquid nitrogen and stored at -80°C.

### 8.10.2 Polymerase chain reaction (PCR)

Cloning was performed by using cDNA (purchased from RZPD, Germany) as template and the regarding primers listed in section 8.3. The Pfu polymerase with the provided buffer containing $MgCl_2$ was used for amplification of DNA. PCR products were analyzed by a 1 % agarose gel electrophoresis containing 0,001 % concentrated ethidiumbromide solution.

| **reaction mix:** | | |
|---|---|---|
| $H_2O$, sterile | 84.5 | µL |
| dNTPs (100 mM) | 2 | µL |
| Pfu polymerase (1 units/µL) | 1 | µL |
| primer | 2 | µL |
| Pfu buffer | 10 | µL |
| template | 0.5 | µL |

| **reaction protocol:** | |
|---|---|
| step 1 | 95 °C, 2 min |
| step 2 (denaturation) | 95 °C, 30 sec |
| step 3 (annealing) | 55-62 °C, 1-10 min |
| step 4 (elongation) | 68 °C, 1 min |
| step 5 | GOTO step 2, 25x |
| step 6 (elongation of short ends) | 68 °C, 10 min |
| step 7 (storage) | 4 °C forever |

Quick change PCRs were performed according to manufactures' protocol (Invitrogen, USA).

### 8.10.3 Purification and storage of DNA

PCR products were purified using the Wizard Plus Gel Extraction Kit following the manufacturers centrifugation protocol. After digestion of DNA fragments or plasmid DNA the Wizard Plus Gel Extraction was used and for mini-preps the Wizard Plus SV Minipreps DNA Purification System was used. DNA was stored in sterile $H_2O$ at -20 °C.

### 8.10.4 Restriciton and ligation protocols

DNA was digested and ligated according the following protocols.

| **restriction protocol** | | |
|---|---|---|
| $H_2O$, sterile | 2 | µL |
| PCR products or plasmid DNA (1 µg) | 40 | µL |
| Enzyme 1 (20 units/µL) | 1.5 | µL |
| Enzyme 2 (20 units/µL) | 1.5 | µL |
| 10x buffer | 5 | µL |
| *incubation at 37 °C for 1 h* | | |

**ligation protocol:**

| | | |
|---|---|---|
| $H_2O$ | 3 | µL |
| insert: digested PCR products (100 ng) | 3 | µL |
| vector: digested plasmid DNA (30 ng) | 1 | µL |
| ligase | 2 | µL |
| ligase-buffer | 1 | µL |
| *incubation at room temperature for 20 min* | | |

### 8.10.5 Sequencing

Plasmid DNA with a concentration ranging from 30 to 100 ng/µL was sent to GATC Biotech AG, Konstanz, Germany.

### 8.10.6 Preparation of chemical competent *E. coli* cells for transformation

10 large colonies were transferred of a fresh overnight cultured plate into 250 mL SOB medium and incubated at 19°C to an $OD_{600}$ of 0.5 (approx. 24 h). After a cold shock of 10 minutes (min) on ice, cells were spinned down at 4000 rpm for 10 min at 4°C. Cells were gently resuspended in 80 ml ice-cold TB medium and stored on ice for 10 min. After spinning the cells down again, the pellet was resuspended in 20 ml ice-cold TB containing 1.4 mL DMSO and the cells aliquoted to 100 µL, frozen in liquid nitrogen and stored at -80 °C.

### 8.10.7 Transformation of competent *E. coli* cells and amplification of plasmid DNA

100 µL of chemical competent *E. coli* cells were incubated with 50 ng of plasmid DNA on ice for 15 min. After a heat step at 42°C for 60 sec, cells were left on ice for another 2 min. 700 µL $LB_0$ were added and the cells incubated at 37°C for 45 min to let the resistance genes be transcribed and the antibiotics converting enzymes be synthesized. Cells were pelleted at 5000 rpm for 5 min and plated on selection media. Plates were incubated at 37°C ON. For amplification of plasmid DNA, single colonies were transferred into 5 ml of LB containing the regarding antibiotics and grown in a shaker at 37°C ON. For plasmid preparation, cells were harvested and treated with the Wizard Plus SV Minipreps DNA Purification System.

## 8.11 Protein chemical methods

### 8.11.1 SDS polyacrylamid gel electrophoresis

SDS-PAGE was performed in accordance to the protocol of Laemmli (Laemmli, 1970). 15% SDS-PAGE gels were poured and contained the following compounds:

Separation gel: 3.75 mL 40% Acrylamide (40% w/v, Acrylamide/Bisacrylamide 38:2)
2.5 mL 4 x SDS-Buffer (0.8% SDS, 1.5 M Tris/HCl, pH 8.8)
3.75 mL bidest. $H_2O$

Stacking gel: 0.625ml 40% Acrylamide (40% w/v, Acrylamide/Bisacrylamide 38:2)
2.5 mL 2 x SDS-Buffer (0.4% SDS, 0.25 M Tris/HCl, pH 6.8)
1.875 mL bidest. $H_2O$

Polymerization of the solution was induced by adding TEMED and APS. Electrophoresis was carried out at constant voltages (150 V) for 1 h. Gels were stained with Coomassie in accordance to the protocol of Fairbanks et al (Fairbanks et al., 1971).

### 8.11.2 Protein expression

The proteins produced in this thesis were expressed in the BL21-CodonPlus(DE3)-RIL strain which carries an additional plasmid encoding extra copies of the *argU*, *ileY* and *leuW* tRNA genes and enables efficient high-level expression of heterologous protein of AT-rich genomes in *E. coli*. Over-expression of proteins can deplete the pool of rare tRNAs and stall translation. BL21-CodonPlus strains encode tRNAs that most frequently limit translation of heterologous proteins.

The pET28b and pProex system was used as expression vector with the regarding genes cloned as described in 8.2 and 8.3. Expression was run on a 6 l scale. After inoculation and growth at 37 °C to an OD of 0.8, expression was induced by the addition of 1 mM IPTG and allowed to proceed for 3 hours for soluble constructs (BiP and J-domain constructs of ERdJ3) or overnight for inclusion body production. Cells were harvested at 6000 rpm and 4 °C for 15 min (JA 10 rotor).

### 8.11.3 Purificartion of soluble proteins

Cell pellets of 6 l cultures were resuspended in 100 mL Ni-NTA buffer A containing 1 ml of Protease Inhibitor Mix HP and processed by a cell disruptor at 1.8 kbar. The lysate was centrifuged at 18,000 rpm and 4°C for 25 min in a JA 25.50 rotor. The supernatant was loaded onto a pre-equilibrated 5 mL HisTrap FastFlow Ni-affinity chromatography column. The purification schemes developed in this thesis are given in section 6.1 including the SEC purification step in HKM buffer.

### 8.11.4 Purification of insoluble proteins

After harvest, cells were resuspended in an appropriate volume of inclusion body (IB) preparation buffer, supplement with DNase I and protease inhibitor mix HP. After cell disruption, 2.5 % Triton X-100 was added and the solution was stirred at 4°C for 30 minutes to solubilize membrane fragments. The inclusion bodies were sedimented by centrifugation (20000 rpm; 20 minutes, 4°C; rotor: JA-25.50) and washed three times with IB preparation buffer. The IB pellet was directly dissolved in urea- containing buffer for purification, or stored at -20°C. The inclusion bodies were dissolved in ~ 100 ml of buffer A supplemented with 10 mM β-mercaptoethanol and stirred at 4°C for 30 minutes. Following this, the

solution was cleared by centrifugation (20000 rpm; 20 minutes; 4°C; rotor: JA25.50) and the supernatant was applied to the ion exchange columns equilibrated in buffer A.

### 8.11.5 Ellman assay

The Ellman assay was used to determine the oxidation status of sulfhydryl groups following the principle described by Ellman (ELLMAN, 1959). The reaction volume was 1 ml in HKM buffer and 40-100 µg/ml protein (final concentration) were used. The reaction of 200 µg DTNB with free sulfhydryl groups was allowed to proceed for 20 min at room temperature. The absorption was determined at λ = 412 nm and the concentration of bound DTNB (equivalent to the concentration of free SH-groups) was calculated with Lambert-Beer-law with the extinction coefficient $\varepsilon_{412\,nm}$ = 13600 $M^{-1}$ $cm^{-1}$ of the reacted DTNB.

### 8.11.6 Protein and peptide labeling

Proteins were labeled at cysteine residues using Atto 532 and or Atto 647maleimide (AttoTec, Germany) or Lucifer yellow for peptides. These dyes react with cysteines to give tioether-coupled products. Labeling was performed at 25°C for 1 hour by addition of a 3-fold excess to a 100 µM solution in HKM buffer and subsequently quenched by the addition of a 10-fold excess of reduced glutathione. For double labeled BiP constructs, a 3-fold excess of Atto 532 and Atto 647 in the engineered BiP variants.

Proteins and peptides were separated from free label by SEC-HPLC on a Superdex 200 10/300 column for BiP or a Superdex 200 10/300 column for $C_H1$ or peptides equilibrated in HKM buffer. The labeling efficiency was determined using UV spectroscopy and the extinction coefficients provided by the manufacturer.

### 8.11.7 MALDI-TOF/TOF-MS

The molecular weight analysis of purified proteins, the fragmentation pattern of the limited proteolysis and the hydrogen deuterium exchange experiments were all performed on a Bruker Ultraflex-2 MALDI-TOF/TOF mass spectrometer.

A Zip Tip preparation was performed for all samples following the instructions of the manufacturer (Millipore). The HCCA matrix was dissolved in 0.1 % TCA, 80 % acetonitrile and 20 % dd$H_2O$. For the hydrogen deuterium exchange experiment, the solvent was 0.1 %

TCA, 90 % acetonitrile and 10 % dd$H_2O$ to reduce the possibility of exchange during the sample preparation. The full-length proteins and peptides were spotted in the matrix solution and analyzed after the evaporation of the solvent. For each spectrum, the MS analysis at different points of the preparation was averaged and the evaluation was done with the program m/z (Moverz).

## 8.12 Spectroscopic methods

### 8.12.1 UV-absorption spectroscopy

Proteins and peptides contain two important functional groups that absorb UV light. Amid groups like those forming the peptide bond absorb at 180 to 240 nm and the aromatic amino acids mainly phenylalanine, tyrosine and tryptophane at 250 to 300 nm.

| | $\lambda_{max}$ (nm) | $\varepsilon_{max}$ ($M^{-1}$ $cm^{-1}$) |
|---|---|---|
| Trp | 280 | 5700 |
| Tyr | 274 | 1400 |
| Phe | 257 | 200 |
| disulphide bond | 250 | 300 |

UV spectroscopy was used to determine the concentration of purified protein by using the law of Lambert-Beer

$$A = \varepsilon * c * d$$

with *A* Absorbance, $\varepsilon$ molar extinction coefficient ($M^{-1}$ $cm^{-1}$), *c* protein concentration (M) and *d* cell length, that correlates the measured absorbance with the protein concentration.

The *protparam* tool provided by www.expasy.org was used to determine the molar extinction coefficients of the purified proteins for concentration determination.

Spectra from 230 to 400 nm were recorded with a 0.5 nm interval. Protein solutions were measured in UV Quartz cuvettes with a thickness of 1 cm and a total volume of 180 µL and spectra were buffer corrected. If necessary, proteins were diluted to A = 0.5 – 1 to guarantee the linearity of Lambert-Beers law.

### 8.12.2 Circular dichroism spectroscopy

Structural features of asymmetric molecules can be assessed by CD-spectroscopy. In chiral molecules such as α-helical structures or asymmetric carbon atoms the electric and magnetic transition dipole moment possesses a parallel component. This leads to a mutual influence of the fields and therefore to a different absorption coefficient of the molecule for left and right circular polarized light.

$$\Delta\varepsilon=\varepsilon_l-\varepsilon_r$$

In the case of proteins, the most important chiral elements with a significant absorption coefficient are the peptide backbone ($n \rightarrow \pi^*$ and $\pi \rightarrow \pi^*$ transition) and aromatic amino acids ($\pi \rightarrow \pi^*$ transition). The chiroptical characteristics of the peptide backbone originate from the secondary structure whereas the one of the aromatic residues depends on the asymmetric environment within the native structure of the protein. Normally the far-UV (FUV; 180 – 250 nm) CD-spectrum of a native protein represents the sum of the signals for the different secondary structure elements, turns and loops (summarized in the following table).

| secondary structure | FUV CD-signal (absorption of carbonyl groups) |
|---|---|
| α-helix | maximum at 192 nm ($\pi \rightarrow \pi^*$ / $\perp$), minima at 209 nm ($\pi \rightarrow \pi^*$ /$\parallel$ ) and at 222 nm ($n \rightarrow \pi^*$) |
| β-sheet | maximum at 196 nm ($n \rightarrow \pi^*$), minimum at 218 nm ($\pi \rightarrow \pi^*$) |
| random coil | minimum at 195 nm ($n \rightarrow \pi^*$), maximum at 212 nm ($\pi \rightarrow \pi^*$) |

The CD measurements were performed in a Jasco J-715 CD spectropolarimeter equipped with a PTC343 Peltier element under the following conditions.

| Parameter | FUV |
|---|---|
| Wavelength [nm] | 250 – 190 |
| Scan speed [nm/min] | 20 |
| Data pitch [s] | 0.2 |
| Band width [nm] | 1 |
| Response time [s] | 4 |
| Temperature [°C] | 25 |
| Path length [cm] | 0.1 |
| Accumulations | 16 |
| Concentration [mg/ml] | 0.1 |

All spectra were buffer corrected and normalized to the mean residual weight ellipticity $\Theta_{MRW}$ according to the following equation

$$\Theta_{MRW} = \frac{\Theta \cdot 100}{d \cdot c \cdot N_{aa}}$$

with $\Theta$ as the obtained ellipticity (mdeg), d cell length (cm), c concentration (mM) and $N_{aa}$ number of amino acids.

For determination of thermal stability, 0.1 mg/ml protein samples were heated with 0.2°C/min in a 1 mm Quartz cuvette and changes in CD signal at a certain wavelength was observed. The midpoint of the equation was determined by a Boltzmann fit.

### 8.12.3 Fluorescence spectroscopy

After excitation of an aromatic system with delocalized π electrons, fluorescence may occur if an electron shifts back from an excited singulet state to the ground state. During the lifetime of the excited state a variety of interactions may influence this process. For FRET, spFRET and fluorescence anisotropy, synthetic fluorophores were coupled to proteins or peptides via cysteine residues following maleimide chemistry. The excitation and emission parameters of the dyes are given in the following table.

| | **excitation wavelength (nm)** | **emission wavelength (nm)** |
|---|---|---|
| **Atto 532** | 532 | 550 |
| **Atto 647** | 645 | 650 |
| **lucifer yellow** | 430 | 525 |

#### 8.12.3.1 spFRET measurements

spFRET measurements were performed and evaluated by Matthias Höller (Ludwig-Maximilians-Universität, München) as described in his PhD thesis. Shortly, experiments were performed on a home built two-color confocal system constructed around a Nikon TE2000 base (Nikon, Germany) with pulsed interleaved excitation and multiparameter fluorescence detection. The labeled proteins were incubated in micromolar concentrations at 37°C in the respective environments: HKM buffer (15 min), HKM buffer with 1mM ADP (15 min), with 1mM AMP-PNP (15 min), with 1mM ADP and > 14 µM unlabeled $C_H1$ (120 min),

with 1mM ADP and > 70 µM HFTPAVL binding peptide (120 min), or with 5 µM ERdJ3 (15 min). The labeled proteins were subsequently diluted to a concentration of <100 pM to ensure a minimal probability of multimolecular events, whereas the concentration of all nucleotides and/or binding partners was held constant. For an individual experiment, at least a total of 1000 individual molecules were measured (Marcinowski et al., 2011).

#### 8.12.3.2 Ensemble FRET measurements

For ensemble FRET experiments, 2 µM Atto532 labeled BiP 636 was incubated with 1 mM ADP or ATP and change in donor (550 nm) and acceptor (650 nm) signal was observed after addition of 3 µM Atto647 labelled $C_H1$ N-Cys and excitation at the wavelength $\lambda_{ex}$ = 532 nm in a Spex FluoroMaxIII spectrofluorimeter (Jobin Yvon). ATP chase experiments were performed by adding 5 U of pyruvate kinase (Roche, Germany) and 10 mM phosphoenolepyruvate (Roche, Germany) to the sample. Rate constants were obtained by single exponential fits.

#### 8.12.3.3 Fluorescence anisotropy measurements

For anisotropy measurements in a Spex FluoroMaxIII spectrofluorimeter equipped with anisotropy polarizers (Jobin Yvon), 1 µM lucifer yellow labelled peptide and varying concentrations of BiP and ERdJ3 were used in HKM buffer supplemented with 1 mM ADP. Lucifer yellow fluorescence was excited at 430 nm and detected at 525 nm. The change in quantum yield of the chromophore was less than 3% upon association of the labelled peptide with BiP. Rate constants were obtained by single exponential fits and the $K_d$ was determined by fitting the data to a single binding site.

### 8.12.4 Surface plasmon resonance spectroscopy

Surface plasmon resonance (SPR) spectroscopy is a common tool to characterize protein-protein-interactions. The method is based on the reflection of plasmons created by an incoming light beam which is irradiated in a certain angle and has to match the impuls of the surface plasmons on a thin goldlayer for their excitation. The excitation of the electrons in the conducting gold layer produces an evanescent wave. A particle or irregularity on a coated gold surface leads to the reemission of the excitation light beam as light which can be detected behind the metal film in various directions. This leads to a loss of reflection intensity at the exact resonance conditions. The distance at which a particle still influences

the refractive index is defined by the range of the evanescent field that attenuates within one wavelength and reaches only 600 nm into the medium. The signal measured in resonance units (RU) is directly correlated to the amount of protein bound. Typically 1000 RU equal 1 ng of protein per $mm^2$.

For SPR measurements, ERdJ3 was immobilized on the gold surface coupled with carboxymethylated dextran. Immobilization was done by activating the carboxyl groups on the surface using 50 mM N-hydroxy-succimid and 200 mM 1-ethyl-3-(3-dimethylaminopropyl)carbodiimide (EDC crosslinker) followed by the incubation of ERdJ3 on the activated surface at pH 4.0. 2000 RU was coupled before the surface was inactivated by ethanolamine. HKM was used as running buffer for measurements at 25°C with a flow rate of 20 µl/min and 35 µl samples were injected.

BiP was preincubated at 30°C with 1 mM ADP or 1 mM ATP where indicated to allow efficient nucleotide binding. The observed association rate constant $k_{obs}$ was determined for a series of BiP or $C_H1$ concentrations by fitting the kinetic time course for each concentration to a single exponential function. $k_{on}$ and $k_{off}$ were determined from the slope and the y-axis intercept, respectively, of the determined $k_{obs}$ values. The $K_d$ was calculated as

$$K_d = \frac{k_{off}}{k_{on}}$$

## 8.13 Regenerative ATPase assay

In order to analyze protein activity, a regenerative ATPase assay, which prevents product inhibition by accumulation of ADP during the hydrolysis reaction, was carried out. This assay uses a coupled-enzymatic approach that rapidly converts produced ADP to ATP in the presence of phosphoenolpyruvate, pyruvate kinase, NADH and lactate dehydrogenase. The consumption of NADH to $NAD^+$ can be followed spectroscopically at a wavelength of $\lambda$ = 340 nm.

The following premix was prepared:

| | |
|---|---|
| 8500 µl | HKM buffer (50 mM Hepes/KOH pH 7.5, 150 mM KCl, 10 mM $MgCl_2$) |
| 240 µl | 100 mM phosphoenolpyruvate |
| 35 µl | 50 mM NADH |
| 12 µl | Pyruvate kinase suspension (Roche, Mannheim, Germany) |
| 44 µl | Lactate dehydrogenase suspension (Roche, Mannheim, Germany) |

100 µl of this premix were used for each 150 µl assay. The remaining volume was used for addition of the ATPase, ATP, co-chaperones or HKM buffer. The assays were conducted in a Cary 50 Bio UV/VIS spectrometer at 37 °C. Data were recorded with an average time of 1 sec. After a stable baseline was observed, the reaction was started by adding indicated amounts of ATP and measurements were performed for 20-30 min. The hydrolysis rates were calculated using the differential molar extinction coefficient of NADH and $NAD^+$ of 6200 $cm^{-1}M^{-1}$ at 340 nm.

$$v_{spez} = \frac{m}{d \cdot \left(-6200 \frac{1}{cm \cdot M}\right) \cdot c_{ATPase}}$$

m is the slope of the resulting lines, d is the thickness of the cuvette in cm and $c_{ATPase}$ is the concentration of the respective ATPase in µM.

$K_M$ values for ATP were obtained by fitting the resulting plot with the Michaelis-Menten equation

$$v_{spez} = k_{cat} \cdot \frac{c}{c + K_M}$$

## 8.14 SEC-HPLC

For all experiments, a Shimadzu HPLC system (Shimadzu, München, Germany) was used. Complex formation between BiP and $C_H1$ was analyzed on a Superdex 200 10/300GL column in HKM buffer at a flow rate of 0.5 ml/min. For the determination of the dissociation constant as well as binding kinetics, peak intensities at the retention time of 28.4 min corrected for baseline drifts were plotted against the $C_H1$ concentration or the incubation

time and normalized. The rate constants $k_{obs}$ of the binding reaction were determined from single exponential fits and evaluated with a linear equation to derive $k_{on}$ and $k_{off}$. Detection of all proteins was performed by the intrinsic fluorescence excited at 280 nm and monitored at 350 nm. Incubation steps were performed in HKM buffer with 1 mM ADP.

## 8.15 Cross-linking

For crosslinking experiments, BiP 636 Cys and BiP 518 Cys were reacted with a 5-fold excess of benzophenone-4-maleimide (Invitrogen, USA) for 1 h at RT. 10 µM BiP were incubated with 35 µM $C_H1$ in the presence of 1 mM ADP at 37°C for 2 hours to allow complex formation. After 10 minutes irradiation at λ = 350 nm in a CL 1000 UV Crosslinker (UVP, Upland, USA), samples were diluted in 2x Lämmli buffer and separated on a 12.5 % SDS-PAGE. For tryptic digests, crosslinking bands were excised and treated as published (Schafer et al., 2001).

# 9 References

Alder,N.N., Shen,Y., Brodsky,J.L., Hendershot,L.M., and Johnson,A.E. (2005). The molecular mechanisms underlying BiP-mediated gating of the Sec61 translocon of the endoplasmic reticulum. J Cell Biol *168*, 389-399.

Andreasson,C., Fiaux,J., Rampelt,H., Druffel-Augustin,S., and Bukau,B. (2008). Insights into the structural dynamics of the Hsp110-Hsp70 interaction reveal the mechanism for nucleotide exchange activity. Proc. Natl. Acad. Sci U. S. A *105*, 16519-16524.

Andreasson,C., Rampelt,H., Fiaux,J., Druffel-Augustin,S., and Bukau,B. (2010). The endoplasmic reticulum Grp170 acts as a nucleotide exchange factor of Hsp70 via a mechanism similar to that of the cytosolic Hsp110. J Biol Chem. *285*, 12445-12453.

Anfinsen,C.B. (1973). Principles that govern the folding of protein chains. Science *181*, 223-230.

Anttonen,A.K., Mahjneh,I., Hamalainen,R.H., Lagier-Tourenne,C., Kopra,O., Waris,L., Anttonen,M., Joensuu,T., Kalimo,H., Paetau,A., Tranebjaerg,L., Chaigne,D., Koenig,M., Eeg-Olofsson,O., Udd,B., Somer,M., Somer,H., and Lehesjoki,A.E. (2005). The gene disrupted in Marinesco-Sjogren syndrome encodes SIL1, an HSPA5 cochaperone. Nat. Genet. *37*, 1309-1311.

Aponte,R.A., Zimmermann,S., and Reinstein,J. (2010). Directed evolution of the DnaK chaperone: mutations in the lid domain result in enhanced chaperone activity. J Mol Biol *399*, 154-167.

Bertelsen,E.B., Chang,L., Gestwicki,J.E., and Zuiderweg,E.R. (2009). Solution conformation of wild-type E. coli Hsp70 (DnaK) chaperone complexed with ADP and substrate. Proc. Natl. Acad. Sci U. S. A *106*, 8471-8476.

Blond-Elguindi,S., Cwirla,S.E., Dower,W.J., Lipshutz,R.J., Sprang,S.R., Sambrook,J.F., and Gething,M.J. (1993). Affinity panning of a library of peptides displayed on bacteriophages reveals the binding specificity of BiP. Cell *75*, 717-728.

Bole,D.G., Hendershot,L.M., and Kearney,J.F. (1986). Posttranslational association of immunoglobulin heavy chain binding protein with nascent heavy chains in nonsecreting and secreting hybridomas. J Cell Biol *102*, 1558-1566.

Braakman,I. and Bulleid,N.J. (2010). Protein Folding and Modification in the Mammalian Endoplasmic Reticulum. Annu. Rev. Biochem.

Brewer,J.W. and Hendershot,L.M. (2005). Building an antibody factory: a job for the unfolded protein response. Nat. Immunol *6*, 23-29.

Brodsky,J.L., Goeckeler,J., and Schekman,R. (1995). BiP and Sec63p are required for both co- and posttranslational protein translocation into the yeast endoplasmic reticulum. Proc. Natl. Acad. Sci U. S. A *92*, 9643-9646.

Buczynski,G., Slepenkov,S.V., Sehorn,M.G., and Witt,S.N. (2001). Characterization of a lidless form of the molecular chaperone DnaK: deletion of the lid increases peptide on- and off-rate constants. J Biol Chem. *276*, 27231-27236.

Bukau,B., Weissman,J., and Horwich,A. (2006). Molecular chaperones and protein quality control. Cell *125*, 443-451.

Buxbaum,J. and Gallo,G. (1999). Nonamyloidotic monoclonal immunoglobulin deposition disease. Light-chain, heavy-chain, and light- and heavy-chain deposition diseases. Hematol. Oncol. Clin. North Am. *13*, 1235-1248.

Calfon,M., Zeng,H., Urano,F., Till,J.H., Hubbard,S.R., Harding,H.P., Clark,S.G., and Ron,D. (2002). IRE1 couples endoplasmic reticulum load to secretory capacity by processing the XBP-1 mRNA. Nature *415*, 92-96.

Chaplin,M. (2006). Do we underestimate the importance of water in cell biology? Nat. Rev. Mol Cell Biol *7*, 861-866.

Chen,Y., Zhang,Y., Yin,Y., Gao,G., Li,S., Jiang,Y., Gu,X., and Luo,J. (2005). SPD--a web-based secreted protein database. Nucleic Acids Res. *33*, D169-D173.

Chung,K.T., Shen,Y., and Hendershot,L.M. (2002). BAP, a mammalian BiP-associated protein, is a nucleotide exchange factor that regulates the ATPase activity of BiP. J Biol Chem. *277*, 47557-47563.

Daugaard,M., Rohde,M., and Jaattela,M. (2007). The heat shock protein 70 family: Highly homologous proteins with overlapping and distinct functions. FEBS Lett. *581*, 3702-3710.

Dill,K.A. (1990). Dominant forces in protein folding. Biochemistry *29*, 7133-7155.

Dill,K.A. and Chan,H.S. (1997). From Levinthal to pathways to funnels. Nat. Struct. Biol *4*, 10-19.

Dobson,C.M. and Karplus,M. (1999). The fundamentals of protein folding: bringing together theory and experiment. Curr. Opin. Struct. Biol *9*, 92-101.

Dong,M., Bridges,J.P., Apsley,K., Xu,Y., and Weaver,T.E. (2008). ERdj4 and ERdj5 are required for endoplasmic reticulum-associated protein degradation of misfolded surfactant protein C. Mol Biol Cell *19*, 2620-2630.

Dragovic,Z., Broadley,S.A., Shomura,Y., Bracher,A., and Hartl,F.U. (2006). Molecular chaperones of the Hsp110 family act as nucleotide exchange factors of Hsp70s. EMBO J *25*, 2519-2528.

Dudek,J., Greiner,M., Muller,A., Hendershot,L.M., Kopsch,K., Nastainczyk,W., and Zimmermann,R. (2005). ERj1p has a basic role in protein biogenesis at the endoplasmic reticulum. Nat. Struct. Mol Biol *12*, 1008-1014.

Easton,D.P., Kaneko,Y., and Subjeck,J.R. (2000). The hsp110 and Grp1 70 stress proteins: newly recognized relatives of the Hsp70s. Cell Stress. Chaperones. *5*, 276-290.

Ellis,R.J. (2001). Macromolecular crowding: obvious but underappreciated. Trends Biochem Sci *26*, 597-604.

ELLMAN,G.L. (1959). Tissue sulfhydryl groups. Arch. Biochem Biophys. *82*, 70-77.

Fairbanks,G., Steck,T.L., and Wallach,D.F. (1971). Electrophoretic analysis of the major polypeptides of the human erythrocyte membrane. Biochemistry *10*, 2606-2617.

Feige M.J. and Buchner J. The role of disulfide bonds in protein folding and stability. 2010. Oxidative Folding of Peptides and Proteins, edited by Luis Moroder and Johannes Buchner.
Ref Type: Generic

Feige,M.J., Groscurth,S., Marcinowski,M., Shimizu,Y., Kessler,H., Hendershot,L.M., and Buchner,J. (2009). An unfolded CH1 domain controls the assembly and secretion of IgG antibodies. Mol Cell *34*, 569-579.

Feige,M.J., Groscurth,S., Marcinowski,M., Yew,Z.T., Truffault,V., Paci,E., Kessler,H., and Buchner,J. (2008). The structure of a folding intermediate provides insight into differences in immunoglobulin amyloidogenicity. Proc. Natl. Acad. Sci U. S. A *105*, 13373-13378.

Feige,M.J. and Hendershot,L.M. (2011). Disulfide bonds in ER protein folding and homeostasis. Curr. Opin. Cell Biol *23*, 167-175.

Feige,M.J., Hendershot,L.M., and Buchner,J. (2010). How antibodies fold. Trends Biochem Sci *35*, 189-198.

Fersht,A.R. and Daggett,V. (2002). Protein folding and unfolding at atomic resolution. Cell *108*, 573-582.

Fink,A.L. (2005). Natively unfolded proteins. Curr. Opin. Struct. Biol *15*, 35-41.

Fischer,G., Tradler,T., and Zarnt,T. (1998). The mode of action of peptidyl prolyl cis/trans isomerases in vivo: binding vs. catalysis. FEBS Lett. *426*, 17-20.

Gething,M.J., Blond-Elguindi,S., Buchner,J., Fourie,A., Knarr,G., Modrow,S., Nanu,L., Segal,M., and Sambrook,J. (1995). Binding sites for Hsp70 molecular chaperones in natural proteins. Cold Spring Harb. Symp Quant. Biol *60*, 417-428.

Goeckeler,J.L. and Brodsky,J.L. (2010). Molecular chaperones and substrate ubiquitination control the efficiency of endoplasmic reticulum-associated degradation. Diabetes Obes. Metab *12 Suppl 2*, 32-38.

Goloubinoff,P. and De los,R.P. (2007). The mechanism of Hsp70 chaperones: (entropic) pulling the models together. Trends Biochem Sci *32*, 372-380.

Goossens,T., Klein,U., and Kuppers,R. (1998). Frequent occurrence of deletions and duplications during somatic hypermutation: implications for oncogene translocations and heavy chain disease. Proc. Natl. Acad. Sci U. S. A *95*, 2463-2468.

Gragerov,A. and Gottesman,M.E. (1994). Different peptide binding specificities of hsp70 family members. J Mol Biol *241*, 133-135.

Gregersen,N. and Bross,P. (2010). Protein misfolding and cellular stress: an overview. Methods Mol Biol *648*, 3-23.

Haas,I.G. and Wabl,M. (1983). Immunoglobulin heavy chain binding protein. Nature *306*, 387-389.

Hageman,J., van Waarde,M.A., Zylicz,A., Walerych,D., and Kampinga,H.H. (2011). The diverse members of the mammalian HSP70 machine show distinct chaperone-like activities. Biochem J *435*, 127-142.

Harding,H.P., Zhang,Y., and Ron,D. (1999). Protein translation and folding are coupled by an endoplasmic-reticulum-resident kinase. Nature *397*, 271-274.

Haslbeck,M., Franzmann,T., Weinfurtner,D., and Buchner,J. (2005). Some like it hot: the structure and function of small heat-shock proteins. Nat. Struct. Mol Biol *12*, 842-846.

Haze,K., Yoshida,H., Yanagi,H., Yura,T., and Mori,K. (1999). Mammalian transcription factor ATF6 is synthesized as a transmembrane protein and activated by proteolysis in response to endoplasmic reticulum stress. Mol Biol Cell *10*, 3787-3799.

Hebert,D.N. and Molinari,M. (2007). In and out of the ER: protein folding, quality control, degradation, and related human diseases. Physiol Rev. *87*, 1377-1408.

Helenius,A. and Aebi,M. (2004). Roles of N-linked glycans in the endoplasmic reticulum. Annu. Rev. Biochem *73*, 1019-1049.

Horwich,A.L. and Fenton,W.A. (2009). Chaperonin-mediated protein folding: using a central cavity to kinetically assist polypeptide chain folding. Q. Rev. Biophys. *42*, 83-116.

Huber,R., Deisenhofer,J., Colman,P.M., Matsushima,M., and Palm,W. (1976). Crystallographic structure studies of an IgG molecule and an Fc fragment. Nature *264*, 415-420.

Jiang,J., Lafer,E.M., and Sousa,R. (2006). Crystallization of a functionally intact Hsc70 chaperone. Acta Crystallogr. Sect. F. Struct. Biol Cryst. Commun. *62*, 39-43.

Jin,Y., Zhuang,M., and Hendershot,L.M. (2009). ERdj3, a luminal ER DnaJ homologue, binds directly to unfolded proteins in the mammalian ER: identification of critical residues. Biochemistry *48*, 41-49.

Kanehara,K., Kawaguchi,S., and Ng,D.T. (2007). The EDEM and Yos9p families of lectin-like ERAD factors. Semin. Cell Dev. Biol *18*, 743-750.

Karlin,S. and Brocchieri,L. (1998). Heat shock protein 70 family: multiple sequence comparisons, function, and evolution. J Mol Evol. *47*, 565-577.

Kelley,W.L. (1998). The J-domain family and the recruitment of chaperone power. Trends Biochem Sci *23*, 222-227.

Kelley,W.L. (1999). Molecular chaperones: How J domains turn on Hsp70s. Curr. Biol *9*, R305-R308.

Knarr,G., Gething,M.J., Modrow,S., and Buchner,J. (1995). BiP binding sequences in antibodies. J Biol Chem. *270*, 27589-27594.

Knarr,G., Modrow,S., Todd,A., Gething,M.J., and Buchner,J. (1999). BiP-binding sequences in HIV gp160. Implications for the binding specificity of bip. J Biol Chem. *274*, 29850-29857.

Laemmli,U.K. (1970). Cleavage of structural proteins during the assembly of the head of bacteriophage T4. Nature *227*, 680-685.

Lee,Y.K., Brewer,J.W., Hellman,R., and Hendershot,L.M. (1999). BiP and immunoglobulin light chain cooperate to control the folding of heavy chain and ensure the fidelity of immunoglobulin assembly. Mol Biol Cell *10*, 2209-2219.

Leopold,P.E., Montal,M., and Onuchic,J.N. (1992). Protein folding funnels: a kinetic approach to the sequence-structure relationship. Proc. Natl. Acad. Sci U. S. A *89*, 8721-8725.

Mannick,J.B. and Schonhoff,C.M. (2002). Nitrosylation: the next phosphorylation? Arch. Biochem Biophys. *408*, 1-6.

Mapa,K., Sikor,M., Kudryavtsev,V., Waegemann,K., Kalinin,S., Seidel,C.A., Neupert,W., Lamb,D.C., and Mokranjac,D. (2010). The conformational dynamics of the mitochondrial Hsp70 chaperone. Mol Cell *38*, 89-100.

Marcinowski,M., Holler,M., Feige,M.J., Baerend,D., Lamb,D.C., and Buchner,J. (2011). Substrate discrimination of the chaperone BiP by autonomous and cochaperone-regulated conformational transitions. Nat. Struct. Mol Biol *18*, 150-158.

Mayer,M.P., Rudiger,S., and Bukau,B. (2000). Molecular basis for interactions of the DnaK chaperone with substrates. Biol Chem. *381*, 877-885.

McCarty,J.S., Rudiger,S., Schonfeld,H.J., Schneider-Mergener,J., Nakahigashi,K., Yura,T., and Bukau,B. (1996). Regulatory region C of the E. coli heat shock transcription factor, sigma32, constitutes a DnaK binding site and is conserved among eubacteria. J Mol Biol *256*, 829-837.

Meunier,L., Usherwood,Y.K., Chung,K.T., and Hendershot,L.M. (2002). A subset of chaperones and folding enzymes form multiprotein complexes in endoplasmic reticulum to bind nascent proteins. Mol Biol Cell *13*, 4456-4469.

Meusser,B., Hirsch,C., Jarosch,E., and Sommer,T. (2005). ERAD: the long road to destruction. Nat. Cell Biol *7*, 766-772.

Moro,F., Fernandez-Saiz,V., and Muga,A. (2004). The lid subdomain of DnaK is required for the stabilization of the substrate-binding site. J Biol Chem. *279*, 19600-19606.

Munro,S. and Pelham,H.R. (1986). An Hsp70-like protein in the ER: identity with the 78 kd glucose-regulated protein and immunoglobulin heavy chain binding protein. Cell *46*, 291-300.

Munro,S. and Pelham,H.R. (1987). A C-terminal signal prevents secretion of luminal ER proteins. Cell *48*, 899-907.

Nawa,D., Shimada,O., Kawasaki,N., Matsumoto,N., and Yamamoto,K. (2007). Stable interaction of the cargo receptor VIP36 with molecular chaperone BiP. Glycobiology *17*, 913-921.

Normington,K., Kohno,K., Kozutsumi,Y., Gething,M.J., and Sambrook,J. (1989). S. cerevisiae encodes an essential protein homologous in sequence and function to mammalian BiP. Cell *57*, 1223-1236.

Okamura,K., Kimata,Y., Higashio,H., Tsuru,A., and Kohno,K. (2000). Dissociation of Kar2p/BiP from an ER sensory molecule, Ire1p, triggers the unfolded protein response in yeast. Biochem Biophys. Res. Commun. *279*, 445-450.

Olsen,J.V., Blagoev,B., Gnad,F., Macek,B., Kumar,C., Mortensen,P., and Mann,M. (2006). Global, in vivo, and site-specific phosphorylation dynamics in signaling networks. Cell *127*, 635-648.

Otero,J.H., Lizak,B., and Hendershot,L.M. (2010). Life and death of a BiP substrate. Semin. Cell Dev. Biol *21*, 472-478.

Pace,C.N. (1990). Conformational stability of globular proteins. Trends Biochem Sci *15*, 14-17.

Pandya,M.J., Bendz,H., Manzenrieder,F., Noessner,E., Kessler,H., Buchner,J., and Issels,R.D. (2009). Interaction of human heat shock protein 70 with tumor-associated peptides. Biol Chem. *390*, 305-312.

Pellecchia,M., Montgomery,D.L., Stevens,S.Y., Vander Kooi,C.W., Feng,H.P., Gierasch,L.M., and Zuiderweg,E.R. (2000). Structural insights into substrate binding by the molecular chaperone DnaK. Nat. Struct. Biol *7*, 298-303.

Polier,S., Dragovic,Z., Hartl,F.U., and Bracher,A. (2008). Structural basis for the cooperation of Hsp70 and Hsp110 chaperones in protein folding. Cell *133*, 1068-1079.

Ptitsyn,O.B. (1995). Structures of folding intermediates. Curr. Opin. Struct. Biol *5*, 74-78.

Ptitsyn,O.B., Bychkova,V.E., and Uversky,V.N. (1995). Kinetic and equilibrium folding intermediates. Philos. Trans. R. Soc Lond B Biol Sci *348*, 35-41.

Qiu,X.B., Shao,Y.M., Miao,S., and Wang,L. (2006). The diversity of the DnaJ/Hsp40 family, the crucial partners for Hsp70 chaperones. Cell Mol Life Sci *63*, 2560-2570.

Richter,K. and Buchner,J. (2006). hsp90: twist and fold. Cell *127*, 251-253.

Richter,K., Haslbeck,M., and Buchner,J. (2010). The heat shock response: life on the verge of death. Mol Cell *40*, 253-266.

Rodriguez,F., Arsene-Ploetze,F., Rist,W., Rudiger,S., Schneider-Mergener,J., Mayer,M.P., and Bukau,B. (2008). Molecular basis for regulation of the heat shock transcription factor sigma32 by the DnaK and DnaJ chaperones. Mol Cell *32*, 347-358.

Ron,D. and Walter,P. (2007). Signal integration in the endoplasmic reticulum unfolded protein response. Nat. Rev. Mol Cell Biol *8*, 519-529.

Rose,M.D. and Fink,G.R. (1987). KAR1, a gene required for function of both intranuclear and extranuclear microtubules in yeast. Cell *48*, 1047-1060.

Rudiger,S., Germeroth,L., Schneider-Mergener,J., and Bukau,B. (1997). Substrate specificity of the DnaK chaperone determined by screening cellulose-bound peptide libraries. EMBO J *16*, 1501-1507.

Schafer,H., Nau,K., Sickmann,A., Erdmann,R., and Meyer,H.E. (2001). Identification of peroxisomal membrane proteins of Saccharomyces cerevisiae by mass spectrometry. Electrophoresis *22*, 2955-2968.

Seckler,R. and Jaenicke,R. (1992). Protein folding and protein refolding. FASEB J *6*, 2545-2552.

Senderek,J., Krieger,M., Stendel,C., Bergmann,C., Moser,M., Breitbach-Faller,N., Rudnik-Schoneborn,S., Blaschek,A., Wolf,N.I., Harting,I., North,K., Smith,J., Muntoni,F., Brockington,M., Quijano-Roy,S., Renault,F., Herrmann,R., Hendershot,L.M., Schroder,J.M., Lochmuller,H., Topaloglu,H., Voit,T., Weis,J., Ebinger,F., and Zerres,K. (2005). Mutations in SIL1 cause Marinesco-Sjogren syndrome, a cerebellar ataxia with cataract and myopathy. Nat. Genet. *37*, 1312-1314.

Sevier,C.S. and Kaiser,C.A. (2002). Formation and transfer of disulphide bonds in living cells. Nat. Rev. Mol Cell Biol *3*, 836-847.

Shen,Y. and Hendershot,L.M. (2005). ERdj3, a stress-inducible endoplasmic reticulum DnaJ homologue, serves as a cofactor for BiP's interactions with unfolded substrates. Mol Biol Cell *16*, 40-50.

Shen,Y., Meunier,L., and Hendershot,L.M. (2002). Identification and characterization of a novel endoplasmic reticulum (ER) DnaJ homologue, which stimulates ATPase activity of BiP in vitro and is induced by ER stress. J Biol Chem. *277*, 15947-15956.

Sitia,R. and Braakman,I. (2003). Quality control in the endoplasmic reticulum protein factory. Nature *426*, 891-894.

Slepenkov,S.V., Patchen,B., Peterson,K.M., and Witt,S.N. (2003). Importance of the D and E helices of the molecular chaperone DnaK for ATP binding and substrate release. Biochemistry *42*, 5867-5876.

Strub,A., Zufall,N., and Voos,W. (2003). The putative helical lid of the Hsp70 peptide-binding domain is required for efficient preprotein translocation into mitochondria. J Mol Biol *334*, 1087-1099.

Swain,J.F., Dinler,G., Sivendran,R., Montgomery,D.L., Stotz,M., and Gierasch,L.M. (2007). Hsp70 chaperone ligands control domain association via an allosteric mechanism mediated by the interdomain linker. Mol Cell *26*, 27-39.

Swain,J.F., Schulz,E.G., and Gierasch,L.M. (2006). Direct comparison of a stable isolated Hsp70 substrate-binding domain in the empty and substrate-bound states. J Biol Chem. *281*, 1605-1611.

Tirasophon,W., Welihinda,A.A., and Kaufman,R.J. (1998). A stress response pathway from the endoplasmic reticulum to the nucleus requires a novel bifunctional protein kinase/endoribonuclease (Ire1p) in mammalian cells. Genes Dev. *12*, 1812-1824.

Tokunaga,M., Kato,S., Kawamura-Watabe,A., Tanaka,R., and Tokunaga,H. (1998). Characterization of deletion mutations in the carboxy-terminal peptide-binding domain of the Kar2 protein in Saccharomyces cerevisiae. Yeast *14*, 1285-1295.

Travers,K.J., Patil,C.K., and Weissman,J.S. (2001). Functional genomic approaches to understanding molecular chaperones and stress responses. Adv. Protein Chem. *59*, 345-390.

Tsai,J. and Douglas,M.G. (1996). A conserved HPD sequence of the J-domain is necessary for YDJ1 stimulation of Hsp70 ATPase activity at a site distinct from substrate binding. J Biol Chem. *271*, 9347-9354.

van,A.E. and Braakman,I. (2005). Versatility of the endoplasmic reticulum protein folding factory. Crit Rev. Biochem Mol Biol *40*, 191-228.

Vanhove,M., Usherwood,Y.K., and Hendershot,L.M. (2001). Unassembled Ig heavy chains do not cycle from BiP in vivo but require light chains to trigger their release. Immunity *15*, 105-114.

Vembar,S.S., Jonikas,M.C., Hendershot,L.M., Weissman,J.S., and Brodsky,J.L. (2010). J domain co-chaperone specificity defines the role of BiP during protein translocation. J Biol Chem. *285*, 22484-22494.

Vogel,M., Mayer,M.P., and Bukau,B. (2006). Allosteric regulation of Hsp70 chaperones involves a conserved interdomain linker. J Biol Chem. *281*, 38705-38711.

Walter,S. and Buchner,J. (2002). Molecular chaperones--cellular machines for protein folding. Angew. Chem. Int. Ed Engl. *41*, 1098-1113.

Wandinger,S.K., Richter,K., and Buchner,J. (2008). The Hsp90 chaperone machinery. J Biol Chem. *283*, 18473-18477.

Wegele,H., Muller,L., and Buchner,J. (2004). Hsp70 and Hsp90--a relay team for protein folding. Rev. Physiol Biochem Pharmacol. *151*, 1-44.

Wei,J. and Hendershot,L.M. (1995). Characterization of the nucleotide binding properties and ATPase activity of recombinant hamster BiP purified from bacteria. J Biol Chem. *270*, 26670-26676.

Weitzmann,A., Volkmer,J., and Zimmermann,R. (2006). The nucleotide exchange factor activity of Grp170 may explain the non-lethal phenotype of loss of Sil1 function in man and mouse. FEBS Lett. *580*, 5237-5240.

Wolynes,P.G., Onuchic,J.N., and Thirumalai,D. (1995). Navigating the folding routes. Science *267*, 1619-1620.

Woo,H.J., Jiang,J., Lafer,E.M., and Sousa,R. (2009). ATP-induced conformational changes in Hsp70: molecular dynamics and experimental validation of an in silico predicted conformation. Biochemistry *48*, 11470-11477.

Yon,J.M. (2001). Protein folding: a perspective for biology, medicine and biotechnology. Braz. J Med. Biol Res. *34*, 419-435.

Yoshida,H., Haze,K., Yanagi,H., Yura,T., and Mori,K. (1998). Identification of the cis-acting endoplasmic reticulum stress response element responsible for transcriptional induction of mammalian glucose-regulated proteins. Involvement of basic leucine zipper transcription factors. J Biol Chem. *273*, 33741-33749.

Young,J.C., Agashe,V.R., Siegers,K., and Hartl,F.U. (2004). Pathways of chaperone-mediated protein folding in the cytosol. Nat. Rev. Mol Cell Biol *5*, 781-791.

Zhu,X., Zhao,X., Burkholder,W.F., Gragerov,A., Ogata,C.M., Gottesman,M.E., and Hendrickson,W.A. (1996). Structural analysis of substrate binding by the molecular chaperone DnaK. Science *272*, 1606-1614.

Zimmermann,R., Eyrisch,S., Ahmad,M., and Helms,V. (2011). Protein translocation across the ER membrane. Biochim. Biophys. Acta *1808*, 912-924.

# 10 Declaration

I, Moritz Marcinowski, hereby declare that this thesis was prepared by me independently and using only the references and resources stated here. The work has so far not been submitted to any audit commission. Parts of this work have been published in scientific journals.

Hiermit erkläre ich, Moritz Marcinowski, dass ich die vorliegende Arbeit selbständig verfasst und keine anderen als die angegebenen Quellen und Hilfsmittel verwendet habe. Die Arbeit wurde bisher keiner Prüfungskommission vorgelegt. Teile dieser Arbeit wurde in wissenschaftlichen Journalen veröffentlicht.

_____

Moritz Marcinowski
München,

# 11 Publications

Marcinowski M, Seitz C, Elfrich J, Behnke J, Feige MJ, Becker CFW, Antes I, Buchner J

Conformational selection of client sequences by the molecular chaperone BiP

*Manuscript submitted*

Schroeder B, Wu Z, Nuding S, Groscurth S, Marcinowski M, Beisner J, Buchner J, Schaller M, Stange EF, Wehkamp J (2011)

Reduction of disulfide bonds unmasks potent antimicrobial activity of human β-defensin 1

*Nature* 469:419-23

Marcinowski M, Höller M, Feige MJ, Baerend D, Lamb DC, Buchner J (2011)

Substrate discrimination of the molecular chaperone BiP by autonomous and cochaperone-regulated molecular transitions

*Nat Struct Mol Biol* 18:*150-8*

Feige MJ, Groscurth S, Marcinowski M, Shimizu Y, Kessler H, Hendershot LM, Buchner J (2009)

An unfolded $C_H1$ domain controls the assembly and secretion of IgG antibodies

*Mol Cell* 34:569-79

Feige MJ, Groscurth S, Marcinowski M, Yew ZT, Truffault V, Paci E, Kessler H, Buchner J (2008)

The structure of a folding intermediate provides insight into differences in immunoglobulin amyloidogenicity

*Proc Natl Acad Sci USA* 105:13373-8

# 12 Danksagung

Ich möchte mich bei Johannes Buchner sehr herzlich für die Betreuung meiner Dissertation, sowie den stets produktiven Austausch bedanken, der diese Arbeit erst ermöglich hat. Zusätzlich möchte ich ihm für seine stete Unterstützung und die Möglichkeit die zahlreichen Kooperationen während meiner Dissertation einzugehen danken.

Dank gebührt auch Matthias Feige, der mein Interesse an Antikörpern und ER spezifischen Fragestellungen geweckt hat und über die Jahre ein wertvoller Ansprechpartner für viele Fragen und Diskussionen war. Ich möchte mich auch bei allen Mitgliedern der Antikörper Gruppe ebenso wie beim ganzen Lehrstuhl für Biotechnologie für tolle Jahre im und außerhalb des Labors bedanken.

Ich möchte mich bei Prof. Don Lamb und Matthias Höller für die sehr produktive und spannende Zusammenarbeit bei den single particle FRET Experimenten bedanken ohne die ein Teil dieser Arbeit nicht möglich gewesen wäre. Christian Becker danke ich für seine Ideen und Synthesen der Peptide mit nicht-natürlichen Aminosäuren. Dank gilt auch Linda Hendershot für ihre Unterstützung und Förderung. Ich möchte auch Danae Baerend für ihre Arbeit zur Rückfaltung des ERdJ3 danken.

Ich möchte mich bei Julia Behnke und Ruoyu Sun und Moritz Kahlig für ihre Unterstützung im Labor während ihren Praktika bedanken.

Bei der Studienstiftung des deutschen Volkes möchte ich mich für die großzügige Unterstützung meiner Dissertation bedanken.

Großer Dank gilt meinen Eltern die mich mein gesamtes Studium unterstützt haben und mir stets den Rücken freigehalten haben und meinen Geschwistern für eine tolle gemeinsame Zeit in München.